A PROBABILISTIC APPROACH TO ESTIMATE EFFECTIVE ABSOLUTE PERMEABILITY

A THESIS
SUBMITTED TO THE DEPARTMENT OF APPLIED EARTH SCIENCES
AND THE COMMITTEE ON GRADUATE STUDIES
OF STANFORD UNIVERSITY
IN PARTIAL FULFILLMENT OF THE REQUIREMENTS
FOR THE DEGREE OF
MASTER OF SCIENCE

BY
CLAYTON VERNON DEUTSCH
MARCH 1987

Approved for the Department:

_____

Approved for the University Committee
on Graduate Studies:

_____

Dean of Graduate Studies and Research

Acknowledgements

It is a great pleasure to thank my advisor, Professor André Journel, for all the guidance, support, and assistance given during the preparation of this thesis.

I would like to thank André, the Applied Earth Sciences department and the Stanford Center for Reservoir Forecasting (SCRF) for providing the financial assistance that made this thesis possible.

Finally, and most importantly, I would like to thank my wife, Pauline, for her love, friendship, and encouragement throughout my studies.

Abstract

In virtually all engineering and science disciplines it is necessary to determine average or effective properties. Certain rock properties, in particular permeability, do not average linearly i.e., the permeability of a block is not an arithmetic average of the component permeabilities. The averaging process is more complex and will depend on the spatial arrangement of the component permeabilities.

The absolute permeability in the most common reservoir rock, a sandstone/shale sequence, is affected most by the presence of the low permeability shales. The estimation of block effective permeability in this composite sandstone/shale reservoir rock is the topic of this thesis.

The sensitivity of reservoir forecasting to the averaging of absolute permeability has been studied using data from the Prudhoe Bay reservoir. As a result of this case study the most critical step in averaging was determined to be the averaging of the contrasting sandstone and shale permeabilities. The block effective absolute permeability has been modeled as a power average of the sandstone and shale permeabilities. The spatial arrangement of the shales will determine the averaging power that correctly identifies the block effective permeability.

Some statistical measures, that are available from obtainable data, are introduced to characterize the spatial arrangement of the shale heterogeneities. The averaging power can then be more accurately estimated knowing these statistics of the sandstone/shale sequence. The results were established on the basis of repeated network flow simulations. The power averaging approach makes the estimation of block effective absolute permeability in sandstone/shale sequences more manageable.

Table of Contents

List of Tables

List of Figures

Chapter 1

Introduction

Overview

Almost everyone will have seen different sedimentary rock formations along roadways. Rarely are the sandstone and shale structures uniform for hundreds or thousands of feet. This, however, is the scale at which reservoir engineers require rock property information. If the rock properties for the large scale rock units do not accurately describe the important smaller scale heterogeneities of the reservoir, the behavior predicted by flow simulation programs may be inaccurate. Since production practices and revenue projection are based on reservoir simulation it is important to characterize the reservoir accurately.

The most common reservoirs are sandstone reservoirs with some shale present. In an oil reservoir most of the rock property information is available at the scale of a core plug and the scale that is observed by well logs. This information must be averaged into effective large scale information. The averaging of permeability from one scale to another is a process that is not yet completely understood. The essentially impermeable shales will affect the permeability of large rock units differently depending on how they are distributed in space. If the shales are aligned in the direction of flow the impact will be minimized. The other extreme is when the shales are aligned opposing flow which will maximize the impact of the shales.

This thesis considers the problem of scale averaging of absolute permeability. Some statistical measures will be introduced to describe the spatial arrangement

of shale and sandstone. These measures can then be used to predict averaging processes to compute effective permeability.

Throughout this research the practical relevance of the approaches taken and the solutions proposed have been critically assessed. The following questions have been considered in detail:

- What practical impact will incorrect averaging processes have on reservoir production forecasting?
- How can block effective absolute permeability be estimated from core measured permeability and statistical parameters about the proportion and spatial arrangement of the rock components?

To address these problems simplifying assumptions must be made. A binary permeability distribution for the core data will be considered to represent the sandstone/shale sequence. This is a valid assumption if there is very little mixing of the two components at the scale of measurement. It is also necessary to assume that some information is available about the spatial distribution of the shales. Indeed, if there is no information outside of the well region then nothing can be said about oil saturation, porosity, and other crucial reservoir parameters. Throughout the thesis the assumptions made are noted and their practical implications are discussed.

Published research related to the problems addressed in this thesis is documented in the next section. The topic of each subsequent chapter is as follows:

- Chapter 2 contains a more detailed description of the problem and a summary of the concepts of permeability and geostatistics.
- Chapter 3 presents the results of a sensitivity study. The sensitivity of predicted reservoir performance to different averaging techniques for

absolute permeability was investigated using data from the Prudhoe Bay reservoir.

- Chapter 4 addresses the problem of determining the appropriate distribution of permeability in a two component sandstone/shale mixture.
- Chapter 5 shows how spatial statistics characterizing the sandstone/shale sequence may be used to estimate effective absolute permeability.
- Chapter 6 summarizes the results of the thesis and shows where future research may be conducted.

Related Research

The calculation of effective flow properties in heterogeneous media is a topic that is receiving a great deal of attention [Freeze, 1975; Gelhar, 1976; Gelhar and Axness, 1983; Haldorsen and Lake, 1984; Haldorsen 1983; Begg and King, 1985]. This problem is important for petroleum engineers who must plan recovery schemes and predict reservoir performance. In the field of hydrology the problem of predicting recharge and discharge rates for aquifers requires calculation of effective flow properties. When considering the underground disposal of hazardous wastes it is necessary to know the rate at which the fluids may move through the rock.

This review section is not intended to be comprehensive but is rather an overview that will highlight important and relevant published research. The author has no access to internal reports or technology developed "in-house" by major oil companies therefore this review will be limited to published research.

A comprehensive discussion of the techniques available to average permeability can be found in the Ph.D. dissertation by A.J. Desbarats (Stochastic modeling of flow in sand - shale sequences, Stanford University, 1986) Most of the research devoted to estimation of effective permeability has considered relatively homogeneous materials. An initial assumption that the distribution of permeability is lognormal is usually made, although, the very nature of a heterogeneous medium does not suggest a lognormal distribution for permeability (Fogg,1986). If the medium is truly heterogeneous, i.e. with sandstone and shale, there should be two main modes in the permeability distribution. A continuous unimodal distribution will only be observed for each of the components independently, or if there has been substantial averaging within the volume of measurement.

For a number of different unimodal permeability distributions Warren and Price (1961) show that the geometric average may be used as an estimate of the

effective permeability when there is no spatial correlation. Other researchers (Gutjahr et.al. 1978; Dagan 1979; Gelhar and Axness 1983) propose solutions for spatially uncorrelated and continuous low variance permeability data distributions. Another, more appropriate averaging technique for permeability in presence of the distinctly bimodal and spatially correlated case of a sandstone reservoir is proposed by Haldorsen and Lake (1984).

The method proposed by Haldorsen and Lake calls for the explicit generation of shale bodies within a flow field by Monte Carlo simulation of their locations and size. The horizontal and vertical effective permeability is then approximated by a formula based on a stream - tube concept. Begg and King (1985) remove the need for Monte Carlo simulation by incorporating statistics of shale size and abundance into the analytical formulas for effective permeability. A.J. Desbarats (1986) has shown that the model does not work well for volume fractions of shale greater than 10%. The implicit assumption that the pressure field surrounding each shale is not affected by other shales is valid only for low shale fractions; for shale fractions greater than 10% this assumption breaks down.

Weber (1982) approaches the problem from a geological position. Knowing the sedimentology and diagenesis background, models can be created that will predict the possible influence of sedimentary structures on fluid flow. The attention is focused on computing the permeability anisotropy rather than volume averages of permeability. However, the geological basis of this research is fundamental to any comprehensive treatment of the scale averaging problem.

Research relevant to the problem of scale averaging can also be found outside of the earth sciences. Percolation theory which is discussed in physics literature (Hammersley and Welsh, 1978) provides another approach to the problem of scale averaging. However, there appears to be no easy way yet to incorporate spatial correlation into percolation theory.

One of two directions is typically taken to solve the problem of estimating effective permeability. A numerical approach (Warren and Price 1961; Freeze 1975; Smith and Freeze 1979; Desbarats 1986) based on numerical simulations, and an analytical method based on a perturbation approach are the two common approaches. Alternately, a more empirical approach similar to that of Haldorsen and Lake (1984), Begg and King (1985) may be adopted. The research presented here falls loosely into this third category.

In the practical case of estimating effective permeability there are some specific considerations that make many of the proposed earlier solutions not fully satisfactory:

- The univariate distribution of the permeability in a sandstone/shale reservoir is bi or multimodal at the scale of measurement and is not continuous. The permeability distribution (if correctly sampled) for a heterogeneous medium as commonly found in actual sandstone reservoirs is most often the combination of two or more distributions.

- Perturbation approaches require that the permeability distribution have a low variance. Variances of multimodal distributions are generally high. In fact a binary distribution has the greatest variance of all possible distributions with a given range.

- Spatial correlation is present. This spatial correlation is introduced through the process of sedimentation and is crucial to the problem: assuming a spatially uncorrelated media is not a valid assumption for most reservoirs.

- The shales interact with each other, thus for volume fractions of shale that commonly exist in sand-shale reservoirs this interaction must be accounted for.

Instead of an empirical estimation algorithm, the effective permeability may be directly calculated by numerical means (Warren and Price, 1961, Desbarats 1986). This is a reasonable alternative but it is cumbersome to implement. Implementation requires a network model for the sandstone/shale sequence of each block. In many practical cases the only information available is core data, well logs and possibly some geological inference about the spatial arrangement of the sandstone and shale. These limitations may make it difficult to create an appropriate numerical model.

A prediction algorithm that is initially calibrated on numerical results but requiring input in the form of statistics (univariate and spatial) relevant to the flow system would be more appropriate. The idea is to fit network simulation results by a heuristic formula whose parameters are statistically linked to geometric characteristics that can be inferred directly. Such techniques performing well for different ranges of shale proportion and spatial distribution are not currently available.

Ideally, the prediction algorithm should integrate all sources of information. The geological input of Weber (1982), the shale simulation of Haldorsen (1983), and various numerical techniques to calculate block permeability can all be used to assist development of a new model. The research presented in this thesis will draw from the results found in the works noted above.

Chapter 2

Problem Statement and Background Information

Problem Statement

The problem of calculating block effective absolute permeability on the basis of small scale measurements is very general. If the reservoir were completely homogeneous the calculation of block averages would not be a problem; the permeability would be constant and uniform throughout the reservoir. However, real reservoirs are not that simple and contain different types of heterogeneity which affect the calculation of block averages. The dominant heterogeneity is considered to be the presence of low permeability shales (Pryor and Fulton, 1976; Fogg, 1985; and Haldorsen and Chang, 1985). Although some authors now suspect that connected fractures may be the most important feature. The impact of heterogeneity within the sandstone and within the shales is dwarfed by the transition sand-shales and their spatial location.

To begin the study of heterogeneity and scale averaging one may ask: how much does reservoir heterogeneity affect simulation results and at what scale heterogeneity is important? To partially answer this general question the following specific problem has been addressed: How will reservoir simulation results for a waterflooding production scheme be affected by the averaging of absolute permeability, and perturbations in other multiphase rock property data? The sensitivity of predictions to perturbations in the multiphase flow properties (relative permeability, capillary pressure, etc) of the medium is important because the fluid heterogeneity may be more important than the rock heterogeneity.

The impact of averaging absolute permeability on waterflooding performance has been studied with the SCRF II heterogeneous reservoir model. When considering this question answers to additional questions will become apparent:

- At what scale is the averaging procedure for absolute permeability important?
- What parameters, that are required input to reservoir flow simulators, impact most the simulation results?

This case study will allow work to be directed more closely toward where the problems are. The second phase of this thesis considers the specific problem of determining effective or averaged medium properties, in particular, the averaging of absolute permeability. A binary permeability distribution is proposed and the effective permeability of a block is modeled as the power average of the component permeabilities.

The effective permeability will be related to statistical measures of the spatial arrangement of shale heterogeneities. The goal is to develop statistical parameters that characterize a heterogeneous system and that may be used to predict effective absolute permeability.

One limitation is that any statistical parameter must be inferred in practical circumstances. Therefore the estimation of such statistics from real data (core, well logs, well testing, seismic, and geologic knowledge) must be realistically possible.

Flow Properties

Absolute Permeability:

The concept of absolute permeability is recalled. Permeability is a property of a porous medium which characterizes how easily a fluid can be made to flow through it. Permeability is defined by an empirical relationship known as Darcy's Law:

$$K = \frac{q\ \mu}{A\ (\delta P\ /\ L\ )} \tag{2.1}$$

where:

K = permeability (md)

q = volumetric flow rate (cm^3/sec)

μ = viscosity (cp)

A = cross sectional area (cm^2)

δP = difference in pressure across the sample (atm)

L = the length of the sample (cm)

The limitations of Darcy's law are well documented in the literature (Collins 1961; Hubbert 1956; Whitaker 1966,1969; and Scheidegger 1974) and will not be discussed here.

The permeability of a porous media is a macroscopic property and has significance for samples sufficiently large with respect to the pore size. Also, permeability is not an additive scalar like saturation. The permeability of a sample may be directional and will depend on the directional size of the sample or rock unit that is being considered.

Relative Permeability:

If more than one fluid phase (ex. oil and water) is flowing through a porous medium, the effective permeability of the rock to each phase is reduced. The sum of the effective permeabilities for all flowing phases is found to be less than the absolute permeability. The effective permeability of a fluid phase may be expressed as the product of the relative permeability (dimensionless value between 0 and 1) and the absolute permeability of the rock. Relative permeability is largely a function of the wetting phase saturation. Water is usually the wetting phase in an oil-water system. Relative permeability is also a function of saturation history as well as of saturation. For example: the relative permeability of the oil phase in an oil-water system depends not only on the water saturation but on whether the water is displacing the oil (drainage) or the oil is displacing the water (imbibition).

A set of typical relative permeability curves and the associated terminology are shown on figure 2.1. Relative permeability curves are determined in the laboratory from core. Three phase relative permeability is rarely measured but is usually constructed through two sets of two phase data. Relative permeability curves vary for different rock characteristics, fluid properties, and flow regimes. Among the parameters that affect the measurement of relative permeability:

1. **Temperature.** It is well documented throughout the literature that temperature affects relative permeability. Recently Bennion, etal. (1985) has shown that the effect of temperature can be significant.

2. **Flow conditions.** The flow conditions used to determine relative permeability may be steady state or unsteady state. Experimental methods to determine relative permeability characteristics have been developed for both flow conditions. Since flow in a reservoir is suspected to be at unsteady state the appropriate method to experimentally determine the relative permeability would be for this flow condition. However, the solutions

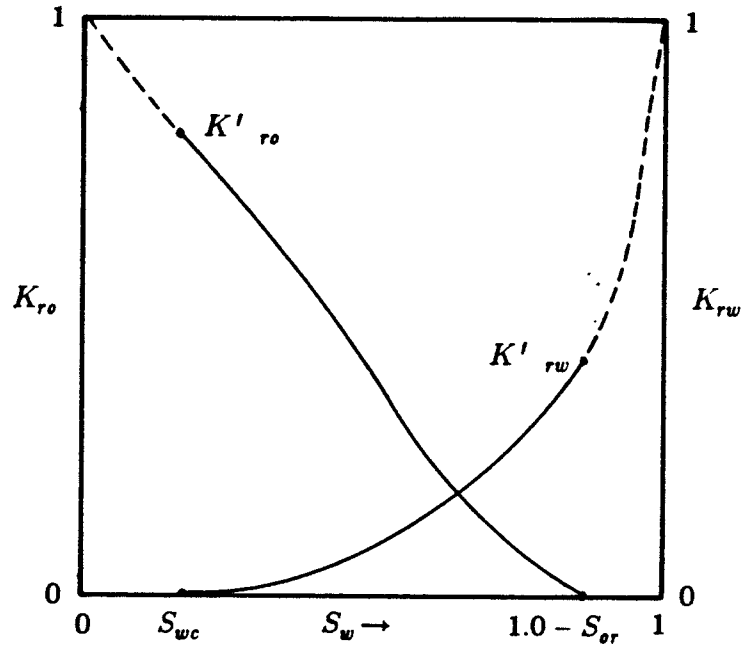

K_{ro} = Relative permeability of the oil phase

K_{rw} = Relative permeability of the water phase

S_w = Saturation of water phase

S_{wc} = Connate water saturation

S_{or} = Residual oil saturation

$1.0 - S_{or}$ = Maximum water saturation

K'_{ro} = Maximum relative permeability of the oil phase

K'_{rw} = Maximum relative permeability of the water phase

Figure 2.1: Relative Permeability as typical functions of the water saturation. The curves are representative of simultaneous flow of oil and water through a porous media (after Dake 1979).

obtained for this condition are not unique. Disregarding conceptual problems with uniqueness and physical meaning there are newer techniques that address this problem (Islam and Bentson, 1986). It is also apparent that this problem has not been fully resolved and that the resulting relative permeabilities are affected.

3. **Measurement fluid** Water-oil relative permeability measured using reservoir fluids and fresh preserved cores differ considerably from those routinely obtained using refined fluids and extracted cores (Mungan, 1972). The effect of the saturating fluid on the determination of relative permeability is significant. It should be noted that using the native crude oil, which would provide the most correct results, is not common practice.

Relative permeability is sensitive to many different parameters that are not easily accounted for in laboratory conditions. The concept of relative permeability seems flawed but as yet there is no alternative to this approach. Some means must be used to quantify the observed phase behavior. Laboratory measured relative permeability curves are usually altered to create pseudo-relative permeability curves that match the performance history of the reservoir. Unfortunately the relative permeability appears to be the most important parameter for many performance forecasting tasks. Consequently the inherent uncertainty in measuring such relative permeability may mask the influence of other possibly more intrinsic rock properties, and may leave the impression that scale averaging is not important. A practical assessment of the impact of relative permeability heterogeneities on flow performance forecasting is documented in the next chapter.

Capillary Pressure:

Another important parameter describing multiphase flow is capillary pressure. If there are two phases present in a porous media the pressure in each phase tends to be different. This pressure difference is called the capillary pressure. The fluid that preferentially "wets" (attracted to) the rock has a lower pressure than the non-wetting fluid phase. The expression commonly written for capillary pressure:

$$P_c = P_{nw} - P_w = f(S_w) \tag{2.2}$$

where:

P_c = Capillary pressure.

P_{nw} = Pressure in the non-wetting phase.

P_w = Pressure in the wetting phase.

$f(S_w)$ = The capillary pressure is a function of the wetting phase saturation.

Capillary pressure is, in some respects, similar to relative permeability. The properties of P_c that make it similar to relative permeability are:

- Reliable measurement is difficult and the impact of various measurement techniques is difficult to assess.
- The capillary pressure depends on the wetting phase saturation and the saturation history.

The capillary pressure is, in most circumstances, not as important as the relative permeability. In fact, the capillary pressure is sometimes set to zero as a first approximation. The capillary pressure may be important especially in cases of fractured reservoirs, however, the meaning of effective capillary pressure is not clear let alone its averaging from one scale to another.

Averaging and Effective Medium Properties

In virtually all engineering and science fields it is necessary to determine average or effective properties. Often the average property of a heterogeneous media is a linear average (i.e., an arithmetic or volumetric average). Certain properties, in particular permeability, do not have the property of linear averaging. The discussion here will be limited to properties such as permeability where the averaging process is non-linear and unknown for practical cases.

When the averaging process is unknown the problem of averaging could be avoided if measurements are taken at the scale at which they are going to be used. As previously mentioned, the scale of a core plug is considerably different from the scale of a reservoir simulation grid-block. For this reason some averaging must be done.

In Petroleum Engineering one must often calculate an average permeability over a large volume based on permeability measurements at several points within the volume. Permeability is, in some respects, a fluid connectivity. It shares many of the properties of electrical conductivity, one of which is its non-additive averaging nature. The overall permeability of several small blocks, each of which has a known permeability k_i is not simply an arithmetic average of the individual k_i' s. The average is dependent on the spatial arrangement of the block permeabilities, k_i.

This problem can be understood in one dimension where the analogy of electrical resistivity is appropriate. In three dimensions the analogy requires a network of resistors. If one considers the flow of fluid through several blocks in series (ref. figure 2.2) the effective permeability of the composite is the harmonic mean:

$$\frac{1}{K_e} = \frac{1}{n}\sum_{i=1}^{i=n}\frac{1}{k_i} \tag{2.3}$$

If the blocks are arranged in parallel (ref. figure 2.3) the effective permeability is

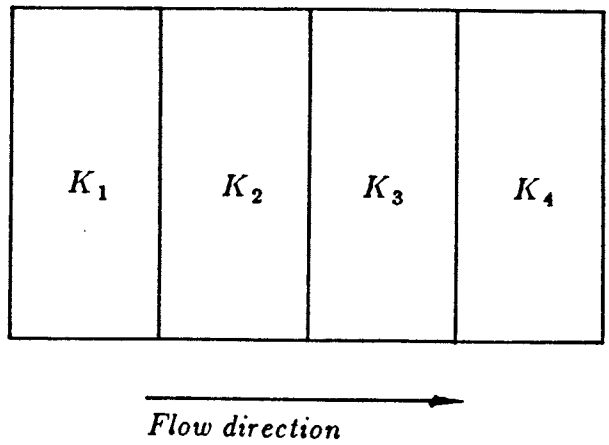

Figure 2.2: Blocks in series - the effective permeability is the harmonic average of the component permeabilities.

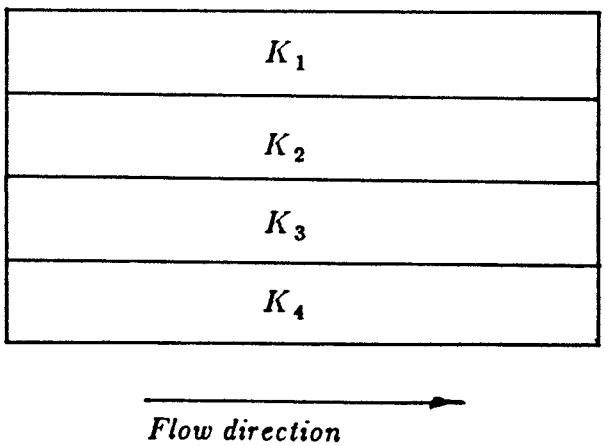

Figure 2.3: Blocks in parallel - the effective permeability is the arithmetic average of the component permeabilities.

given by the arithmetic mean:

$$K_e = \frac{1}{n} \sum_{i=1}^{i=n} k_i \tag{2.4}$$

In two or three dimensions the effective permeability is not given by any simple analytical solution. The effective permeability is bounded by the harmonic mean as a lower limit and the arithmetic mean as an upper limit. The effective permeability of a 3-d network of blocks, each with a known permeability k_i, may take any value between the harmonic average and arithmetic average. The lower bound harmonic mean (2.3) can be seen as a power average of the elementary k_i's with power $\omega = -1$. Similarly, the upper bound arithmetic mean (2.4) can be seen as a power average with power $\omega = +1$. Hence, and heuristically, it can be said that the effective permeability is a power ω average of the elementary permeability values k_i's with a power value $-1 \leq \omega \leq +1$. The problem of determining the effective permeability is now mapped into the more congenial problem of determining an effective power which is a scalar valued between +1 and -1.

The distribution of permeability must be split into n_c modes or classes. At the limit each permeability datum could represent a class. The power averaging formula is written:

$$K_e = \left[\sum_{i=1}^{i=n_c} p_i \cdot k_i^{\omega} \right]^{\frac{1}{\omega}} \tag{2.5}$$

where:

K_e = effective permeability

p_i = volume fraction of class i

1 The power averaging formulation requires that all the permeabilities (k_i) be strictly greater than zero.

k_i = permeability of class i

ω = power of averaging

The geometric average is obtained with $\omega = 0$ (at the limit since the power function is not defined at $\omega = 0$).

The power average provides a convenient formulation for the description of an averaging process. Fractional power values will characterize different spatial arrangements of the elementary k_i values. When dealing with a two component system($n_c = 2$), as done in this thesis, the power averaging formulation is shown to be the *correct* functional form of the solution if certain axiomatic conditions are met. Korvin (1982) outlined eight conditions or axioms that the physical system should meet to unambiguously determine the effective property of a two component system with a power average. The work presented in this thesis makes use of the power averaging formulation and the conditions outlined by Korvin will be recalled. The two component power average formula for effective permeability is written:

$$K_e = \left(p \cdot Ksh^{\omega} + (1-p) \cdot Kss^{\omega} \right)^{\frac{1}{\omega}} \tag{2.6}$$

with:

K_e = Block Effective Permeability.

Ksh = Permeability of the shales (strictly > 0).

Kss = Permeability of the sandstone.

p = Proportion (volume fraction) of shale.

ω = Power of averaging.

The eight conditions will now be given and interpreted in the context of a permeability study.

1. *Reflexivity:* If the sandstone and shale have the same permeability, the permeability of any composite sandstone and shale unit will have that same permeability.

2. *Idempotency:* The permeability of a 100% shale unit is the permeability of the shale and the permeability of a 100% sandstone unit is the permeability of the sandstone.

3. *Homogeneity (of the 0-th order) with respect to the sandstone/shale volume fractions:* The effective permeability does not depend on the size of the composite but only on the volume fraction of each component. The averaging power ω will be made variable to account for the different spatial arrangements of sandstone/shale for a given shale volume fraction.

4. *Internity;* The effective permeability of a composite lies between the permeability of the sandstone and the permeability of the shale.

5. *Bi-symmetry:* If the composite is composed of four components any pair of components may be averaged and the resulting pair of averaged properties may be averaged to obtain the composite effective permeability.

6. *Monotonicity with respect to the volume fractions:* As the proportion of shale increases the permeability decreases (provided that the permeability of the shale is less than that of the sandstone).

7. *Monotonicity with respect to the permeabilities:* For a given system (constant shale permeability and proportion of shale) the effective permeability will decrease for a decrease in sandstone permeability.

8. *Homogeneity (of the first order) with respect to the permeabilities:* If the shale and sandstone permeabilities are scaled by a multiplicative constant the effective permeability will be scaled by the same constant. The implication is that the effective permeability will have the same units as the component permeabilities.

The permeability of a composite mixture is not only a function of the component permeabilities and the volume fraction of each component. The effective permeability is also a function of the spatial arrangement of the

components. This obvious fact leads to the conclusion that permeability can *not* be unambiguously determined from the component permeabilities and volume fractions. The idea of this thesis is precisely to make the averaging power a function of some statistics of this spatial arrangement. This type of empirical approach is not unusual in the earth sciences.

Formulae that make use of a power averaging approach include the Wyllie "time-average equation" (Wyllie et al, 1956), Meese and Walther's "vugular carbonate formula" (Meese and Walther, 1967), (Tegland, 1970, Mateker, 1971) for the sound speed and effective attenuation in an alternating sequence of sand shale layers, and (Beck, 1976; Rzhevsky and Novik, 1971; Schon, 1971; Woodside and Messner, 1961; Grant and West, 1965; Pearce, et al., 1973; etc.) for the estimation of thermal and electric conductivity of fluid filled sedimentary rocks.

The power averaging formulation is not subject to any *a priori* hypothesis that can be validated or refuted. It is simply a model allowing the problem of determining Ke to be shifted to the problem of determining ω. The problem is more manageable due to the following properties (Journel, et.al., 1986, Deutsch, 1986):

1. For a bimodal sandstone/shale system the averaging power has been shown to be reasonably independent of the proportion of shale (see next section).
2. It is more convenient to work with the power of averaging which is a scalar known to be bounded between +1 and -1, than with a complex function of the permeability measurements.
3. On the basis of some prior geologic knowledge about the dimensionality and spatial arrangement of heterogeneities it may be possible to narrow considerably the range of possible averaging powers.

Figure 2.4 shows how the averaging power affects the resulting effective permeability for a bimodal distribution of permeability (Ksh =0.1 md and Kss =1000.0 md). The traditional arithmetic, geometric, and harmonic averages

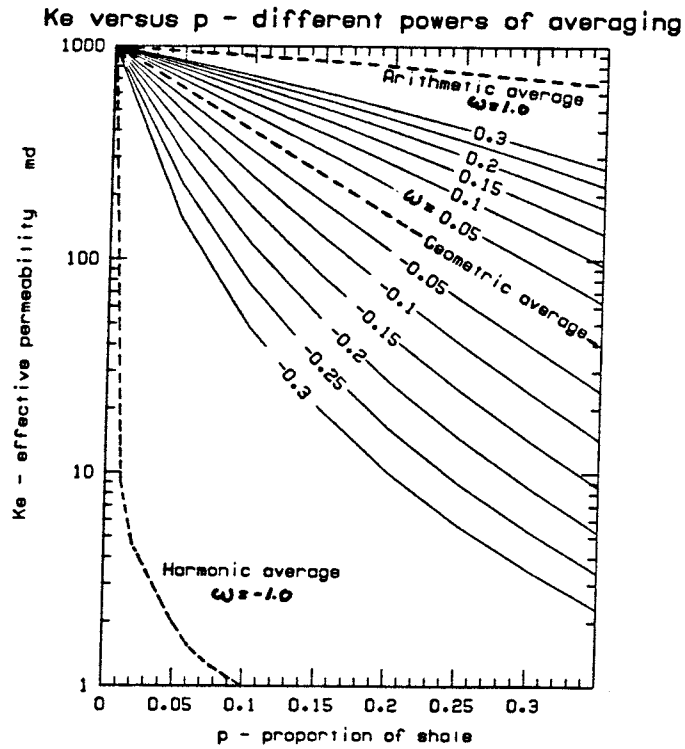

Figure 2.4: Effective permeability for different averaging powers.
A bimodal permeability distribution with $Ksh = 0.1$ md and $Kss = 1000$ md is used. The arithmetic, geometric, and harmonic averages are shown for reference.

are shown for reference. The continuous transition from the arithmetic mean to the harmonic mean allows stable mapping of K_e to ω.

It should be noted that the process of power averaging is distributive, i.e., both of the following processes will yield the same average permeability for a large block:

IMPORTANT

1. The small scale information is averaged directly to the large block scale.
2. The small scale data is averaged to an intermediate scale and subsequently averaged to the large block scale.

In both cases the same averaging power must be used in each step.

Power averaging amounts to transform the data by a power ω, arithmetically average the transformed data, and then back transform (by $\frac{1}{\omega}$) to obtain the average.

To summarize the current knowledge on effective medium properties is easy because there is no analytical solution to calculate the effective absolute permeability in a two component mixture. Methods that are used in different situations are refered to in chapter one. A power averaging formulation is adopted in this thesis because it makes the problem more tractable.

Power Averaging for Block Effective Permeability

Rather than trying to analytically derive the averaging process, it is observed through repeated flow simulations performed on realizations of permeability fields. This forward modeling, common to petroleum engineering practice, allows consideration of any permeability field, not restricted by such hypothesis as continuity or small variance.

Before getting into more sophisticated recovery processes with multiphase flow, a single phase, steady state, flow equation solved by finite difference methods at each grid block will be considered. Because of hardware limitations, the system was limited to a maximum of 500 grid blocks. Constant pressure boundaries were imposed in the direction of flow, and no-flow boundaries were specified in the other two directions perpendicular to flow. The effective permeability K_e of the network is obtained by dividing the total volumetric flux across a section perpendicular to flow by the imposed pressure gradient. The flow simulation was repeated for each realization of the grid block permeability field, yielding each time an effective K_e. The relationship between K_e and the characteristics of the input (grid block) permeability field are observed.

The input permeability field:

Experience and previous simulation works in shaley reservoirs have shown that the recovery, hence the flow conditions do not depend on the fine details of the permeability spatial distribution, but rather on the spatial connectivity of the extreme permeability values, either low such as impervious shale barriers, or high such as open fractures. ref. Haldorsen and Chang (1985).

In other words, and in first approximation for recovery purposes in single phase steady state flow conditions, the permeability field can be approximated by its two extreme modes, K_{sh} for the essentially impermeable phase and K_{ss} for the much coarser grained rock. Thus, the permeability distribution considered hereafter is binary and characterized by the 3 parameters:

$$K_{sh} << K_{ss} \tag{2.7}$$

$0 < p < 1$: volumetric proportion of shales

However these two modes are not distributed at random in space. Rather their spatial distribution obeys the following bivariate distribution:

$$Prob\{x \text{ in shale}, x+h \text{ in shale}\} = S(h) \tag{2.8}$$

$S(h)$ being a function of the three dimensional interdistance vector h.

The function $S(h)$ fully characterizes the bivariate spatial distribution of the binary permeability field, in particular:

$$Prob\{x \text{ in sand}, x+h \text{ in sand}\} = 1 - 2p + S(h) \tag{2.9}$$

$$Prob\{x \text{ in shale}, x+h \text{ in sand}\} = p - S(h)$$

The random function permeability $K(x)$ is stationary with moments:

$$E\{K(x)\} = p \cdot K_{sh} + (1-p) \cdot K_{ss}$$

$$Var\{K(x)\} = \left[K_{ss} - K_{sh}\right]^2 \cdot p(1-p)$$

The correlation between $K(x)$ and $K(x+h)$ is:

$$\rho(h) = \frac{S(H) - p^2}{p(1-p)} \tag{2.10}$$

Several techniques exist to generate realizations of a binary random field with a given univariate and bivariate spatial distribution (equations 2.7 and 2.8). The technique used here is that of indicator simulation, described in Journel and Isaaks (1984), whereby an appropriate threshold is applied on an appropriate Gaussian field generating two spatially correlated phases called sand (above threshold) and shale (below threshold).

The study consists in varying the input statistics: p, $S(h)$, and the contrast K_{ss}/K_{sh}, and observing the resulting network effective permeabilities K_e.

A dispersion of shale and sandstone permeability values can easily be generated around their mode values K_{sh} and K_{ss}, thus generating a continuous bimodal distribution. However, the binary distribution allows studying the impact of the sole transition sandstone/shale, high/low, independently of other and minor sources of variability.

This binary model, although still limited and provisional, goes a long way beyond the limitations of previously used stochastic models, such as small contrasts and no spatial correlation. In the present study contrasts K_{ss}/K_{sh} up to 10^6 and correlation ranges from nought to several times the network dimensions were considered.

Some Results:

In the following, an exponential model with a vertical to horizontal anisotropy 1/15 has been considered for the correlation function $\rho(h)$:

$$\rho(h) = \exp\left[\frac{-3h'}{a}\right] \tag{2.11}$$

with:

$$h' = \sqrt{h_x^2 + h_y^2 + (15h_z)^2}$$

h_x, h_y, h_z being the three rectangular coordinates of the vector h.

Thus, the practical range, i.e., the distance beyond which spatial correlation vanishes is a in the horizontal plane, and $a/15$ in the vertical direction.

Figure 2.5 gives the results for horizontal flow in the x-direction in a network of dimensions (L_x, L_y, L_z) such that: $L_x/a = 1.7$, $L_y/a = 0.8$, $L_z/a = 3$, i.e., of dimensions 1.7, 0.8, and 3 times the respective correlation ranges. The network is discretized into $n_x = 12$, $n_y = 6$, $n_z = 6$, i.e., a total of 432 grid blocks. Each grid block was assigned a permeability (diagonal isotropic tensor) equal to $K_{sh} = 10^{-2} md$ or $K_{ss} = 10^4 md$; the contrast is thus $c = K_{ss}/K_{sh} = 10^6$.

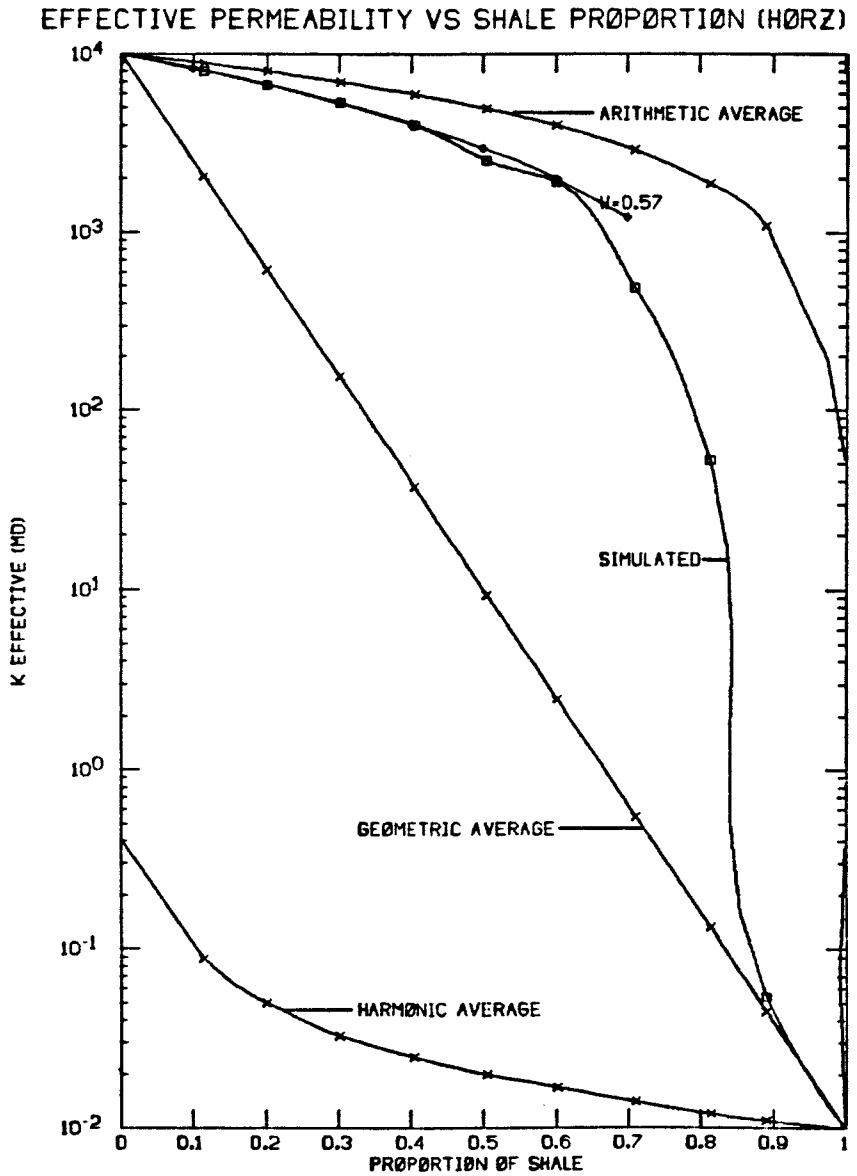

Figure 2.5: The effective permeability versus shale proportion for horizontal flow. Note that for shale fractions less than 0.6 the power average ($\omega = 0.57$) fits the simulated data very well. The traditional arithmetic, geometric, and harmonic averages are shown for reference.

This figure graphs the network effective permeability (in the X-direction) vs. the proportion p of shales. Since the generation of the permeability field is stochastic in nature, an average of 30 to 50 realizations (with each 432 permeability values) were retained for each preassigned shale proportion p ; the flow simulation was run for each such realization to derive the corresponding effective permeability K_e ; finally, it is the arithmetic average of these 30 to 50 realizations of K_e which is plotted vs. p on figure 2.5.

Also plotted for references on figure 2.5 are the arithmetic, geometric and harmonic averages of K_{sh} and K_{ss} .

A power average, with power $\omega = 0.57$ is shown to provide an excellent fit to the curve K_e vs. p for proportion of shales below 0.6.

Next, vertical flow (in the z-direction) was simulated over a network of dimensions (L_x, L_y, L_z) such that: $L_x/a = L_y/a = 1$, $L_z/a = 3.25$,. Recall that the vertical range of correlation is $a/15$. The network is discretized into $n_x = n_y = 6$, $n_z = 12$, i.e., a total of 432 grid blocks. Thus, the vertical distance between two grid blocks is $3.25/12 = .27$ times the vertical range.

The corresponding results are shown on figure 2.6. The results for high proportion of shale $p > 0.6$ show extreme fluctuations in the permeability field from one realization of the permeability field to another and cannot be considered significant.

Again, the average effective permeability K_e appears as significantly greater than the geometric average. The practical conclusions of figures 2.5 and 2.6 are:

- For practical values of shale proportion $p < 0.5$, a power average provides a good fit to the curve K_e vs. p .

- The averaging power increases with the correlation range in the direction of flow. The upper bound $\omega = 1$ corresponds to arithmetic averaging for perfect correlation and laminar flow.

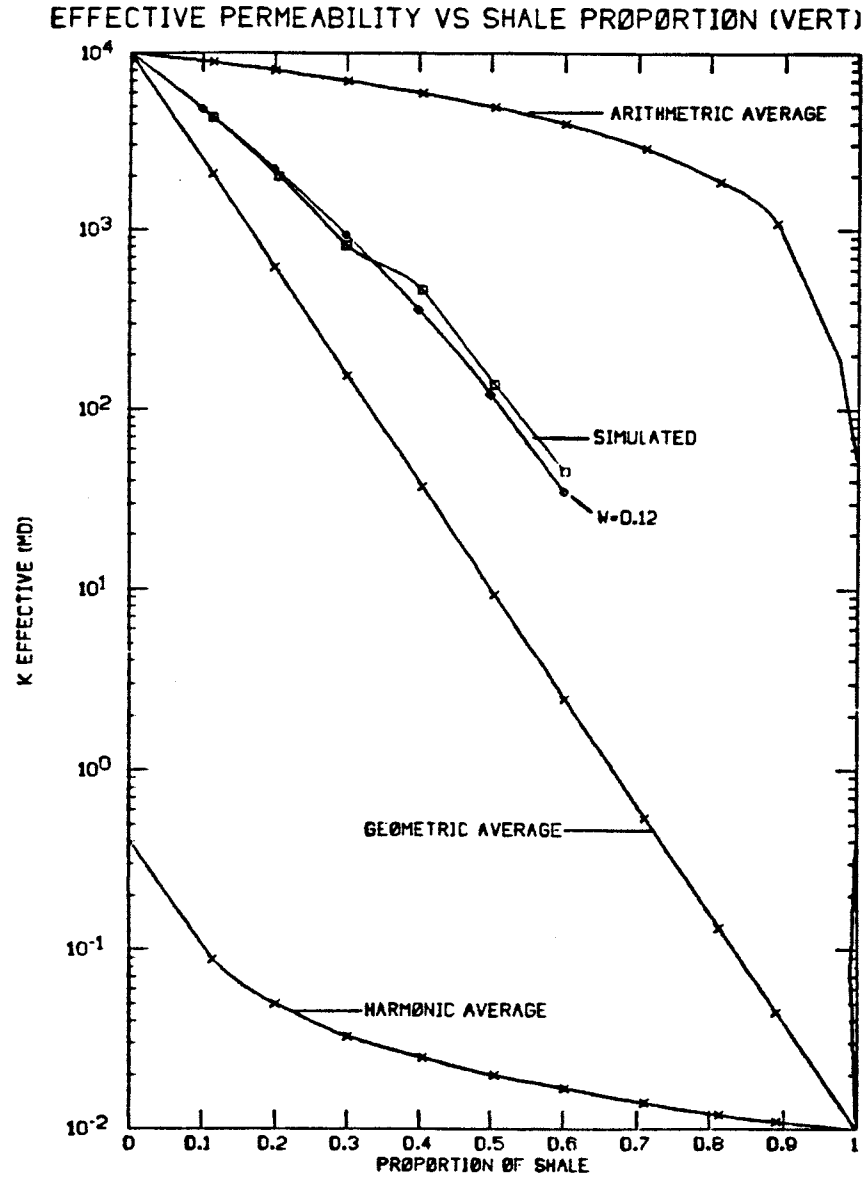

Figure 2.6: The effective permeability versus shale proportion for vertical flow. Note that for shale fractions less than 0.6 the power average ($\omega = 0.12$) fits the simulated data very well. The traditional arithmetic, geometric, and harmonic averages are shown for reference.

- The practice of using the arithmetic average for horizontal flow and the geometric average for vertical flow is sound but could be considerably improved with appropriate power ω - averaging.

The averaging power is shown to be independent of the proportion of shale and dependent on the spatial arrangement of the sandstone/shale network. The spatial arrangement can be summarized by some statistics which can then be used to estimate an appropriate averaging power. The proportion of shale is known through well logs and cores thus, the effective permeability may be calculated. In chapter 5 the problem of estimating the appropriate averaging power is addressed.

Geostatistical Tools

This section contains a general discussion of geostatistics and how some of its tools may be applied to petroleum engineering and to reservoir characterization. Specific statistical measures that have been found appropriate for flow systems are developed in chapter 4. The conventional and commonly applied aspects of geostatistics are emphasized here.

Geostatistics is a branch of applied statistics that studies phenomena spread in space and/or time with some degree of continuity. In petroleum applications the spatial distribution of rock properties such as porosity, permeability, and saturations is of interest. The procedures and techniques of geostatistics call for a model of the spatial continuity of the rock property being considered. A large part of geostatistics is devoted to estimation and, more specifically, interpolation.

The process of estimation must account for all the data available whether it is in the form of hard data (actual observations or measurements) or soft data (ex. in the form of a geologist's interpretation or expert judgement). If a geologist's interpretation of a phenomena is to be used it must be quantified in some manner. Expert knowledge is rarely passed downstream to engineers and process design people if not in the form of numbers. It is unfortunate, but a fact, that most small scale qualitative geologic descriptions of an oil reservoir are often of little use for engineering studies and flow simulations. Using (i.e., coding adequately) expert knowledge in the interpretation and processing of a spatially distributed variable may result in a more accurate reservoir model.

Some of the problems in the petroleum industry where geostatistical tools may be applied are:

1. Interpolating variables (ϕ,K ,S_w ,S_o ,ρ) distributed through space. This may involve gridding a variable towards further reservoir forecasting chores.
2. Defining the spatial continuity of a variable. A quantitative description of the physical size and spatial structure of a phenomena can be obtained

through geostatistical tools such as variograms. For example, the spatial continuity of a shale indicator field may be calculated to assist in predicting the averaging process for absolute permeability (ref. chapter 4).

3. Combining information from different sources to provide a single estimate of a variable. For example, one may wish to combine data from well logs, cores, and seismic to estimate porosity throughout the reservoir. A combined estimate may be generated that accounts for the different precision and resolution of each data source. A M.Sc thesis by F. Alabert (Stanford, 1987) contains a description of a method to do this.

4. Provide means whereby various maps can be generated depending on the objective (ex. the objective may be to generate a smooth, locally accurate map or it may be to produce a map that will reproduce the large scale spatial variability of a variable).

Some basic geostatistical concepts will now be introduced. The intuition and practical meaning of the various concepts will be stressed rather than the mathematical rigor. Refer to Journel and Huijbregts (1978) for a more complete presentation.

To perform any statistical inference it is necessary to assume that the observations belong to the same statistical population. To average a variable or to interpolate its value from different locations it is necessary that these locations are in a statistically "stationary" field. For example, if we were going to interpolate oil saturation it would be necessary to define the area within which interpolation is reasonable. The oil saturations in a particular sandstone lithology could be assumed statistically stationary. Measurements from nearby or imbedded shale/siltstone sequences could not be assumed to come from the same statistical population. The concept of stationarity allows statistical inference (averaging) over a predefined population or scale of variability.

Within a stationary field the expected value of the squared variation between two values of the attribute separated by a distance h does not depend on the location of the two values but only on their relative interdistance. The expected value of the squared deviation is represented by the semi-variogram $\gamma(h)$:

$$\gamma(h) = \frac{1}{2}E\Big([Z(x) - Z(x+h)]^2 \Big) \tag{2.12}$$

where $Z(x)$ is the value of a random variable (ex. porosity) at location x.

Figure 2.7 shows a typical variogram model. The variogram increases with increasing h and often after a certain distance exhibits a plateau, i.e. two values are no longer correlated. If the variogram function is independent of direction the random variable is said to be isotropic. In practice there is no reason for the variable to be as continuous in one direction as another. The range of correlation or the distance where the variogram becomes constant is likely much less in the vertical direction than in the horizontal direction for a horizontally layered structure. If the variogram depends on direction the variable is said to be anisotropic.

In practice the actual variogram must be inferred from the available data. This can be difficult because of lack of information or if the observations are at a scale too large to see any correlation. If there is no correlation structure, no spatial resolution can be obtained from estimates and it is difficult to perform any geostatistical analysis. However, the apparent lack of spatial dependence is most likely due to the too large spacing and/or imprecision of the data observations.

A large part of geostatistical theory is devoted to the problem of estimation. Spatial estimation involves assigning a value of a rock property to a location where there is no data. Where there is no data the true value is never known and may only be estimated, hopefully, in a way that the error in estimation is

A Typical Variogram Model

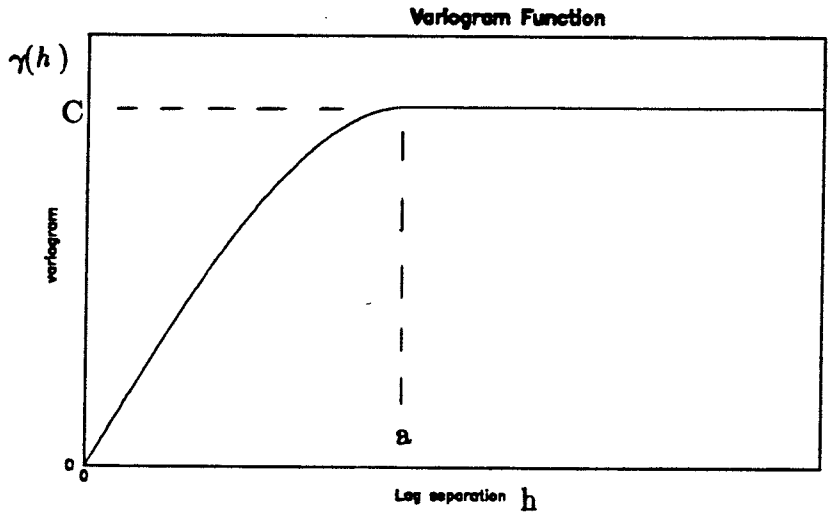

$\gamma(h)$ = Variogram function = $\frac{1}{2}E\{[Z(x) - Z(x+h)]^2\}$

h = lag separation distance.

a = range beyond which measurements are no longer correlated.

C = Sill = variogram value beyond range.

Figure 2.7: Typical Variogram Function.

minimized. Kriging is an estimation technique which minimizes the mean squared error of estimation.

Kriging provides the linear minimum error variance unbiased estimate of an unknown value. The estimate is linear in the sense that it is a weighted linear average of the surrounding data values. Kriging is able to handle information of different volumes of measurement and uncertainty. For example, if one knew the porosity of a large block through well testing and the porosity of a small core plug, both of these observations could be used in the Kriging system. For Kriging to be used a variogram model must be available.

Assigning the weight to be placed on each of the data values is what is formalized in Kriging. Intuition would tell us that data values which are close to the unknown value location should be given more weight. In geostatistics, closeness is expressed in terms of a "structural distance", i.e. a variogram distance specific to the variable and stationary population being considered. Our intuition would also tell us that if there is a cluster of data, these data are to a certain degree redundant. Therefore, a datum that is not in the cluster, but at the same structural distance away from the point to be estimated, should be given proportionally more weight than any of the cluster data.

Kriging is unbiased in the sense that it honors the "mean" of all the data available within the stationary zone. It is also best in the sense that no other linear combination of the surrounding data values will provide an estimate with a smaller average squared error. The Kriging system for determining the weights will not be given here. Refer to Journel and Huijbregts (1978) page 304. An example of Kriging is shown on figure 2.8. The kriging weight given to each datum satisfies our intuition about distance and redundancy.

One important characteristic of Kriging is that the estimated surface is very smooth except at locations very close to the data locations. This is a result of the least squares criteria built into the Kriging system. If the objective of the study is

An Example of Kriging

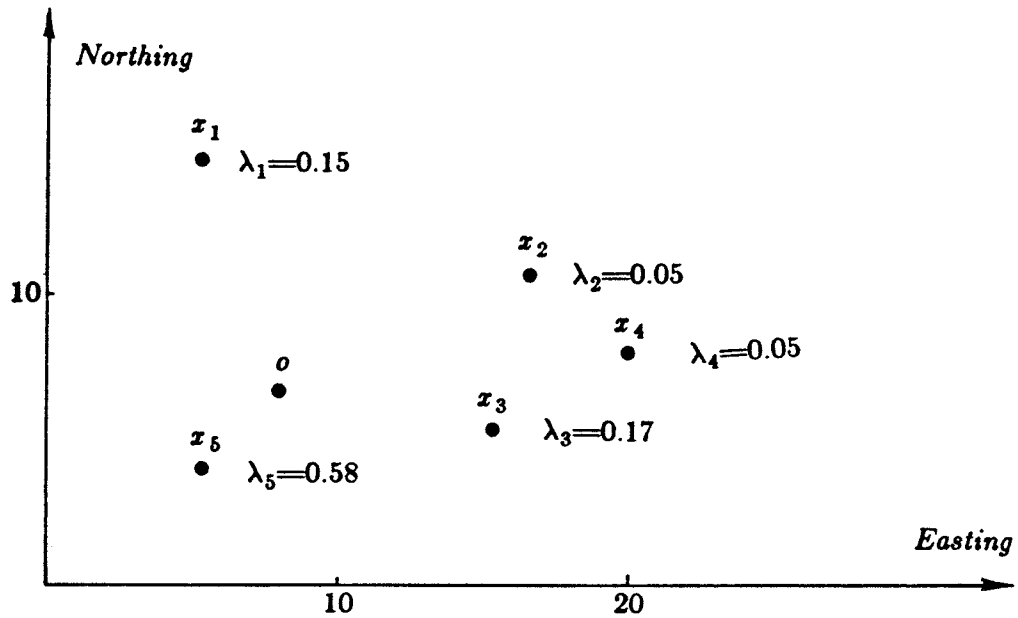

x = data (porosity) location.

o = point where porosity is to be estimated.

i = 1,2,3,4,5 = data points.

ϕ_i = porosity at point i.

ϕ_o^* = estimate of the unknown porosity = $\sum_{i=1}^{5} \lambda_i \phi_i$

λ_i = weight assigned to point i.

NOTE:

1. The variogram model used is the same as in figure 2.5 with a=10. The value of the sill C does not affect the calculation of the weights.
2. The clustered data (2,3,4) receive less weight than data which are not clustered.
3. The data which are close to the point to be estimated (5) receive more weight than data which are further away (1).

Figure 2.8: An Example of Kriging.

to produce an unsmoothed surface the kriged estimate would not be adequate. Another technique such as conditional simulation should be used (see hereafter). A second important characteristic of kriging is that the estimated value at the data points is always equal to the data value. It is said that kriging is an exact interpolator.

Conditional simulation is so called because the simulated profile at the data locations honors the data values. However, the simulation differs from kriging in the sense that the spatial variability of the data is reproduced. When considering flow properties it is important to reproduce the "roughness" of the resulting surface. Conditional simulation provides a mechanism to do this while honoring the data where the data are available. The idea is to add a spatially correlated random noise to the kriged surface.

There are many other aspects to the field of geostatistics and reference books are available. This brief introduction was intended for those people who have not been formally introduced to geostatistics.

Chapter 3

Sensitivity of Reservoir Performance Forecasting to Flow Properties

Introduction to Sensitivity Study

A data base from an actual reservoir was used to perform this sensitivity study. The 200 ft thick reservoir unit considered is within a geologically homogenous reservoir. This sandstone formation contains considerable amounts of drape/eddy/slough and abandoned channel shale deposits.

The sensitivity of the results (production rate, cumulative production, and in some cases gas-oil ratio and reservoir pressure) to the input permeability field was investigated. The results were not found to be sensitive to the averaging procedure used for absolute permeability. This is due to two facts. The permeability distribution averaged from the initial detailed information (well logs and core data) is unimodal. An average of data drawn from a unimodal frequency distribution is not sensitive to the averaging scheme used as will be shown in chapter 4. Secondly, the waterflooding production pattern caused the results to be less sensitive to permeability. The practice of fixed rate injection and fixed rate production does not show sensitivity of the oil production rate to changes in absolute permeability. The well pressures are sensitive to the absolute permeability but, for a fixed total flow rate, the relative rate of oil and water flow will be essentially the same for a uniform increase in absolute permeability. These reasons were not realized by the author prior to the sensitivity study.

Reservoir Description

Data from 22 wells (five of which were cored) were used to create the detailed reservoir model. Figure 3.1 shows a map of the study area with the well locations shown. The field considered is of size 8100ft by 8100ft by 200ft.

A conditional simulation of porosity yielded values for 131220 grid blocks 100ft by 100ft by 10ft. The simulation was conditioned to porosity data derived from well log analysis. The spatial variance structure of the porosity has been modeled with a variogram. The 3-d variogram model used for porosity is made up of the following three components:

1. An isotropic nugget effect (white noise) to account for errors of measurement and other small scale effects.
2. A geometric anisotropy of 25:1 (i.e., the horizontal continuity is 25 times greater than the vertical continuity) has been considered.
3. An additional component of range 100 ft present only in the vertical direction to account for the variability induced by changing beds has also been considered.

The resulting three dimensional variogram model is written:

$$\gamma(h) = 0.03 + 0.37 \cdot Sph_{500}(h') + 0.60 \cdot Sph_{100}(h_z)$$

where:

$h' = \sqrt{h_x^2 + h_y^2 + (25 \cdot h_z)^2}$ = the anisotropic distance (25:1) accounting for the greater horizontal continuity.

The simulation has been conditioned by the well data within and near the study area (ref. figure 3.2). The absolute permeability (horizontal and vertical) was obtained by selecting block permeability on the basis of the block estimated porosity.

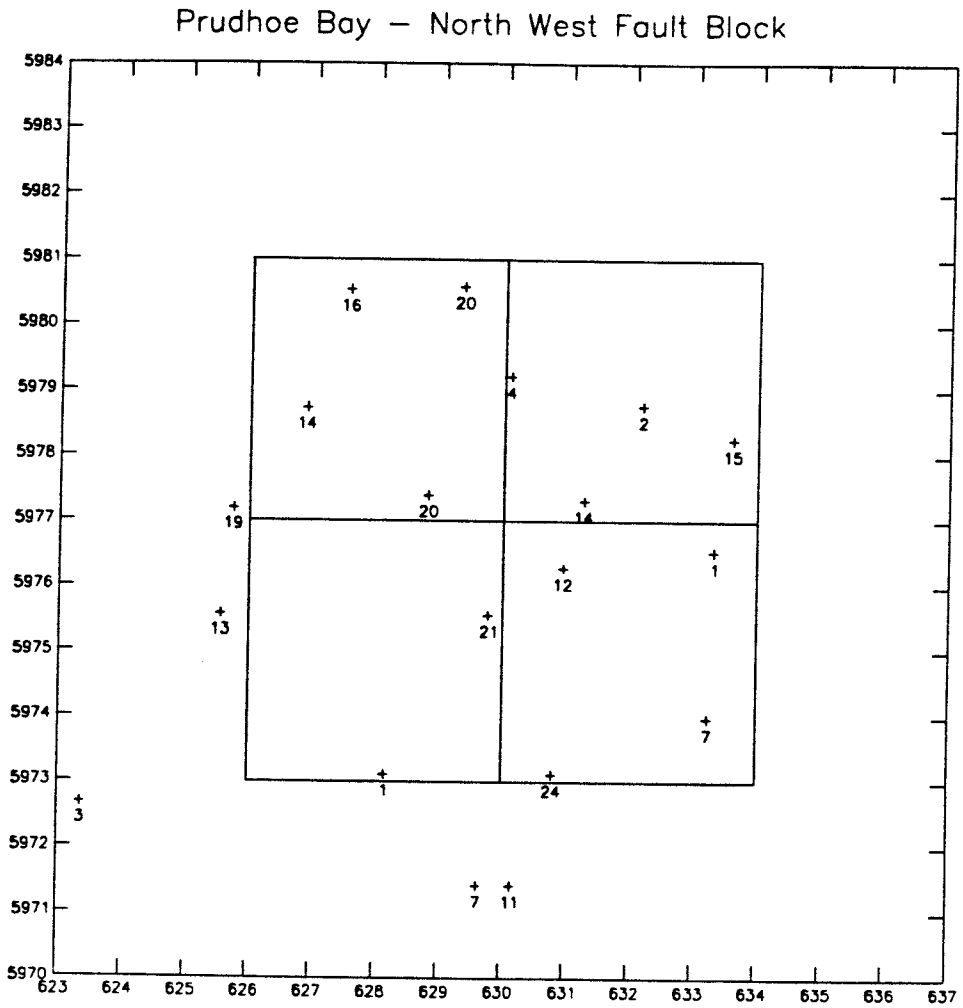

Figure 3.1: The study area is shown with the well locations. The study area has been divided into quarters on the map.

The data base is comprised of porosity, horizontal absolute permeability, and vertical absolute permeability information for 131,220 blocks 100ft by 100ft by 10ft. For all practical purposes, this dense information represents an exhaustive knowledge of the study area.

Summary statistics for the porosity, horizontal permeability (Hperm), and vertical permeability (Vperm) are presented on table 3.1.

Summary Statistics

Description	Porosity(%)	Hperm (md)	Vperm (md)
Arithmetic mean	14.58	295.1	58.7
Minimum	0.00	6.9	3.2
Maximum	40.67	2,598.6	290.0
Geometric mean	-	194.2	45.8
Variance	44.7	111,540.	1,860.
Standard deviation	6.68	334.	43.1
Coefficient of variation	0.459	1.13	0.735

Table 3.1: Summary statistics

Block diagrams of block averaged porosity, horizontal permeability, and vertical permeability are shown on figures 3.2,3.3, and 3.4. The block diagrams are for the rock properties averaged over the vertical extent of the reservoir unit. An arithmetic average was used because representative properties are desired rather than effective properties. From these figures the spatial variability is clearly apparent.

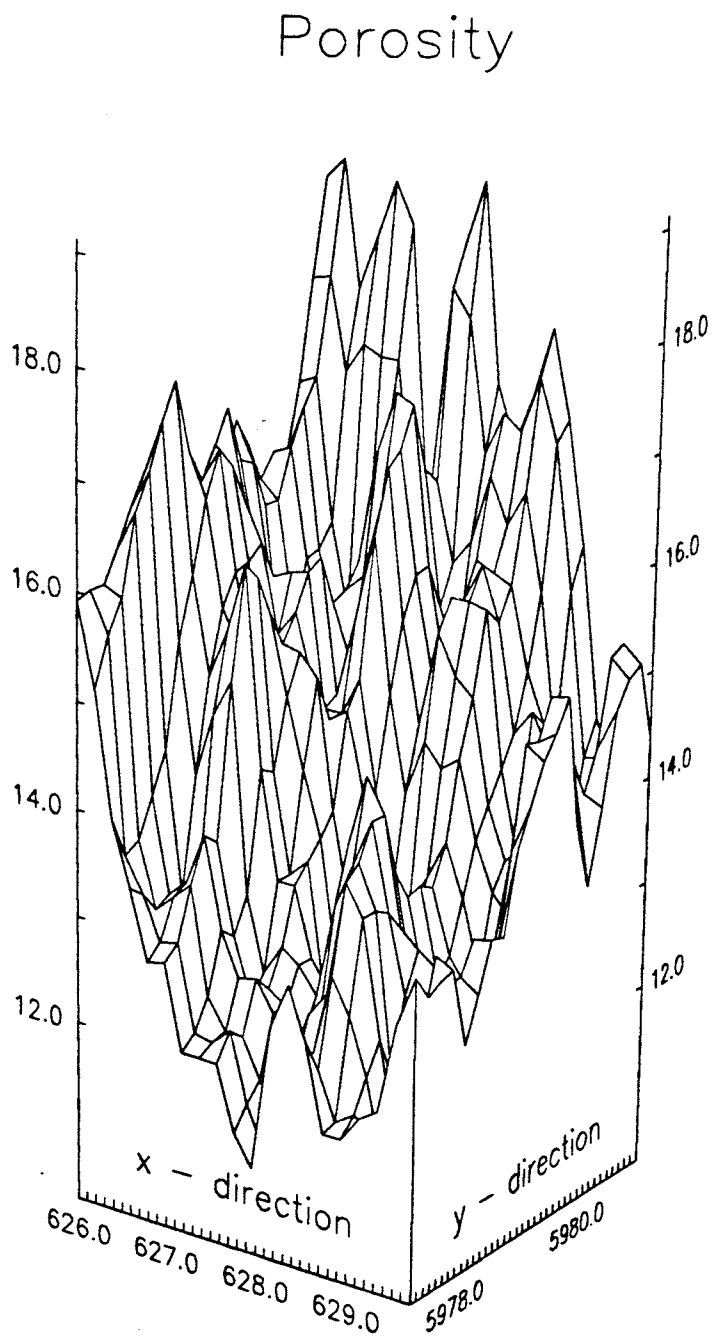

Figure 3.2: Block diagram of porosity over the horizontal extent of the study area.

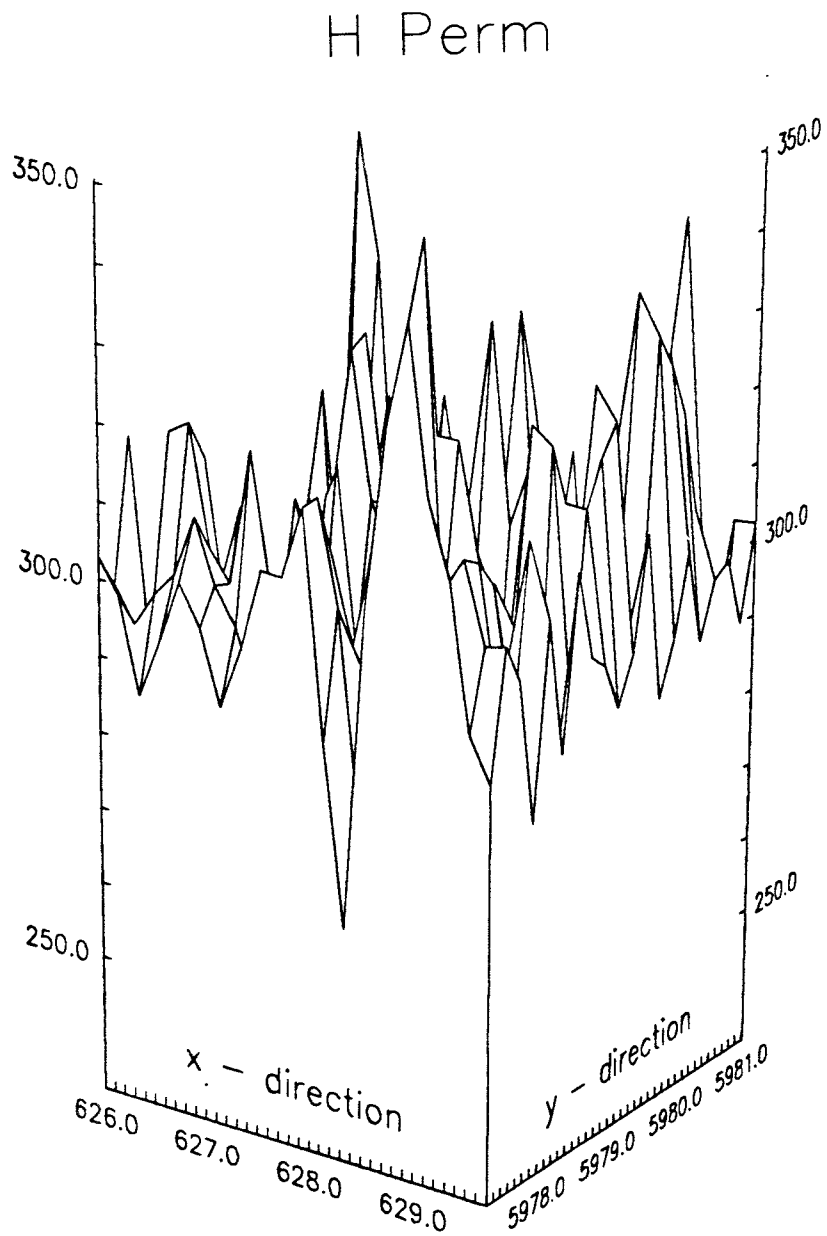

Figure 3.3: Block diagram of horizontal permeability over the horizontal extent of the study area.

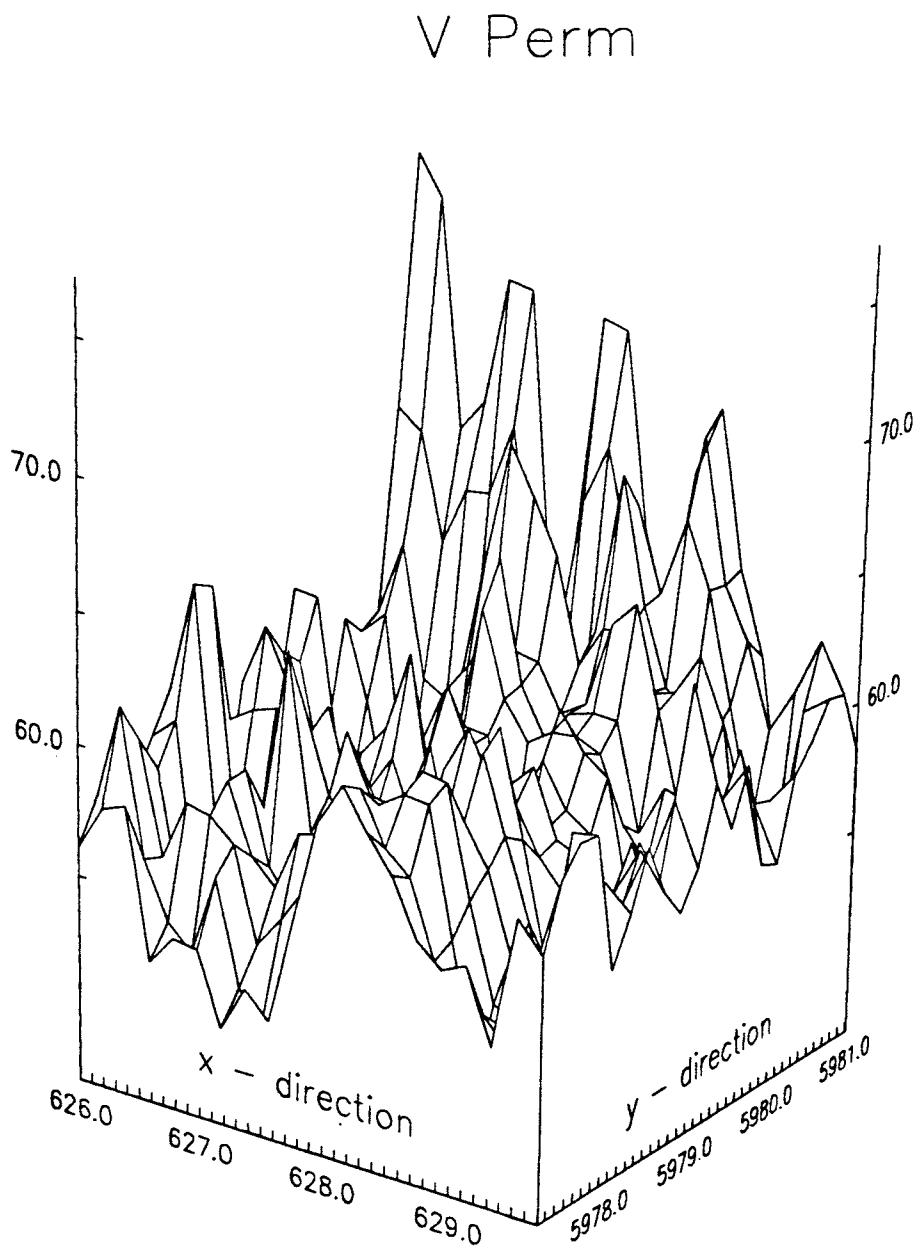

Figure 3.4: Block diagram of vertical permeability over the horizontal extent of the study area.

Reservoir Production

Basic Reservoir Properties and Characteristics:

Most reservoir properties and characteristics were kept unchanged between the sensitivity simulation runs. Among these are the fluid properties and other reservoir characteristics shown on table 3.2. It might be noted that two sets of two phase relative permeabilities were assumed. The simulator uses these data to compute the three phase relative permeability by Stone's method.

Reservoir Characteristics	
Per Well Spacing, acres	78.6
Nine-spot Pattern Spacing, acres	314.3
Production Interval, ft	200
Liquid Production Rate, STB/D	4,800
Voidage Replacement with Water,%	100 and 90
Initial Pressure, psia	5481
Bubble Point Pressure, psia	5015
Surface Oil Density, lb/cubic ft	55.9
Surface Water Density, lb/cubic ft	62.43
Water Formation Volume Factor, RB/STB	1.003
Water Viscosity, cp	0.31
Water Compressibility, 1/psia	3.0E-6
Surface Gas Density, lb/cubic ft	0.0646
Rock Compressibility, 1/psia	3.5E-6
Well Diameter, ft	0.458

Table 3.2: Reservoir characteristics.

Two water injection schemes were considered for a liquid production rate set at 4,800 STB/D. One scheme results in 100% voidage replacement, the other injection scheme results in 90% voidage replacement. Since reservoir pressure is initially above the bubble point, the 100% voidage replacement scheme maintains pressure above the bubble point throughout the simulation run, while, the 90% voidage replacement scheme does not.

A diagram of the inverted nine-spot pattern is shown in Figure 3.5. It consists of a single injection well in the center of the pattern and a total of eight production wells on the periphery of the pattern.

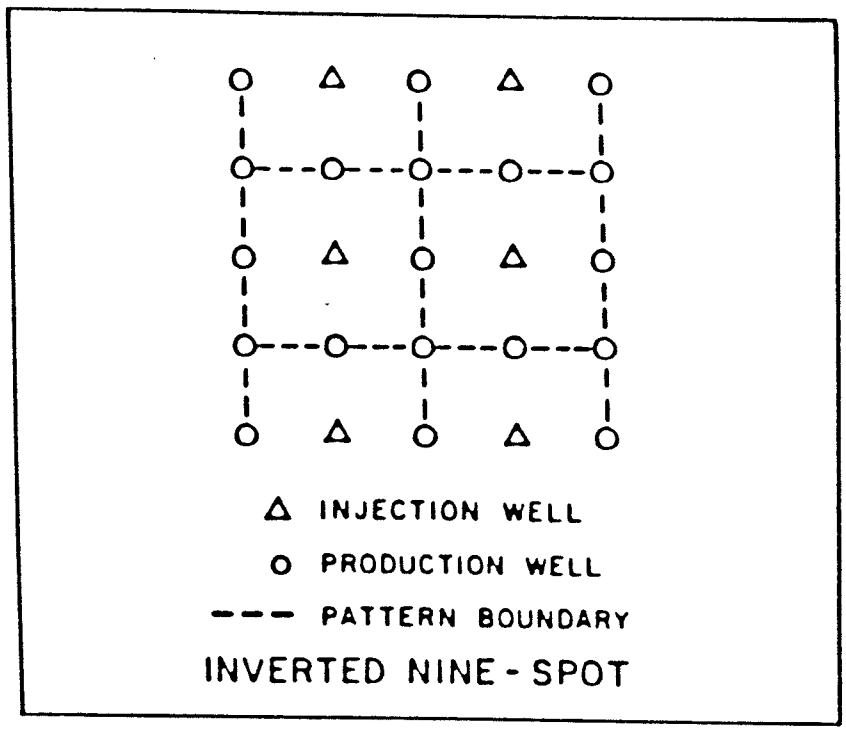

Figure 3.5: Inverted nine spot pattern.

Discretization Error:

This study requires comparisons of production forecasts made from reservoir simulations with different block sizes. It is thus necessary to quantify the error imparted by different block sizes.

The Eclipse reservoir simulator, version 84/9, developed by Exploration Consultants Limited has been used in this study. The reservoir behavior under a production scheme is described by a set of partial differential equations. The finite difference approximation to the partial differential equations sets an upper limit on how large the finite difference grid blocks can be. If the grid blocks are larger substantial numerical dispersion will occur.

To study the question of numerical dispersion the basic reservoir has been considered for different levels of discretization. Uniform rock properties were assigned over the entire reservoir ($\phi = 14.58\%$, $K_h = 295.1\ md$, $K_v = 58.7\ md$). The reservoir was produced for a set period of time using a large block size, the production history was recorded, and progressively smaller blocks were used for the same time period and production scheme. The resulting production histories for the various cases can be compared to judge the impact of numerical dispersion and at what level the numerical dispersion is significant.

For the 100% voidage replacement case the total field oil production rate and the cumulative field oil production can be compared. Figure 3.6 shows the field oil production rate versus time for the five block sizes considered. The five block sizes considered: 5x5x5, 7x7x5, 13x13x5, 17x17x5, and 37x37x5. The results clearly show the problem of numerical dispersion. There are notable decreases in the oil production rate corresponding to breakthrough at the side and then the corner wells respectively. As the block size increases the resolution decreases and the breakthrough times are not as distinct. The first breakthrough appears earlier for cases with coarser discretization. The second breakthrough occurs later as the discretization level gets coarser. All the simulations are ordered as they

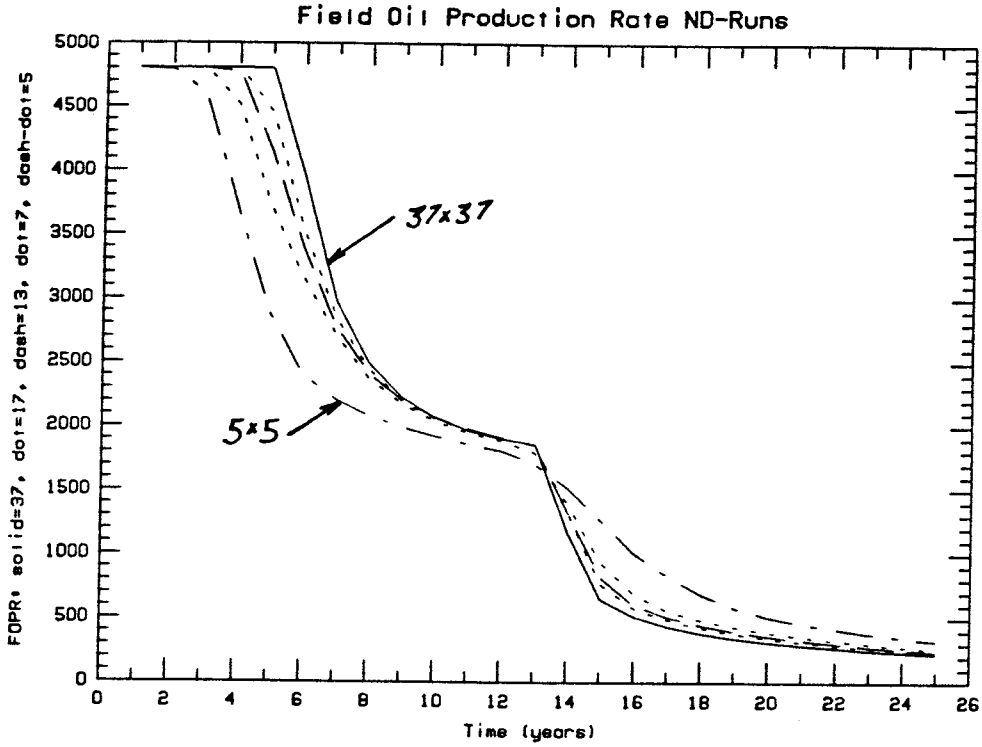

Figure 3.6: Field Oil Production rate versus time for the 100% voidage replacement runs.

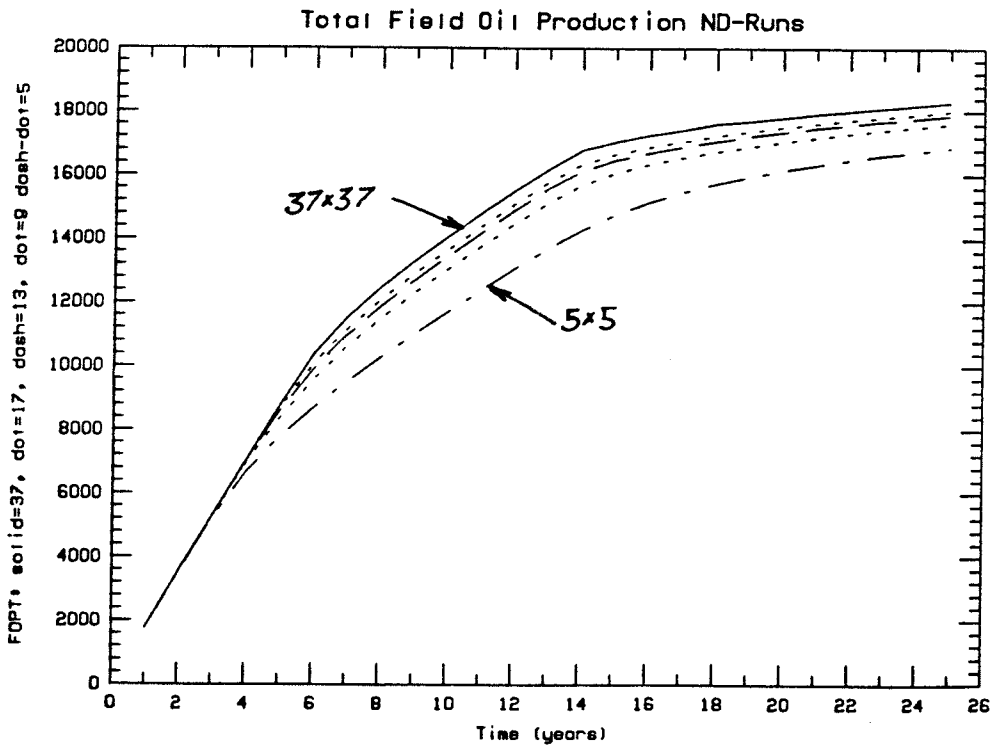

Figure 3.7: Cumulative Field Oil Production versus time for the 100% voidage replacement runs.

should be and as the discretization becomes finer the production history appears to be approaching a unique history. It should be noted that with porosity and permeability heterogeneities present one would expect the results to appear similar to the cases with coarse discretization. In this example the dispersion is caused solely by the size of the grid blocks. In the presence of heterogeneity the cause of dispersion would be the heterogeneity itself and the block size.

Figure 3.7 shows the cumulative field oil production versus time. The curves seem to approach the same result as the discretization becomes finer. The cumulative production at the end of 25 years is greater for the simulation runs made at a finer discretization. The production rate, however, converges at the end of 25 years. If the production history would have been simulated for a longer period of time one would expect the cumulative production for all cases to approach the same value.

Figure 3.8 shows the field oil production rate versus time for the 90% voidage replacement runs. The behavior is very similar to that shown for 100% voidage replacement. Figure 3.9 shows the cumulative field oil production versus time. Again, the results seem close to the results for the 100% replacement case. The average field pressure and field gas oil ratio can be compared in this set of runs. Figures 3.10 and 3.11 show how these two parameters change with time for the different levels of discretization. The average field pressure does not seem to be affected by the level of discretization. The gas oil ratio is more sensitive to the discretization. Table 3.3 summarizes the findings for step 1 of the discretization study. The MOC or Measure Of Closeness is defined as the area between the history being considered and the base case curve divided by the area under the base case curve. This allows a quantitative comparison of the various runs.

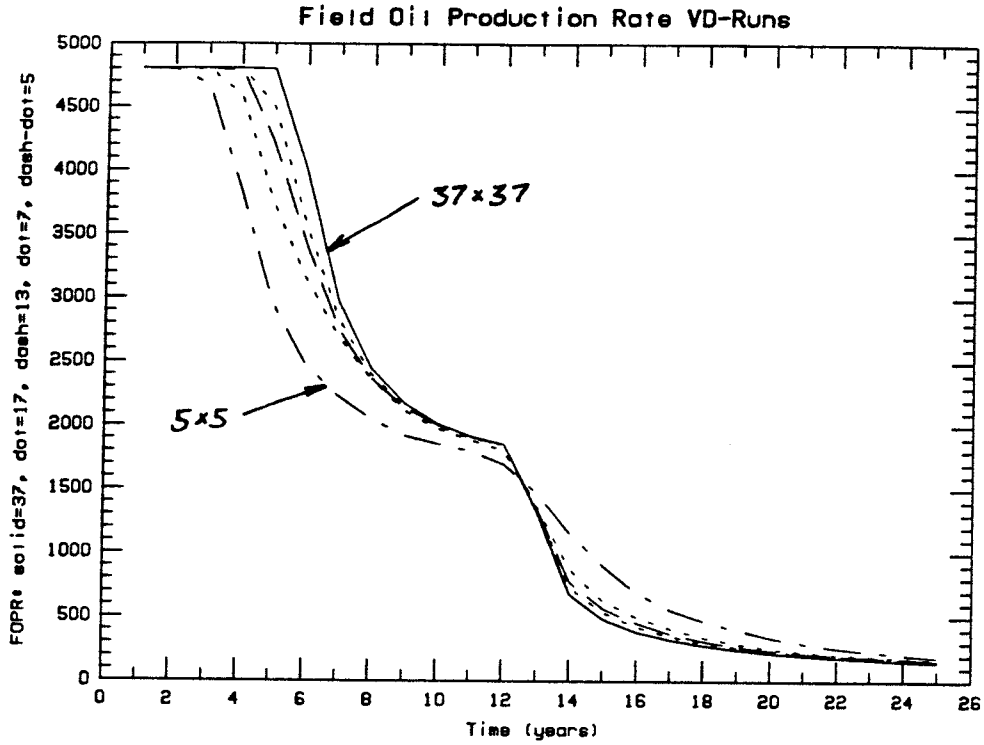

Figure 3.8: Field Oil Production rate versus time for the 90% voidage replacement runs.

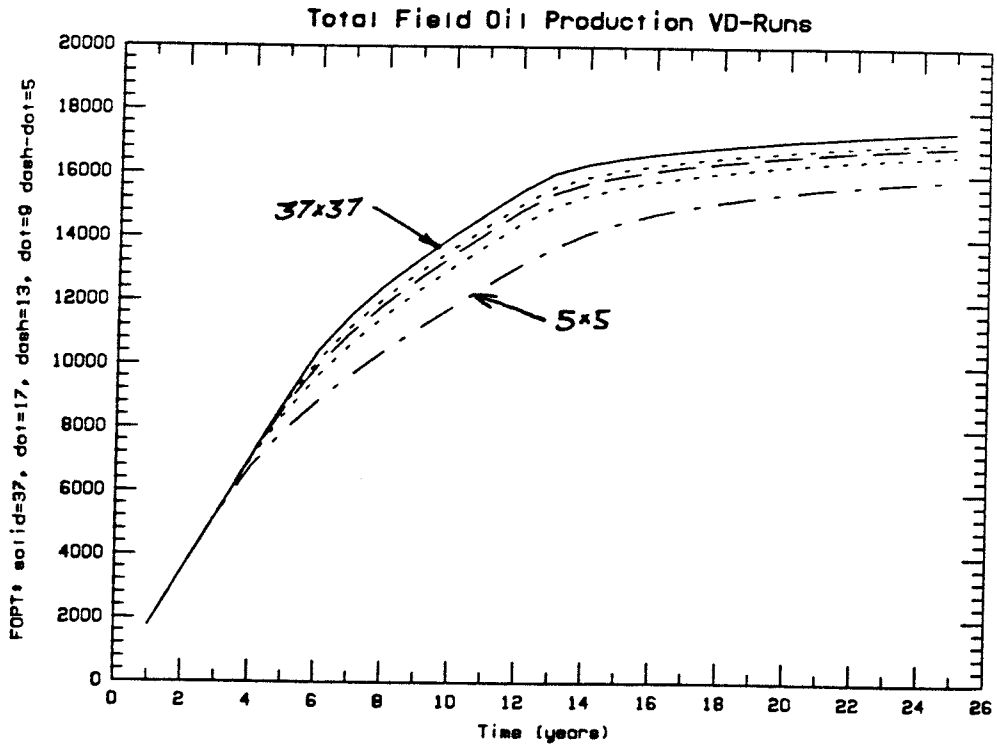

Figure 3.9: Cumulative Field Oil Production versus time for the 90% voidage replacement runs.

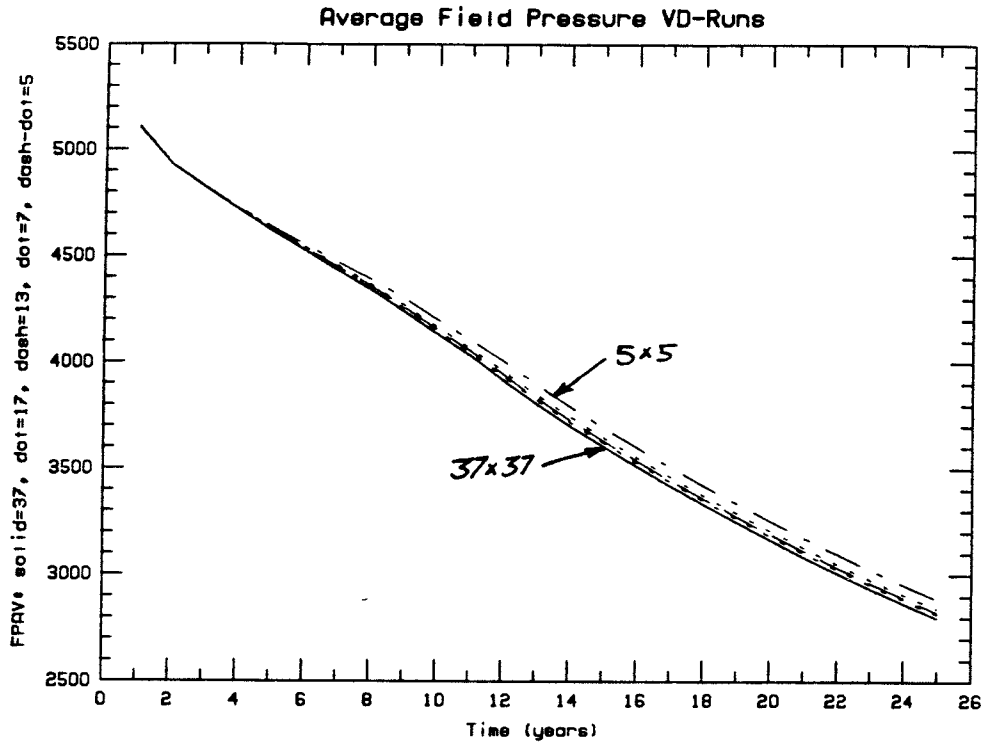

Figure 3.10: Average Field Pressure versus time for the 90% voidage replacement runs.

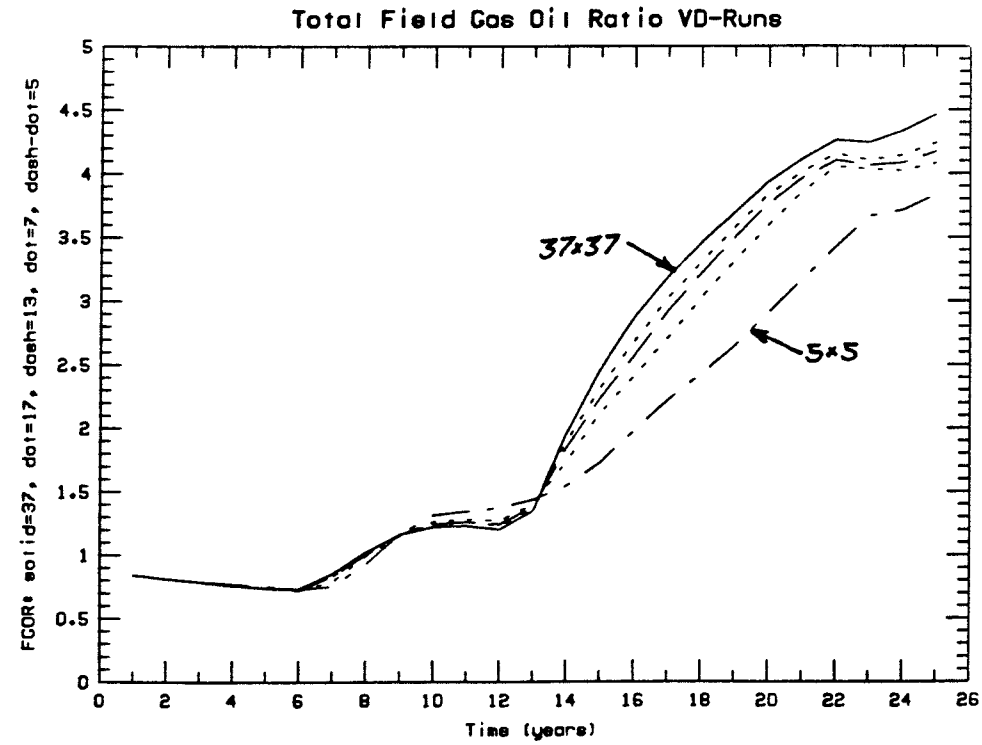

Figure 3.11: Total Field Gas Oil Ratio versus time for the 90% voidage replacement runs.

Summary For Step 1 - Discretization Error					
Description	base case				
# of blocks	37x37x10	17x17x4	13x13x4	9x9x4	5x5x4
MOC (FOPR) (100%)	0	0.034	0.051	0.087	0.215
MOC (FOPT) (100%)	0	0.021	0.031	0.052	0.119
Production (100%)-Mstb	18270.7	18003.1	17869.0	17608.3	16860.2
MOC (FOPR) (90%)	0	0.029	0.045	0.078	0.195
MOC (FOPT) (90%)	0	0.021	0.032	0.053	0.115
MOC (FPAV) (90%)	0	0.0036	0.0051	0.0081	0.017
MOC (FGOR) (90%)	0	0.032	0.048	0.078	0.190
Production (90%)-Mstb	17356.9	17055.8	16907.3	16626.8	15863.3

Table 3.3: Summary for Step 1 - Discretization Error.

FOPR = Field Oil Production Rate.

FOPT = Cumulative Oil Production.

FPAV = Average Field Pressure.

FGOR = Field Gas Oil Ratio.

Remarks:

1. The measure of closeness (MOC) reflects what is seen visually on the plots.
2. The cumulative production at the end of the 25 year period is higher for the cases with finer discretization.
3. The cumulative production for the case of 100% voidage replacement is greater than for the case of 90% voidage replacement.
4. The measure of error in both cases (100% and 90% voidage) is comparable for the different levels of discretization. This implies that a suitable level of discretization for one case would be appropriate for the other case.

5. Using 13 by 13 blocks in the horizontal plane would give adequate resolution for simulation runs to be performed on the Apollo computer.

The second step in the study of discretization looked at vertical discretization. The areal discretization was held constant at 13 by 13 blocks and the vertical discretization was changed to 3 blocks for the 200 foot interval to 4,5,6, and 7. There is no need to present the results in graphical form. The production history was virtually identical regardless of the vertical discretization. The MOC defined above would be on the order of 10^{-6}.

Remarks:

1. The vertical discretization is not an important factor for the case considered here. The flow system that has been considered approximates two dimensional flow and the vertical discretization has very little impact. Two dimensional flow is approximated due to the uniform properties and the production practice of injection and production throughout the entire vertical extent of the reservoir.
2. The reservoir unit considered is thin compared to the horizontal extent. This also decreases the impact of the vertical discretization.
3. Heterogeneous rock properties may enhance the impact of vertical discretization. Flow may bypass low permeability boundaries if the vertical resolution is "good". In future work with heterogeneous properties this aspect should be kept in mind.
4. It is now possible to judge the difference between runs of unequal discretization and see if the numerical dispersion is due to discretization or some other feature of the input data.

Alternate Averaging Processes for Absolute Permeability

Given a particular heterogeneous reservoir model with detailed ϕ , K_h , and K_v information available - how should this small scale information be averaged to obtain simulation block data? Ideally, the small scale information should be used directly in the simulator. However, this is not feasible due to storage and processing limitations and may not be necessary in any case.

The conventional averaging processes for permeability (arithmetic average for horizontal permeability and geometric average for vertical permeability) is compared to more sophisticated averages. The first part of the study is carried out by averaging over small volumes (i.e., block volumes less than the level at which numerical dispersion occurs 13x13x5). A second study is then performed with the permeability being averaged over larger volumes while maintaining the same size of blocks in the simulator.

Averaging Process - Impact on Simulation Results:

In the case being considered, detailed information is in the form of ϕ , K_h , and K_v values for grid blocks 100ft by 100ft by 20ft (200,000 ft^3). Note that a great deal of resolution is already lost when averaging core data (fraction of a ft^3) to these smallest grid block data.

A bench mark run has been made on a Cray with 13690 blocks (100ft by 100ft by 20ft). The subsequent runs will be made at a constant block size of 284ft by 284ft by 67ft (5,400,394 ft^3) or 27 times the volume of the small scale information. The production history obtained with the averaged data will be compared to the results from the bench mark run. The averaging process that provides the most closely matched production history will be taken as the "correct" averaging process for the scale of information considered. After the appropriate averaging process is determined, the scale of averaging is studied.

The different power - ωaveraging schemes that will be considered are: (Note: The porosity is always averaged with an arithmetic average.)

Total Field Oil Production - Selected Runs		
Run ID.	100% replacement	50% replacement
1. Heterogeneous Data(base case)	20896.0	-
2. K_h ω=1.0,K_v ω=0.0 (traditional)	20373.9	7944.4
3. Block Dependent (see chapter 5)	20358.8	9004.0
4. K_h ω=0.6,K_v ω=0.1	20386.0	8242.5
5. K_h ω=0.8,K_v ω=0.1	20380.0	8069.8
6. K_h ω=0.6,K_v ω=0.2	20386.2	8243.0
7. K_h ω=0.8,K_v ω=0.2	20380.9	7620.7

Table 3.4: Total Field Oil Production obtained for alternate averaging of absolute permeability.

Remarks:

- For 100% voidage replacement the impact of averaging absolute permeability is nil.
- The averaging powers for runs 4 through 7 were selected on the basis of numerous network simulations documented in chapter 5. It was observed that the averaging power for horizontal permeability was usually in the range 0.6 to 0.8 and the averaging power for vertical permeability was normally within 0.1 to 0.2. These estimates correspond to the range of shale proportion and shale geometry of the study area.

- The largest difference between final production for the 100% voidage replacement is 0.13% while the difference for 50% voidage replacement is 12%.

- Although the rock property data is identical for the 100% and 50% voidage replacement runs, the case that gives the highest production with the 100% case does not give the highest with the 50% case. There are interactions with phase behaviour characteristics and no conclusions can be drawn from this limited amount of data.

- Since absolute permeability is a constant that relates flow rate and pressure for a fixed geometry and fluid it is not surprising to see the more highly stressed situation (50% replacement) being more sensitive to permeability.

Volume of Averaging - Impact on Simulation Results:

The second stage of the study will attempt to determine over which volume the small scale information can be averaged without affecting the simulation results. It is already known that the simulation results are not sensitive to the averaging procedure used. It is not known yet over which volume the block data can be averaged before affecting the results.

To answer this question the permeability measurements have been averaged over the entire NW corner (corresponding to run ID#1 on table 3.4). The arithmetic average of the horizontal permeability and geometric average of the vertical permeability have been considered. The production history has been simulated with the same heterogeneous porosity data base.

The results were not found to be sensitive to the volume of averaging. The reasons for this are discussed in the next section.

Remarks on Sensitivity Study

The performance forecasting results were not found to be sensitive to the absolute permeability. The oil production rate remains unchanged for different levels of absolute permeability due to the simulated production practice.

The production practice involved injecting water at a fixed rate (within well bore pressure constraints) and producing the equivalent amount of fluid (oil and water). The relative flow of oil and water, the well bore pressure, and other field measurements were recorded. In hindsight it is not surprising that this production scheme shows little sensitivity to absolute permeability. As the absolute permeability is changed the pressure required to inject the target flow rate changes but the other measurements remain unchanged.

The well pressures are thus the sensitive measurements with this production practice. The mathematical model used to relate well bore size, rock properties, productivity and injectivity indices, and other information to compute well flow rates and pressures is beyond the scope of this study.

To illustrate that the relative flow rates of oil and water will remain unchanged consider a single grid block with a fixed total fluid flow rate. The relative flow of oil and water is computed as the ratio of the oil phase transmissibility and the water phase transmissibility. If the absolute permeability is changed this ratio remains unchanged. Thus, with the reservoir model considered the absolute permeability could be changed from 35md to 800md without altering the relative flow of oil and water.

Some interesting avenues for future research have been identified:

- The presence of porosity heterogeneity and its link to permeability heterogeneity and overall recovery has not been considered. This is an important area of sensitivity that should be explored.

- Multiphase flow properties might influence the development of preferential flow and the impact of heterogeneity on "effective" multiphase flow properties should also be investigated.

Chapter 4

Univariate Distribution of Permeability

General Remarks:

The univariate distribution of permeability depends on the scale at which the permeability measurements are observed. Due to the sedimentary nature of a sandstone/shale reservoir the permeability distribution at some scale will be bimodal. There will be a mode corresponding to mostly sandstone and a mode that corresponds to mostly shale. As the scale of observation becomes smaller more modes would become apparent and one will be able to identify different types of sandstone and shale. As the scale of observation increases each measurement will be due to a mixture of sandstone and shale causing the distribution to become unimodal.

The assumption made here is that at some particular scale the two component mixture of sandstone and shale can be approximated by a binary distribution, which only locates the central sandstone and central shale permeabilities. It is intuitively clear that the amount of shale and its spatial arrangement will be very important. Indeed, Pryor and Fulton, 1976; Fogg, 1985; Haldorsen and Chang, 1985; and Desbarats, 1986 have all shown that the dominant heterogeneity affecting flow is the dispersed low permeability shale. On the basis of this well documented practical experience the binary distribution approximation is deemed relevant, at least as a first approximation model.

In the first chapter methods for calculating effective permeability such as the perturbation approach were discounted because they did not consider the two

component aspect of the problem. If the goal were to infer the effective permeability of an essentially clean sandstone (e.g. corresponding to an aquifer), the assumptions required by the perturbation approach would be reasonable. However the problem addressed in this research is more complex: inferring the effective property of a two component spatially correlated, random field.

If the univariate distribution of measured permeability appears unimodal i.e., does not show distinct modes corresponding to shale and sandstone, one of the following explanations is likely:

- The shales are very small relative to the measurement volume, hence some implicit averaging has already been performed yielding the unimodal distribution.
- The shales have not been sampled as systematically as the sandstone, which is not an *un* common practice, however unfortunate.

An average from a unimodal distribution will be less sensitive to the averaging power than an average from a bimodal distribution. Two distributions are shown on figure 4.1, one of which is distinctly bimodal and another which is unimodal but skewed corresponding to what may be observed after a first implicit step of averaging. For each distribution the arithmetic and geometric averages may be compared to see the effect of using a power $\omega = 1$ (arithmetic average) and $\omega = 0$ (geometric average). The difference between the geometric and arithmetic mean in the bimodal case is 506md while in the unimodal case the difference is only 41md. This suggests that for a unimodal distribution the average is less dependent on the averaging power.

Bimodal Distribution

Shale Distribution: Lognormal (mean=5md, s.d.=10) - 20%

Sandstone Distribution: Truncated Normal (mean=1000md, s.d.=200) - 80%

Lower bound = 100.0 Upper bound = 1900.0

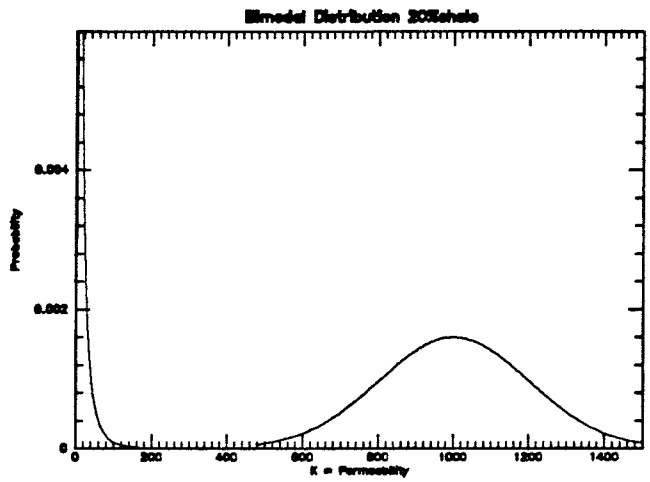

AM = Arithmetic Mean = 801md

GM = Geometric Mean = 295md

HM = Harmonic Mean = 5md

σ = 445md c.v. = 0.56

Unimodal Distribution

Matches Geometric Mean and C.V. of Bimodal Distribution

Distribution: Lognormal (geometric mean=295md, s.d.=188)

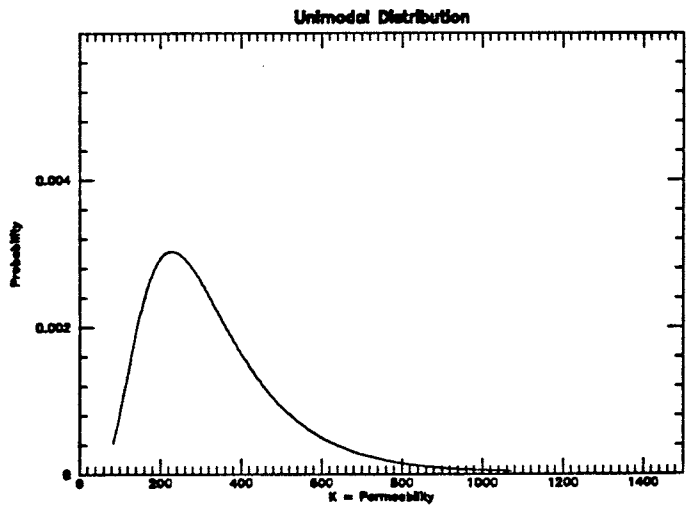

AM = Arithmetic Mean = 336md

GM = Geometric Mean = 295md

HM = Harmonic Mean = 259md

σ = 188md c.v. = 0.56

Figure 4.1: A comparison of a bimodal and unimodal distribution of permeabilities. The bimodal distribution represents a sandstone/shale mixture while the unimodal distribution represents a distribution after averaging. The ω = 1,0, and –1 power averages are shown for each distribution.

Figures 4.2 shows two distributions, one which is asymmetric another which is symmetric. The averaging power will have more impact on an asymmetric permeability distribution while having no effect on the symmetric truncated normal distribution shown. However, the greatest sensitivity is not introduced by the shape of the distribution but rather by the bimodal nature of the permeability distribution.

In other words, averaging absolute permeability is indeed a problem and a severe one provided that one works with the original (essentially) bimodal distribution. If prior averaging, either implicitly through data defined over too large a measurement volume or explicitly through some averaging technique, has been performed yielding a unimodal distribution, further averaging will have little impact. This small impact does not mean that the prior implicit or explicit averaging process was correct, and this process should be critically assessed because it does have an impact on the large scale predictions. In short, all the action resides at the first averaging step, usually performed at the data-taking step and/or well log analysis.

This point is crucial to the entire problem of scale averaging. For this reason some examples will be presented to show the impact of averaging on the distribution of permeability.

Scale Averaging of a Binary Random Variable:

Starting from a sandstone/shale composite media described by a binary permeability distribution it is interesting to see how the distribution of permeability will change as the volume of observation increases. At the limit when the volume of observation becomes the entire composite volume the initial binary distribution reduces to a single effective permeability value (or tensor).

With certain assumptions the distribution of block effective permeabilities, in a given direction, may be approximated by a binomial distribution. The assumptions required are:

Asymmetric Distribution

Distribution: Lognormal (geometric mean=295md, s.d.=188)

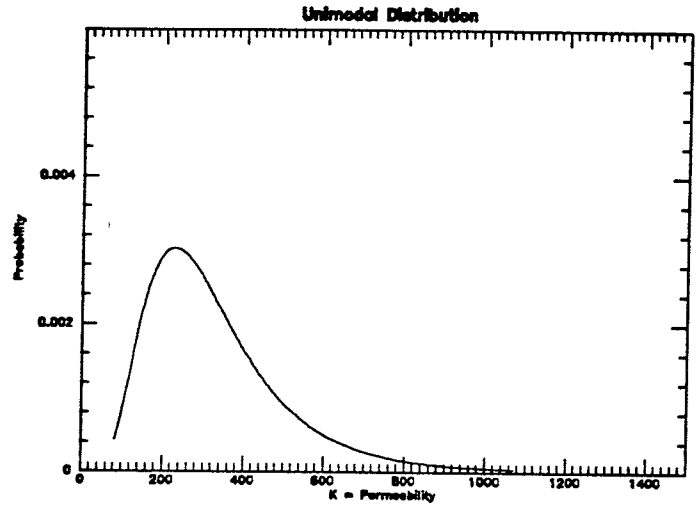

AM = Arithmetic Mean = 336md

GM = Geometric Mean = 295md

HM = Harmonic Mean = 259md

Symmetric Distribution

Matches Arithmetic Mean of Asymmetric Distribution

Distribution: Truncated Normal (mean=336md, s.d.=150)

Lower bound=10.0 Upper bound=666.0

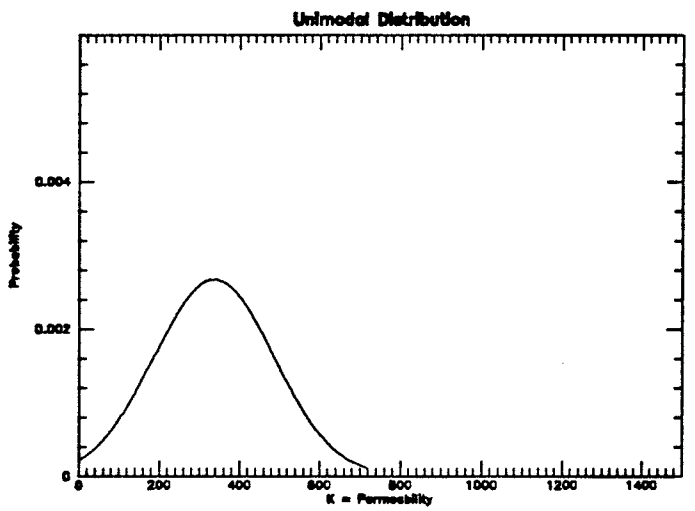

AM = Arithmetic Mean = 336.0md

GM = Geometric Mean = 335.8md

HM = Harmonic Mean = 335.5md

Figure 4.2: A comparison of an asymmetric and symmetric distribution of permeabilities. The $\omega = 1,0$, and -1 power averages are shown for each distribution. As the distribution becomes more symmetric the difference between the different averages becomes less.

1. The sandstone/shale mixture is composed of small equal units that are either 100% sandstone or 100% shale.
2. The sandstone and shale units are located independently one from each other.
3. The effective permeability of a block for a given proportion of shale in the block is determined by a power average with a constant averaging power independent of the shale proportion.
4. The proportion of shale in the sandstone/shale mixture is known or may be approximated.

It is certainly valid to consider the sandstone/shale mixture as composed of small equal volume units of sandstone and shale. However, the strongest assumption is that they are located independently of one another. This assumption is a first approximation and methods to relax this assumption are discussed later. Indeed, the interesting case is when a spatial correlation structure is present.

It has been shown in chapter 2 (p 23) that the averaging power is independent of the proportion of shale for the interesting range of shale proportions i.e., $p < 0.5$. For blocks with a greater amount of shale this does not hold. However, the permeability of these blocks will be very low and the exact value is not practically important. The overall proportion of shale may be estimated by well log analysis and from core data. So, the last two assumptions are deemed less restrictive.

It is illustrative to see how the transition from a binary distribution to a single effective value is made, as the block size increases. Consider a block volume made up of n small elementary volumes. According to the third hypothesis noted above the block effective permeability K_e may take only $n+1$ permeability values, each permeability value corresponding to the number of actual shale units in the block (i.e. 0,1,2, ... ,n). In reality, K_e could take many

possible values corresponding to $-1 \leq \omega \geq 1$ the limitation to $n+1$ permeability values is due to hypothesis 3 which assumes a constant averaging power. The $n+1$ permeabilities are calculated by the equation:

$$K_{e_j} = \left[\sum_{i=0}^{n} \frac{1}{n} K_i^{\omega} \right]^{\frac{1}{\omega}} = \left[p_j \cdot K_{sh}^{\omega} + (1-p_j) \cdot K_{ss}^{\omega} \right]^{\frac{1}{\omega}} \tag{4.1}$$

where:

$j = 0,1,2,....,n$ the number of shale units in the block.

K_{e_j} = effective permeability of the block given j.

$p_j = \frac{j}{n}$ = a fractional volume.

Knowing the overall proportion of shale (p) the probability of each K_{e_j} may be calculated considering a binomial distribution for j:

$$b(j; n, p) = \frac{n!}{j!(n-j)!} p^j (1-p)^{n-j} \tag{4.2}$$

$b(j; n, p) =$ the probability of obtaining j shales after drawing n units randomly with an overall proportion of shale p.

Figure 4.3 shows the effect that averaging has on the cumulative distribution of permeability. The discrete distribution is seen as a series of step probabilities. These probabilities are independent of the averaging process (averaging power) used. The averaging process only changes the scale on the permeability (abcissa) axis. A linear scale results from an arithmetic average. A geometric average amounts to arithmetically average the natural logarithms of the sandstone and shale permeabilities and then take the exponential of the result. Therefore, a log scale on the permeability axis would cause the step probabilities to be equally spaced. The two previous cases are but particular cases of power averages and in general the permeability axis scale depends on the appropriate averaging power.

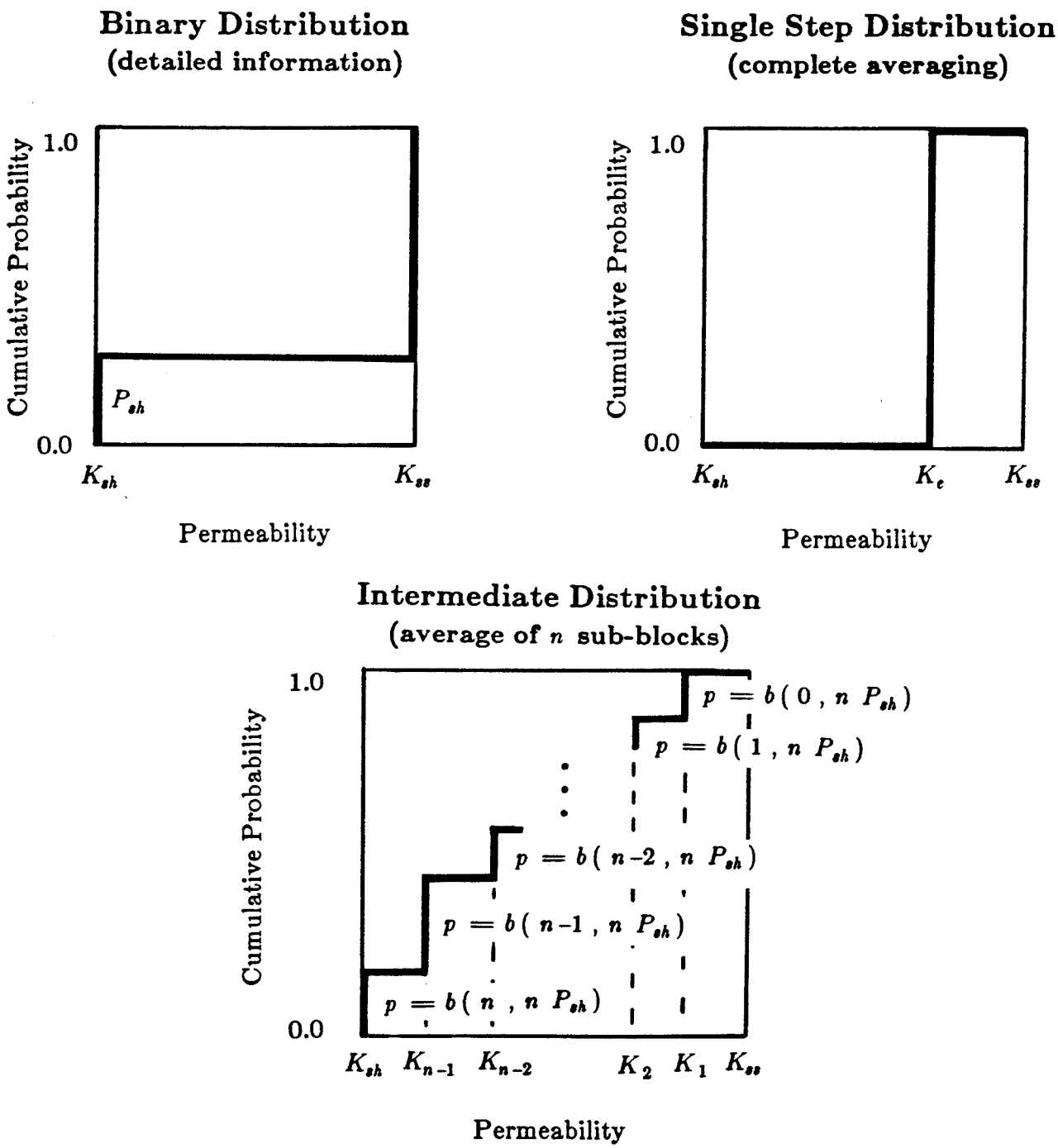

Figure 4.3: The effect of averaging on the cumulative distibution of permeability is illustrated. A binary distribution is obtained when each observation is either shale or sandstone. After complete averaging the permeability is characterized by a single value K_e. In between these extremes a binomial distribution is found. The step probabilities are independent of the averaging process. The location of the permeability values (K_1 through K_{n-1}) is determined by the averaging process.

The formula for the binomial frequency distribution (4.2) is not very handy because for large n it is not possible to realistically compute the corresponding large factorial numbers. However, a normal distribution may be used to approximate the binomial as n becomes large. The development of this approximation for a power averaging process is given in appendix B. Figure 4.4 shows a series of cdfs for averaging powers 0, 0.5 and 1, the proportion of shale is fixed at 0.25 and n took the values: n =4,8,16,32. Figure 4.5 shows a series of cdfs for a fixed averaging power (0.5) and proportion of shale (0.25) with n varying from 4 to 512. Figure 4.6 shows the cdfs for n=32 and ω = 0,0.5, and 1 with the proportion of shale varying from 0.1 to 0.3.

Some remarks:

- As the averaging power increases the expected value of the block distributions also increase. Similarly, but to a lesser degree, as the number of units n increases the expected value increases. With a greater number of units (n) the dimensionality of the network is greater causing more paths for flow and the effective permeability is increased.

- An important observation is that the central location of the distribution depends on the averaging power. If a distribution of already averaged data is used, it is essential that this prior averaging process be correct. If the averaging is performed incorrectly at a small scale it is unlikely that subsequent averaging could yield the correct result.

- As n increases the distribution becomes less dispersed around its central location. This is, in part, due to the assumption of independence of the sandstone-shale elementary volumes.

- For an $\omega = 0$ power average (geometric averaging) the distribution of the block permeabilities is lognormal. That is to say: if a logarithmic axis for permeability is used the distribution would appear as a normal distribution.

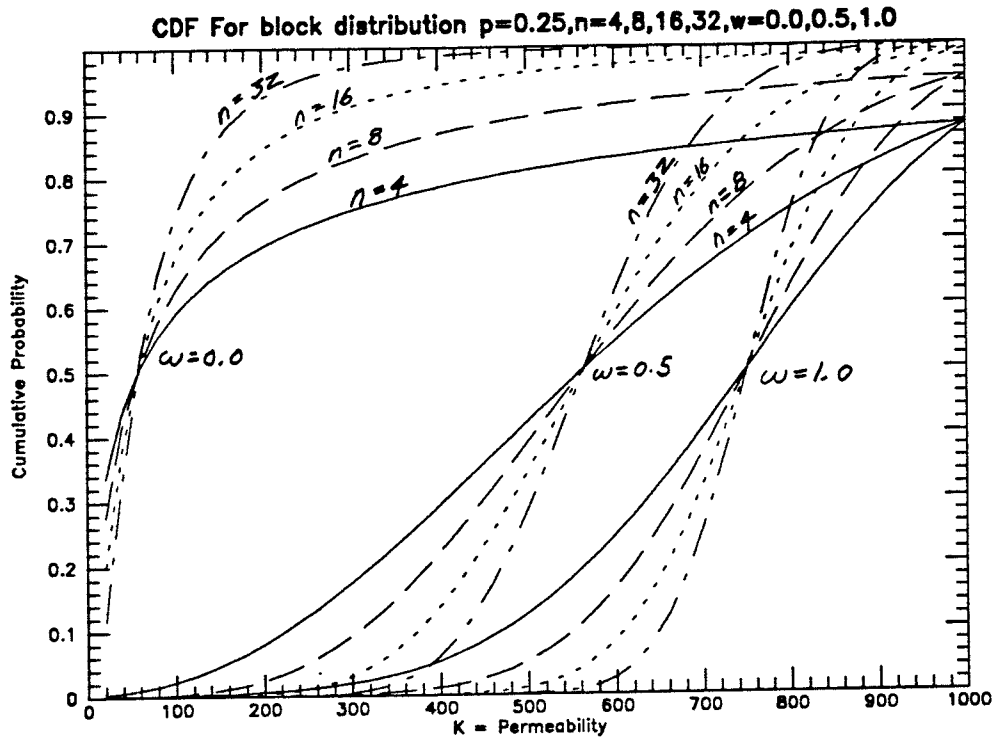

Figure 4.4: The cumulative Distribution Functions (cdfs) for block averaged permeability are shown. The three sets of curves correspond to averaging powers of 0, 0.5 and 1.0. The number of sub-blocks being averaged (size of the block) increases from 4 to 32. The effective permeability increases as ω increases and as ω approaches 1 the distribution becomes more normal.

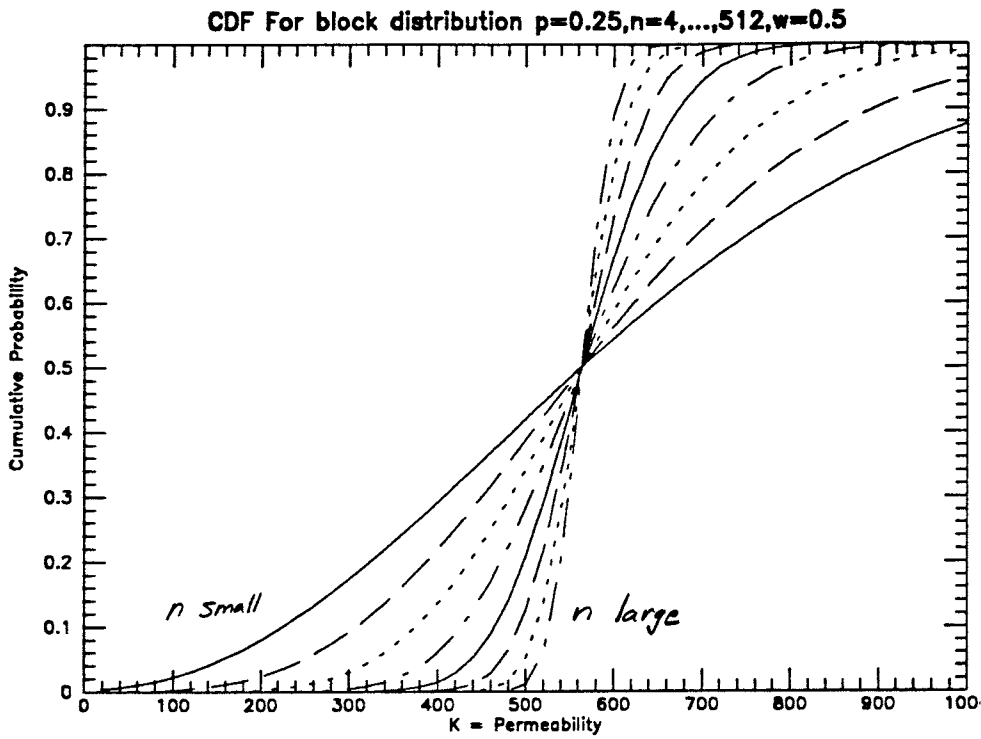

Figure 4.5: The Cumulative Distribution Functions (cdf) for block averaged permeability is shown. The averaging power is fixed at 0.5. The number of sub-blocks increases from 4 to 512. The distribution approaches a step distribution as the number of sub-blocks increases.

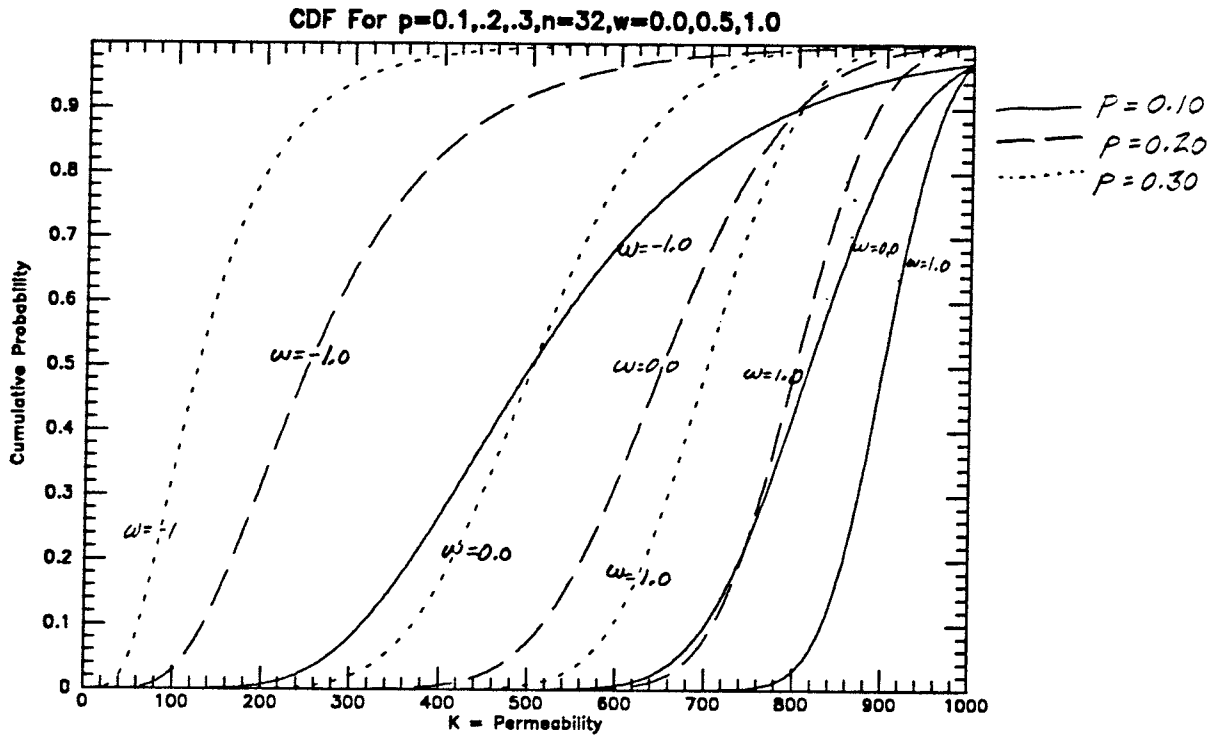

Figure 4.6: The Cumulative Distribution Functions (cdf) for block averaged permeability is shown. The number of units is fixed at 32. Three averaging powers (ω=0.0,0.5,1.0) are used and the proportion of shale is varied from 0.1 to 0.3. The effect of the shale proportion can be compared to the effect of the averaging power.

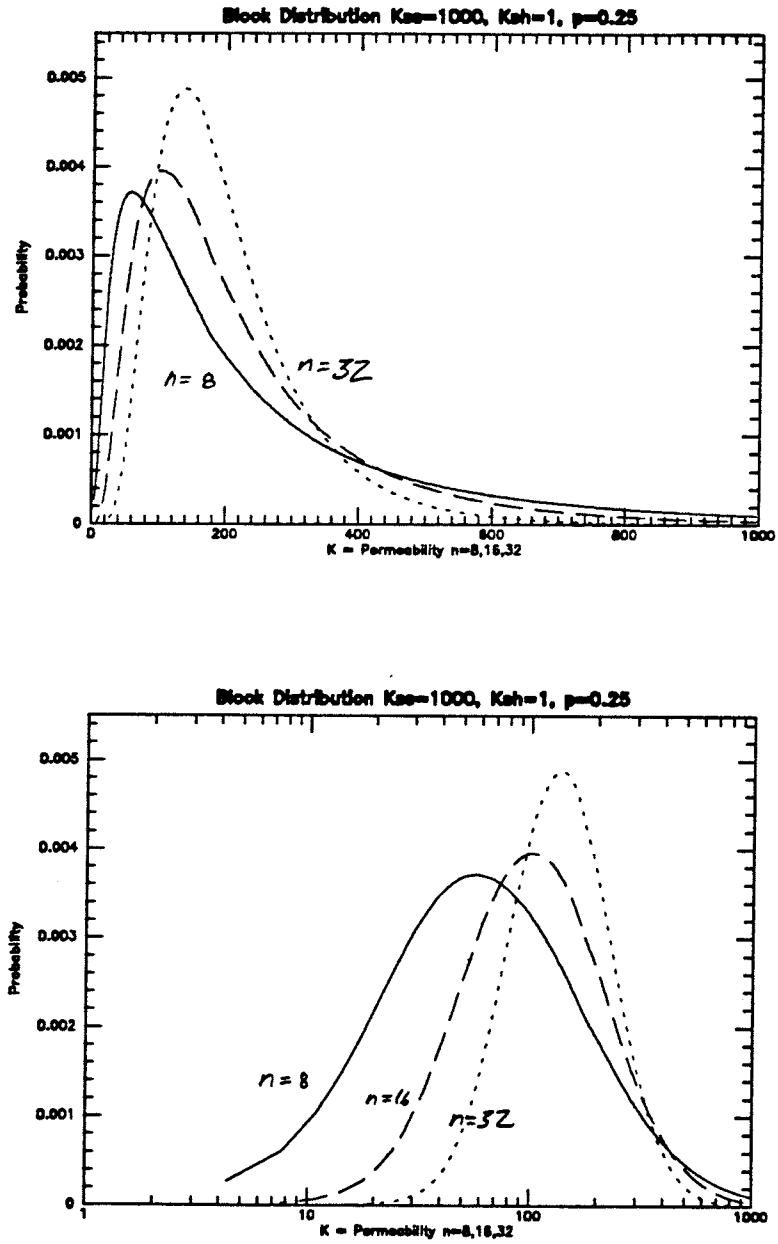

Figure 4.7: Probability Distribution Functions (pdf) for block averaged permeability calculated with a geometric average are shown. If a log permeability scale is used a normal distribution is obtained.

This idea is easily generalized so that the scale is interpreted as a power transformation. Figure 4.7 shows a series of probability distribution functions (pdfs) that correspond to geometric averages. The pdfs appear normally distributed if a log scale is used. The expected value of these pdfs (the peak in the *normal* distribution) increases as the number of units n increases.

- Theoretically ω can vary from -1 to 1, however practical experience has shown that it is most often between 0.0 and 1.0. It is in this range that the averaging power has a large effect on the absolute value of the effective permeability. As the averaging power becomes less than 0 the effective permeability approaches rapidly the shale permeability and for all practical purposes an impermeable sandstone/shale system will exist. Although the relative effect for lower averaging powers is similar, the effective permeability can be considered as very low thus removing the need for determining precisely the corresponding low ω.

Up until this point the sandstone and shale units have been located independently. This is not a realistic assumption due to the sedimentary nature of sandstone/shale sequences. The effect of introducing spatial correlation would cause the distribution of block effective permeability to be more dispersed. To correct for this, an "effective" n_e smaller than the true n could be used. The dispersion introduced by a smaller n_e would mimic the dispersion due to spatial correlation. The dispersion would be corrected by, in effect, grouping the shales and sandstone into larger blocks allowing for the spatial dependence of the sandstone and shale. Implementation of this effective correction is beyond the scope of this research but there is potential for future research in this area.

Selecting the Shale Permeability:

As we have seen before the power average of a a two component mixture is written:

$$K_{eff} = \left[p \cdot K_{sh}^{\omega} + (1-p) \cdot K_{ss}^{\omega} \right]^{\frac{1}{\omega}}$$

For a sandstone/shale mixture the shale permeability is essentially zero. For all realistic pressure gradients applied in practice there will be no flow through the shale component. The shale permeability may be 0.1md or 0.001md but when considered with the high permeability of the sandstone phase (typically 500-1500md) this difference in shale permeability should be of no practical consequence.

In any case, the very low permeability of the shale would be difficult to measure accurately. For a given size of core sample (ex. a cylindrical core plug 2cm radius and 2cm thick) if a 3 atm pressure drop was used to measure the permeability of a sandstone sample ($K_{ss} = 500md$) a 1,500,000 atm pressure drop would be required to obtain the same flow rate in a shale sample ($K_{sh} = 0.01md$). Of course, such pressures are unrealistically high and a lower flow rate would have to be accepted, nevertheless, a reasonable measurement of such a low permeability would be difficult to obtain.

When considering the power average expression of the effective permeability the shale permeability can not be set to zero. If set to zero the geometric average is not defined and for all negative averaging powers the effective permeability is similarly undefined.

As mentioned above there is practically no difference in shale permeability once it is below a certain level because there will be essentially no flow through the shale. The flow through the mixture will be the same regardless of just how low the shale permeability may be. The power average - calculated effective permeability of the shale will, however, depend on the shale permeability chosen.

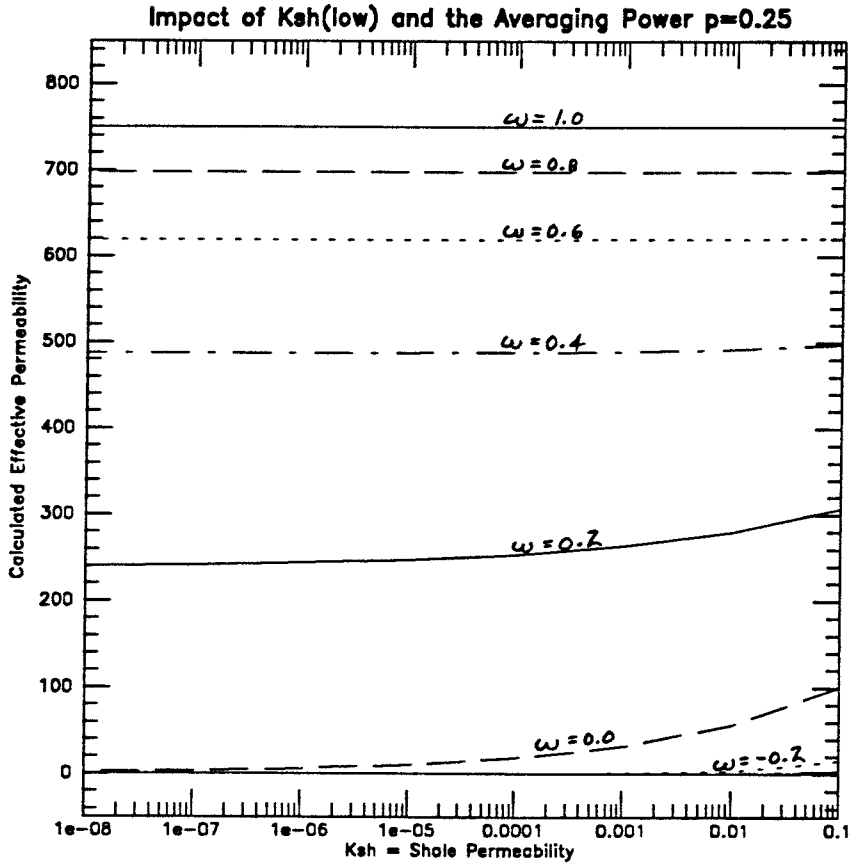

Figure 4.8: The effective permeability is plotted for various averaging powers versus shale permeability. The sandstone permeability is fixed at 1000md and the proportion of shale is fixed at 0.25. The averaging power is the important parameter in determining the effective permeability. The selection of the low shale permeability will affect the resulting effective permeability for low powers ($\omega < 0.2$).

Figure 4.8 shows how the calculated effective permeability will vary for different values of low shale permeability and different powers of averaging. It is clear from these figures that correctly identifying the averaging power is the important issue. For averaging powers less than 0.2 the shale permeability has an important impact on the calculated effective permeability. Figure 4.9 shows the relative change in effective permeability for averaging powers less than zero. The block effective permeability in all of these cases is less than 10md. If the permeability is this low it is not practically important to have an accurate estimate of the effective permeability.

Figure 4.10 shows how the effective permeability for a geometric average is affected by the selection of the shale permeability. It is clear from this figure that the problem is not negligible.

This consequence can not be ignored and the way to avoid complications is as follows:

1. If the shale permeability is known through reliable measurements there is no problem.
2. If the shale permeability is estimated to be zero or is unknown an arbitrarily low shale permeability can be selected. All the regression analysis that is subsequently performed using different statistics for shale geometry will correspond to the value of the shale permeability chosen. The value chosen should be reported and if, at some later time, data is made available the regression should be modified.

This analysis raises the question: what has been done up until this point with the geometric average? Previous work dealing with averaging considered, essentially, homogeneous media and no low permeabilities were encountered. Any geometric average can not accept permeabilities that are zero, and would be very sensitive to any proportion of very low permeabilities.

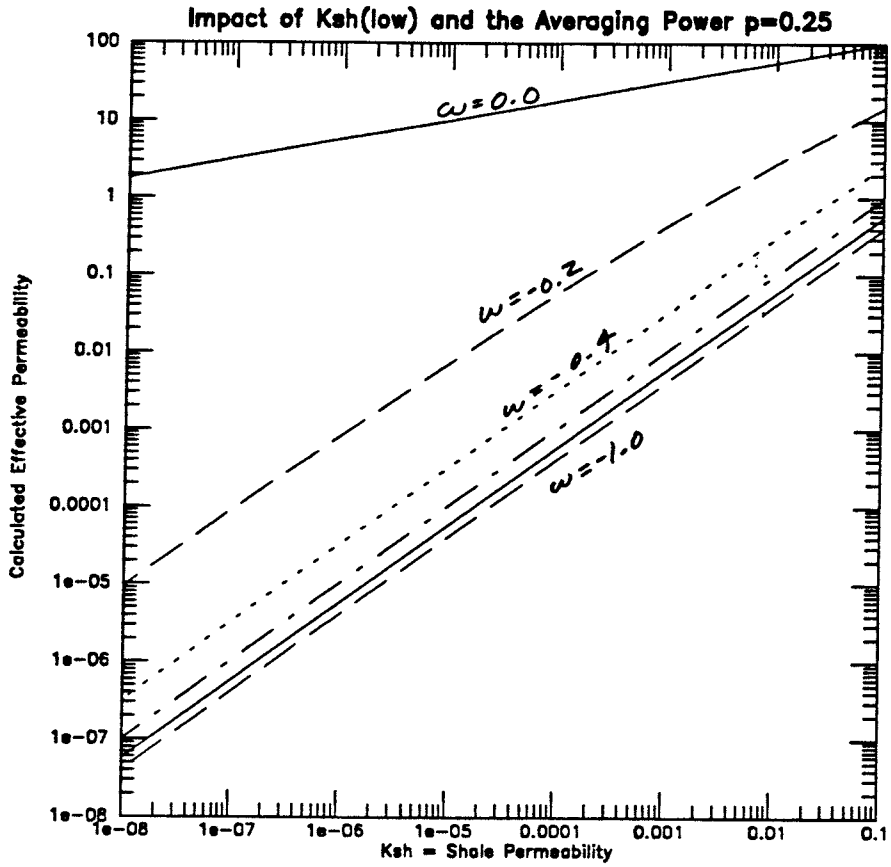

Figure 4.9: The effective permeability is plotted for averaging powers $\omega<0$ versus shale permeability. The sandstone permeability is fixed at 1000md and the proportion of shale is fixed at 0.25. As the averaging power decreases the relative impact of the shale permeability increases. Although in practice for such low permeabilities there will be essentially no flow in any case.

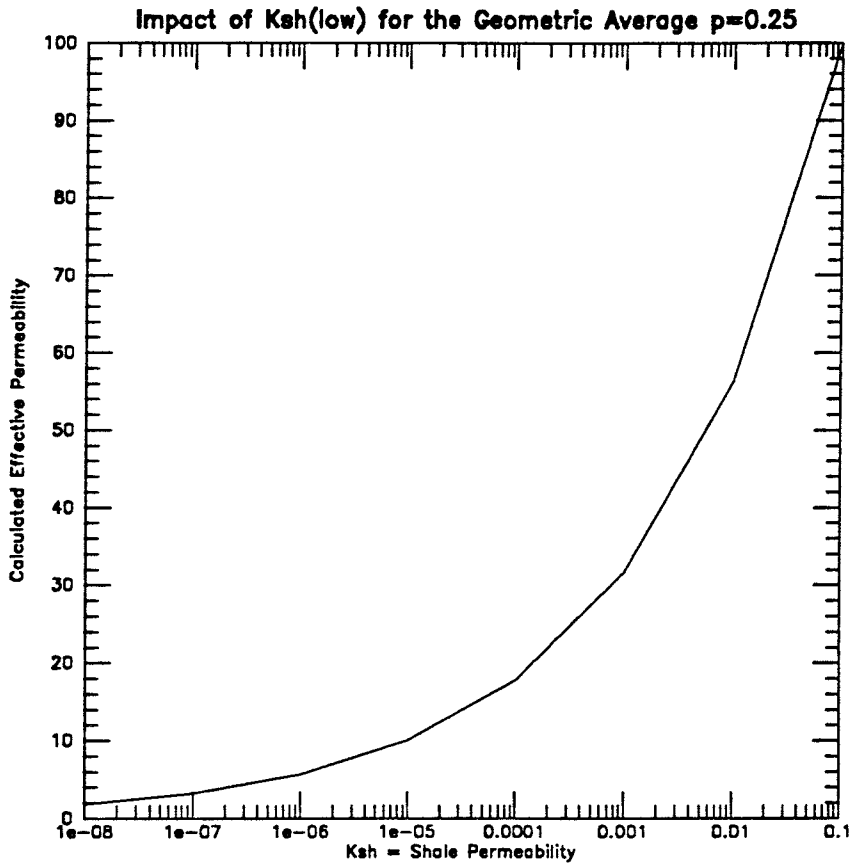

Figure 4.10: The effective permeability versus shale permeability for a geometric average is shown. The sandstone permeability is 1000md and the proportion of shale is 0.25. Note the change in effective permeability due to the shale permeability. If the shale permeability is set to zero the geometric average would always provide a zero effective permeability. In practice, shale is impermeable and a geometric average is used. This shortcoming of the geometric average must be addressed.

Adding Uncorrelatable Shales

Reservoir heterogeneities may be categorized as large scale *deterministic* shales or small scale *stochastic* shales. Large scale shales may be handled deterministically in the finite difference grid block model. The stochastic shales must be accounted for in the creation of the grid block model.

At this point it is important to note that the accuracy of any method used to correct block properties for stochastic shales will only be as good as the information available. As mentioned in the last section; the proportion of shale is a crucial parameter. The spatial distribution of the shales is equally important and much more difficult to assess.

Two apprcaches may be taken to account for the stochastic shales:

1. Correct the flow properties arbitrarily through a history matching procedure. A procedure of this type is not unique and the results can not be expected to represent the *true* block effective permeability.
2. Add the shales into each reservoir block and average the permeability with an appropriate averaging scheme. The averaging must be performed since the stochastic shales (by definition) are too small to be accounted for in the simulation model.

To develop or test any technique to average permeability the small scale shales must be simulated and the resulting sandstone/shale network considered as one possible real situation. The problem of simulating a shale indicator field in a fast (computationally) and realistic manner will now be discussed.

Three methods are proposed to simulate a shale indicator field:

1. Geometric Simulation.
2. Depositional Process Simulation.
3. Geostatistical Simulation.

Geometric simulation was proposed by Haldorsen (1984) and elaborated on by Srivastava (1986). Shale units are characterized by certain geometric parameters such as length and width. The shale centroids may be randomly located and their geometry is randomly drawn from known distributions of length, width, and thickness. The procedure of randomly locating centroids within a matrix is known as the *Bombing model*. The shale shapes are assumed to be rectangular paralellipipeds, ellipsoids, or triangular prisms. Shale units are generated until the correct volume fraction of shale is present. In the procedure proposed the direction of the long axis is controlled so that the local paleocurrent directions may be approximately honored. Other conditions concerning clustering can be imposed so that the resulting model appears realistic.

This method has the advantage of using some geologic knowledge and statistical measurements. This procedure reproduces the geometric parameter distributions that can be measured in the field. However, it is difficult to condition the resulting realizations to known occurences of shale (intersected by well). The simulations are obtained relatively fast.

Depositional process simulation involves simulating the depositional process through time, allowing for sediment influx, erosion, uplift, sediment transport, etc. After several million years of simulated geologic time the resulting grain size distribution will give a sand/shale model. Coarse grained sediments form sandstone while fine grained sediments result in shales. This procedure is documented in a Ph.D. thesis by Tetzlaff (Stanford University, 1987). The advantage of this method is that the simulated indicator field has been obtained through physical process simulation and the models are realistic looking. A number of drawbacks make this method unsuitable for the problems addressed in this thesis.

The initial state (i.e., sediment properties, physical setting, fluid transport properies) is set and the model takes over. Thus, feedback on important

parameters is difficult to obtain. It is also difficult to condition the simulation to known shale occurences. The simulation of flow over several million years requires a considerable amount of computer time which limits the complexity of the model that may be considered.

The third feasible method to simulate a shale indicator field is the method of geostatistical simulation. A standard normal variable that honours the indicator variogram describing the geometrical size and anisotropy of the shale bodies is simulated. If data is available the simulated random field can be conditioned to known data easily. The shale indicator field is obtained by applying a predefined cut off on the simulated Gaussian fields. The cut off is chosen such that the proportion of shale is honoured. Each sub block whose standard normal assignment is greater than the cut off will be defined as e.g. a shale block. The reader is refered to Journel and Isaaks (1983) for a more detailed description of this method.

Once the indicator variogram model describing the presence/absence of shales has been determined and the volume fraction of shale is known; numerous simulations may be quickly obtained. Another advantage of this approach is the possibility to test how sensitive average flow properties are to the statistics that are used (variogram model, anisotropy, range of correlation, and proportion of shale).

The simulated indicator field will on average represent the shales from which the variogram was inferred. However, a particular realization will not necessarily resemble the geometry of the shales. This method is well documented and used successfully in the thesis of Desbarats(1986). An indicator variogram does not relate directly to flow but to the geometry of heterogeneities. The actual flow paths and detailed measures of connectivity are described by the multivariate distribution of the shale indicator field. The variogram or two point correlation structure do not fully capture all the flow characteristics of the mixture.

The indicator simulation approach has been used for this study because its drawbacks were not assessed to be that severe and the advantage of quickly obtaining a great number of realizations was desired. The ability to determine how sensitive the flow is to parameters such as the variogram and characteristcs of a particular realization was also desireable.

Chapter 5

Estimating Effective Absolute Permeability

Introduction to Absolute Permeability Research

In this chapter the problem of estimating block effective absolute permeability in heterogeneous reservoirs is addressed. A binary type permeability distribution is assumed and the effective permeability is taken as a power average of the component permeabilities. The averaging power will be related to statistical parameters characterizing the spatial arrangement of the sandstone and shale. These statistics are chosen such that they can reasonably be inferred in practical cases. It is shown that knowledge of these statistics allows a prediction of effective permeability which is more accurate than traditionally obtained.

The work presented here comprises two steps. The first step corresponds to an evaluation of the power averaging approach considering vertical flow and an indicator simulation of the sandstone/shale sequence.

Then a second type of simulation is considered to provide greater flexibility and control. A bombing type model is used to simulate the sandstone/shale sequence. The bombing model allows generation of large realizations while providing a better control on the geometry of the shale bodies. The Eclipse black-oil simulator is used in this step to allow an easy transition to the evaluation of two phase flow. The Eclipse simulator because of its industry acceptance was chosen in preference of a simulator developed in-house.

To determine if there exists statistical measures that are appropriate for predicting the averaging process the following procedure is used:

1. Different sandstone/shale networks are simulated to provide models for flow simulation. The models can reproduce observed spatial correlation structures or they can reproduce other characteristics of the sandstone/shale sequence such as distribution of lengths, anisotropy ratio, etc.
2. A steady state, single phase flow simulation program is used to determine the effective absolute permeability of each sandstone/shale network.
3. From the component permeabilities and the proportion of shale the averaging power ω which identifies the network effective permeability can be retrieved.
4. The averaging power ω is then related to statistical parameters describing the spatial arrangement. It has been shown (chapter 2) that the averaging power ω is independent of the proportion of shale for a large range of shale proportions ($p < 0.5$). Therefore, ω depends solely on the spatial arrangement (connectivity) of the shales.

In practice the procedure would be reversed: the averaging power would be predicted from experimental spatial statistics and the corresponding block effective permeability would be retrieved.

Estimation of K_e based on a Continuity Parameter

The three dimensional reservoir blocks are made up of elemental sub-blocks that are either 100% shale or 100% sandstone. Figure 5.1 shows such an assemblage of sub-blocks. The permeability of the elemental sub-blocks may take one of two values, that of sandstone or that of shale. Consider the shale indicator random function $I(x)$ defined for each elemental sub-block centered at point x:

$$I(x) = 1 \text{ if } x \text{ is in shale}$$
$$= 0 \text{ if } x \text{ is in sandstone} \qquad (5.1)$$

The indicator function $I(x)$ has the following first and second order moments:

$$E\{I(x)\} = p = \text{volume fraction of shale in the large block}$$
$$Cov\{I(x), I(x+h)\} = C(h) = p(1-p)\rho(h)$$
$$Var\{I(x)\} = C(0) = p(1-p)$$
$$\gamma(h) = C(0) - C(h) \quad \text{and: } \rho(h) = C(h)/C(0)$$

with $\rho(h)$ and $\gamma(h)$ being respectively the correlogram and variogram of the random function $I(x)$. Controlling the shale indicator variogram $\gamma(h)$ i.e. $\rho(h)$, allows controlling the probability that two 1's will be connected. For a sandstone/shale realization the connectivity of the shales can be measured by $\rho(h)$.

The dimensions of the simulated reservoir blocks have been expressed in terms of the variogram range in the three coordinate directions. It has been assumed that there is a finite range for $\gamma_I(h)$ and that it will be isotropic in the horizontal plane. There is a vertical to horizontal geometric anisotropy with the vertical range less than the horizontal range. The discretization is expressed as the number of points that describe the variogram range. For example: if the variogram range in a particular direction is 15 m (ie. $a_x = 15$ m), and the block

Typical Discretized Reservoir Block

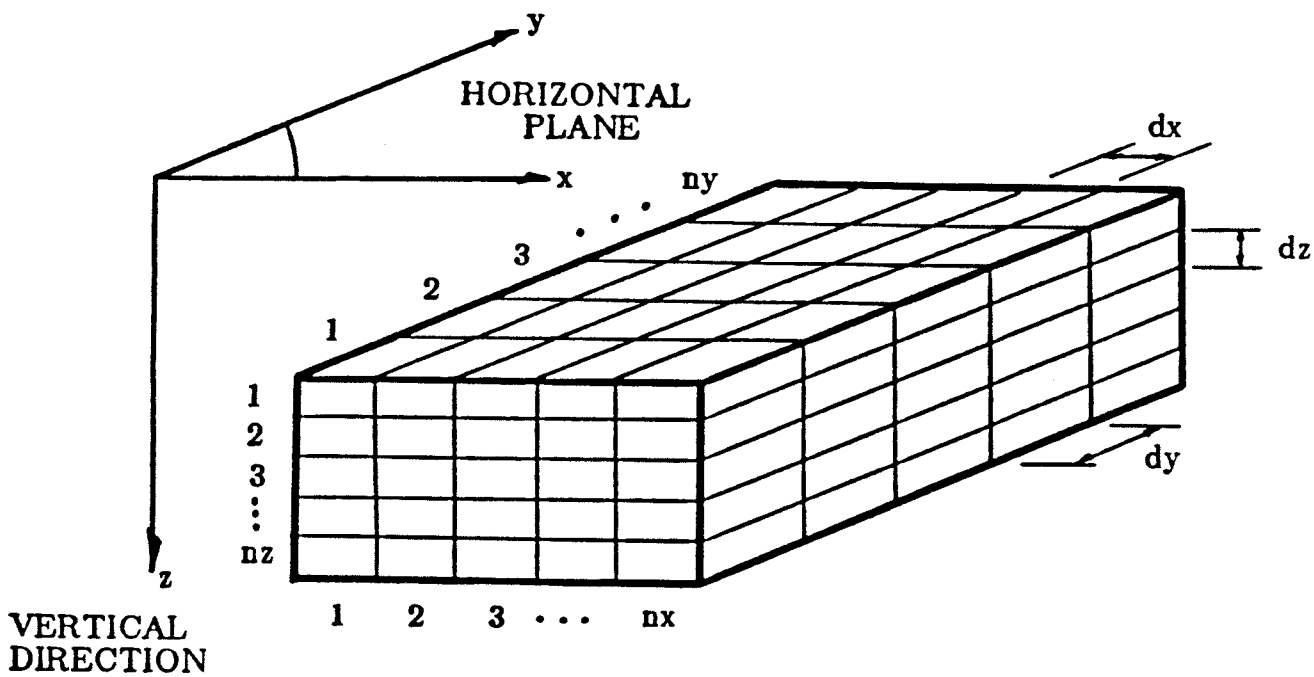

BLOCK SIZE:

$$Lx = dx \cdot nx$$

$$Ly = dy \cdot ny$$

$$Lz = dz \cdot nz$$

Figure 5.1: A typical discretized block.

size L_x is 30 m with sub-blocks each 2 m (d_x). The block length given will be $30/15 = 2 \cdot a_x$ and the number of discretization points will be presented as $15/2 = 7.5$.

A constant shale permeability (Ksh) of 0.1 md, and sandstone permeability (Kss) of 1000 md has been used throughout. An exponential model with a vertical to horizontal anisotropy 1/15 has been considered for the indicator correlogram $\rho(h)$:

$$\rho(h) = e^{\left(\frac{-3h'}{a}\right)} \tag{5.2}$$

$$h' = \sqrt{h_x^2 + h_y^2 + (15 \cdot h_z^2)}$$

h_x, h_y, h_z = rectangular coordinates of the vector h.

The geometrical anisotropy of 1/15 implies that the range of correlation in the vertical direction is one fifteenth the horizontal range of correlation.

A large number of simulations for vertical flow were initially performed. The block size was $0.8 \cdot a_x$ by $0.8 \cdot a_y$ by $1.5 \cdot a_z$, with a discretization of 5 by 5 by 10. A scatterplot of the averaging power versus the proportion of shale (see figure 5.2) shows that the averaging power is independent of the volume fraction of shale. The correlation between the averaging power ω and the volume proportion of shale p for the 4000 runs was found to be 0.07. Thus, the earlier result (chapter 2) that ω does not depend on p is verified.

Given a 3-d indicator field it is necessary to extract some simple and easily inferable statistics that would relate the 3-d configuration of shale to the ability of the field to flow fluid (effective permeability). Two such statistics would be a measure of spatial continuity along the flow lines and a measure of spatial continuity perpendicular to flow. As the spatial continuity of the shales in the flow direction increases it is expected that the flow would increase, thus the

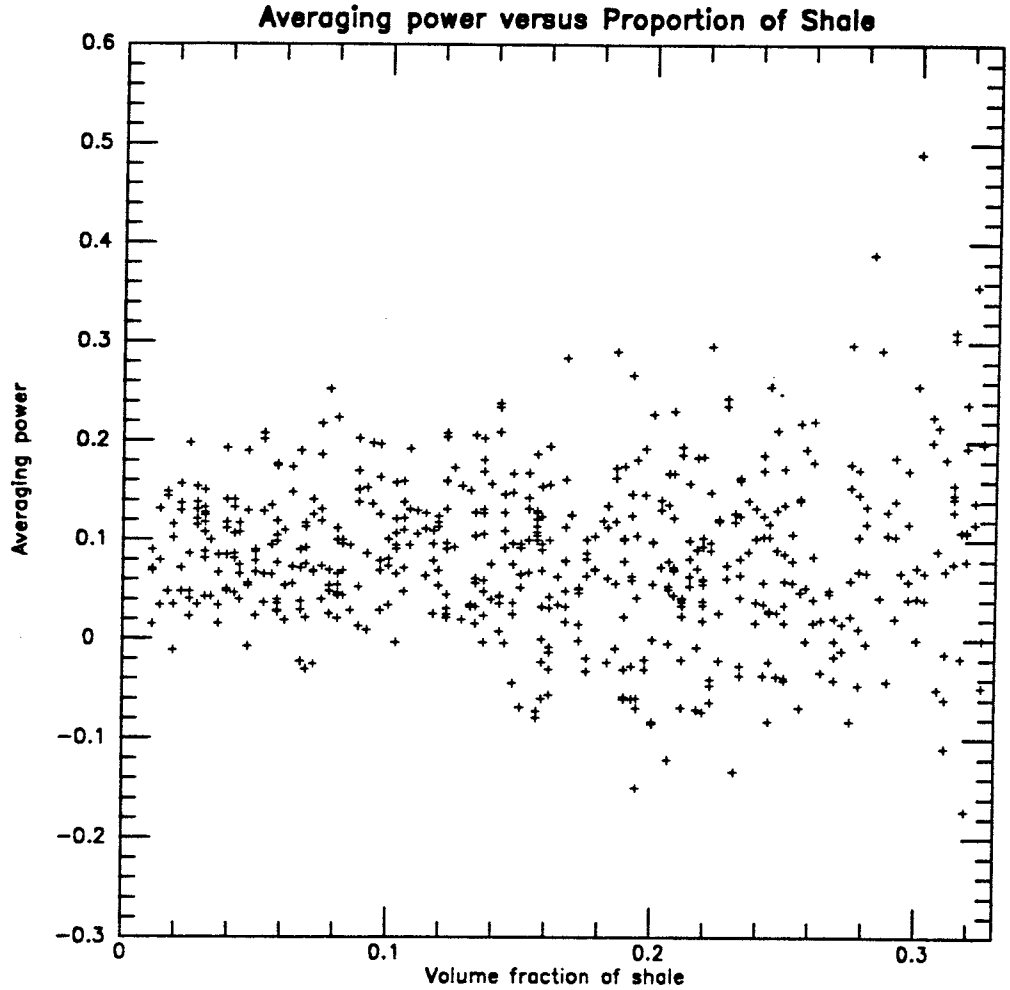

Figure 5.2: A scatterplot of the averaging power versus the proportion of shale. The averaging power appears independent of the proportion of shale over the range observed on this figure.

averaging power should increase entailing an increase of the effective permeability. Similarly, as the spatial continuity of the shales in the plane perpendicular to flow increases, the power of averaging should decrease.

Such a measure of average continuity is a weighted average of the shale indicator correlation for all distances h either in the direction of flow or perpendicular to flow. The general form of such a statistic follows:
(Note: Appendix B contains a full development of this statistic.)

$$\overline{\rho}(L) = \sum \lambda_l \ \rho(h_l) \tag{5.3}$$

with:

$\overline{\rho}(L)$ = weighted shale indicator correlation..

L = length of the network in the direction of flow.

h_l = separation vector in the grid network.

$\rho(h_l)$ = correlogram of the shale indicator at lag h_l.

λ_l = weights on the $\rho(h_l)$, with $\sum_l \lambda_l = 1$.

As $\overline{\rho}(L)$ increases the *average* spatial continuity in the direction of L increases. An equal weighted average will be considered first denoted by a subscript ew.

Figures 5.3 and 5.4 show, as expected, a positive correlation existed between ω and $\overline{\rho}_{ew}(L)$ and a negative correlation between ω and $\overline{\rho}_{ew}(S)$. However, a great deal of scatter was observed. The corresponding median and quartiles of the distribution of ω within small classes of $\overline{\rho}_{ew}$ are also shown. They allow a fast visual appreciation of the amount of scatter. Presenting the results in this manner is consistent with the ultimate objective of having parameters that can predict an effective ω.

Although a clear relation between ω and the two $\overline{\rho}$'s appears, the overall correlation is poor. The correlation between ω and $\overline{\rho}_{ew}(L)$ is only 0.46, and the correlation between ω and $\overline{\rho}_{ew}(S)$ is -0.21. Recall however that traditionally the

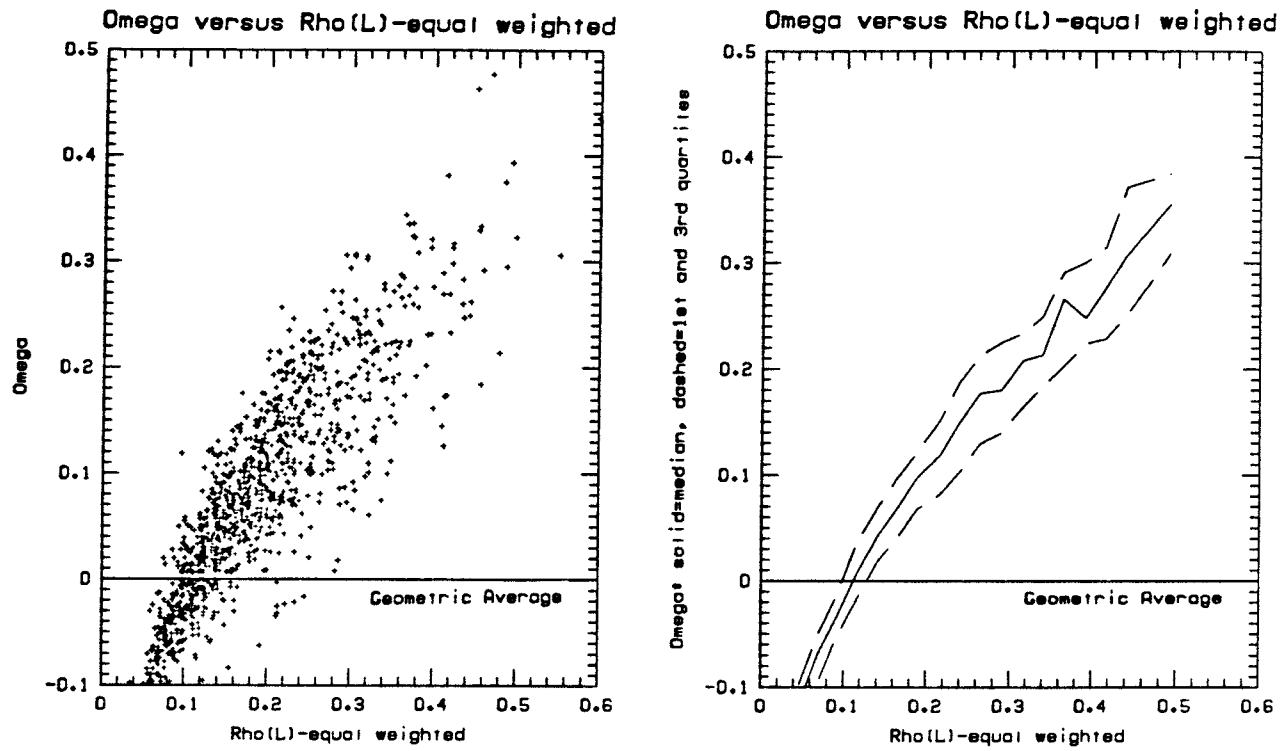

Figure 5.3: Power of Averaging (ω) versus mean indicator correlation $\overline{\rho}_{ew}(L)$. The scattergram of the effective power average ω vs. the mean indicator correlation $\overline{\rho}_{ew}(L)$ for each of the 4000 network simulations. In the right figure, the median, 1st and 3rd quartiles of the distribution of ω conditioned over classes of $\overline{\rho}_{ew}(L)$ values are given. $\overline{\rho}_{ew}(L)$ is the mean, equal weighted, shale indicator correlation within the length L of vertical flow. Note the positive correlation between ω and the statistic $\overline{\rho}_{ew}(L)$.

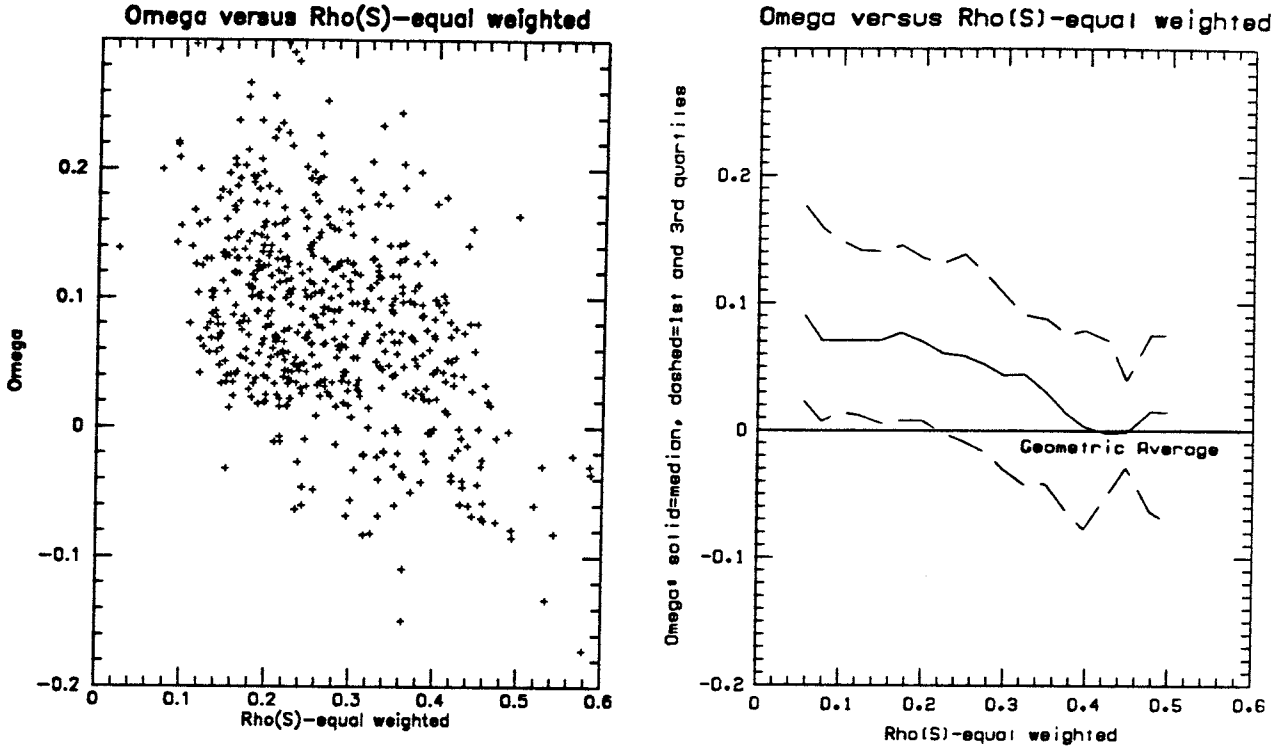

Figure 5.4: Power of Averaging (ω) versus mean indicator correlation $\overline{\rho}_{ew}(S)$. The scattergram of the effective power average ω vs. the mean indicator correlation $\overline{\rho}_{ew}(S)$ for each of the 4000 network simulations. In the right figure, the median, 1st and 3rd quartiles of the distribution of ω conditioned over classes of $\overline{\rho}_{ew}(S)$ values are given. $\overline{\rho}_{ew}(S)$ is the mean, equal weighted, shale indicator correlation over the plane S perpendicular to flow. Note the negative correlation between ω and the statistic $\overline{\rho}_{ew}(S)$.

effective vertical permeability is taken as the geometric average of the component permeabilities which corresponds to an averaging power equal to zero. From figures 5.3 and 5.4 the possibility of improving on this traditional approach can be appreciated.

Upon a detailed look at the $\overline{\rho}(h_l)$ component terms of the expression 5.3 it was considered that ω should be more correlated to the $\rho(h_l)$ terms for small lags h_l see figure 5.14 p111. The influence, i.e., the weight λ_l, was considered to vanish beyond twice the indicator range. Indeed it has been found from network simulations that the block effective permeability becomes independent of the length of the block if that length exceeds double the variogram range (see figure 5.5). On the basis of these observations the following weighting system was considered:

1. $\sum\lambda_l = 1$ (see equation 5.3).

2. λ_l decreases linearly to zero at twice the variogram range.

A complete development is given in appendix B (ref equations B.5 and B.7).

The equal weighted and unequal weighted $\overline{\rho}$ were calculated for the grid networks. Figure 5.6 shows the averaging power versus the equal weighted $\overline{\rho}_{ew}(L)$ and the unequal weighted $\overline{\rho}(L)$ The correlation between ω and the weighted $\overline{\rho}(L)$ is 0.81, a substantial improvement over the correlation between ω and the unweighted $\overline{\rho}_{ew}(L)$ found to be 0.64. Figure 5.7 shows that $\overline{\rho}(S)$ is not very helpful for predicting the averaging power. For $\overline{\rho}(S)$ both cases yielded a correlation of -0.2.

Various block sizes and degrees of discretization have been considered. In each set of test runs the relationship between the averaging power and the experimentally calculated indicator correlation have been observed. The characteristics of the five test runs considered are given in table 5.1.

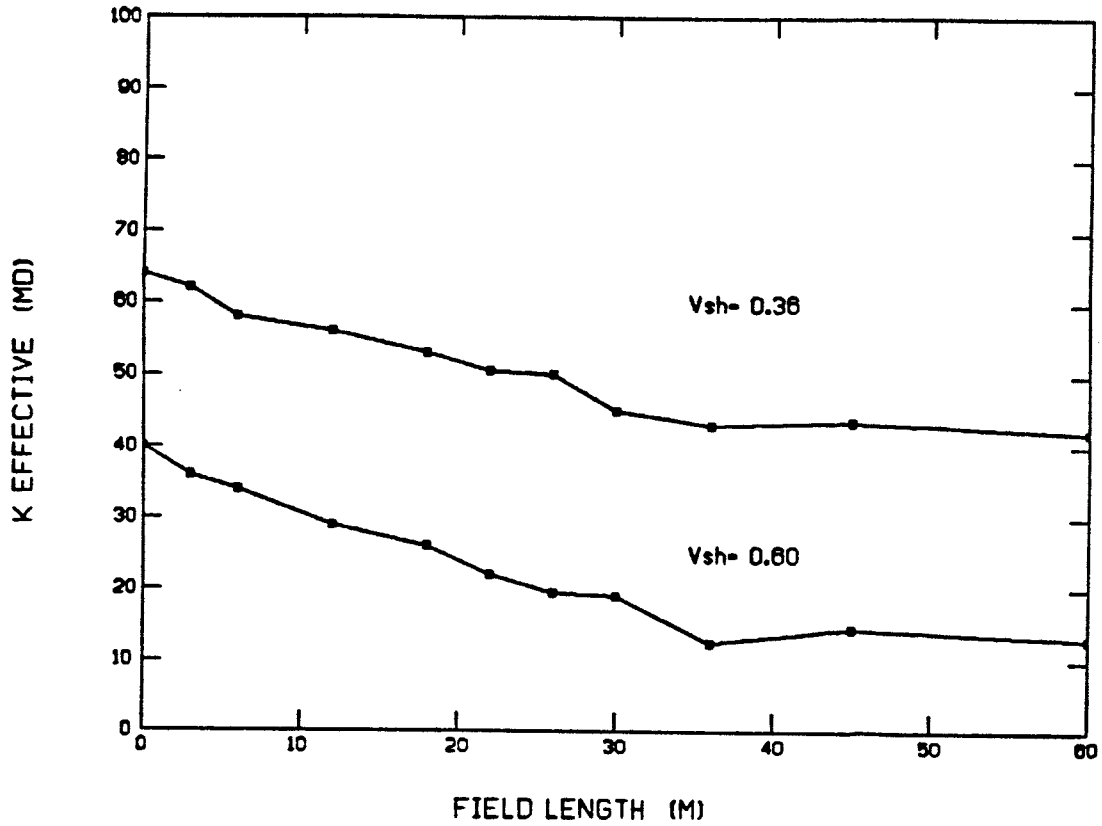

Figure 5.5: The effective permeability versus field length in the direction of flow for shale fractions of 0.36 and 0.64 (from Desbarats, 1986). The indicator range of correlation in the direction of flow is 15m. The effective permeability changes very little after 30m or twice the range of correlation.

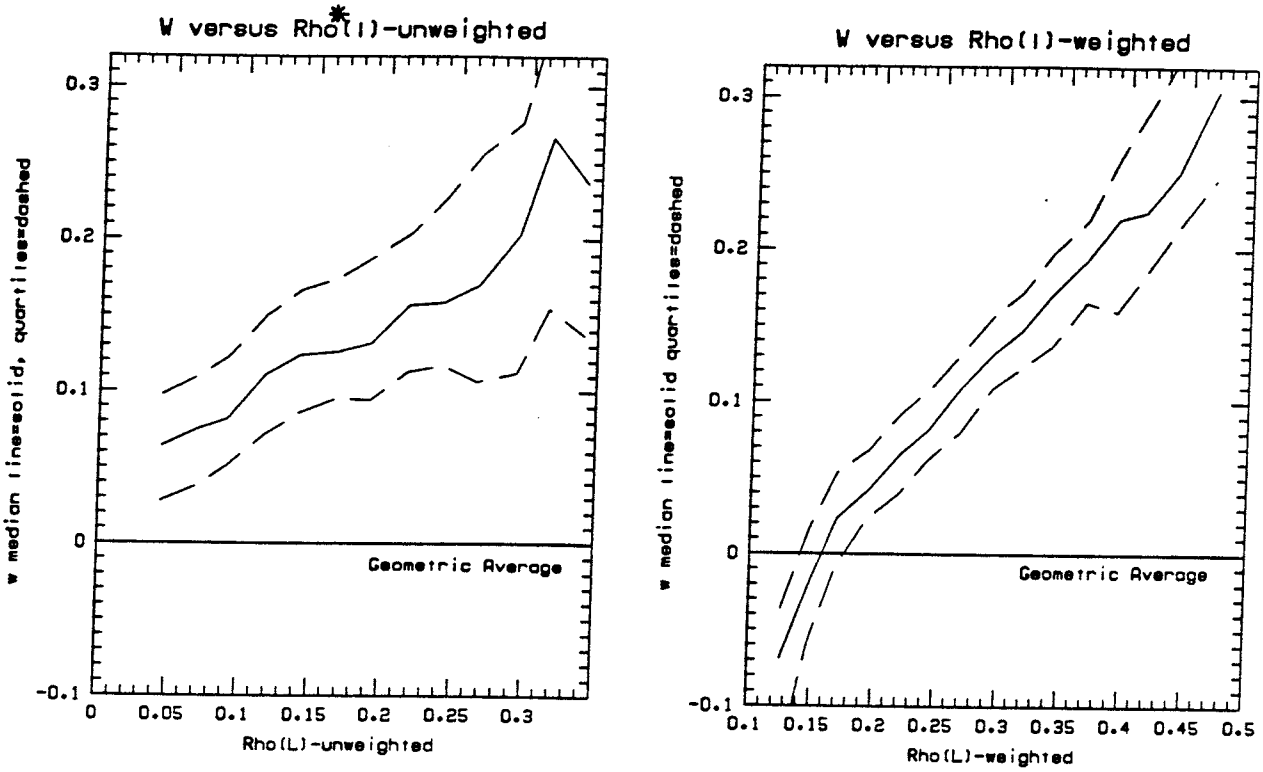

Figure 5.6: Power of Averaging (ω) versus $\overline{\rho}_{ew}(L)$ and $\overline{\rho}(L)$. All the test cases presented in table 5.1 have been combined to determine the median and quartiles of ω based on small classes of $\overline{\rho}(L)$. The 2500 effective ω's have been grouped per classes of either $\overline{\rho}_{ew}(L)$ or $\overline{\rho}(L)$. The resulting class medians for ω were all positive in one case, and negative for low $\overline{\rho}(L)$ classes in the other case.

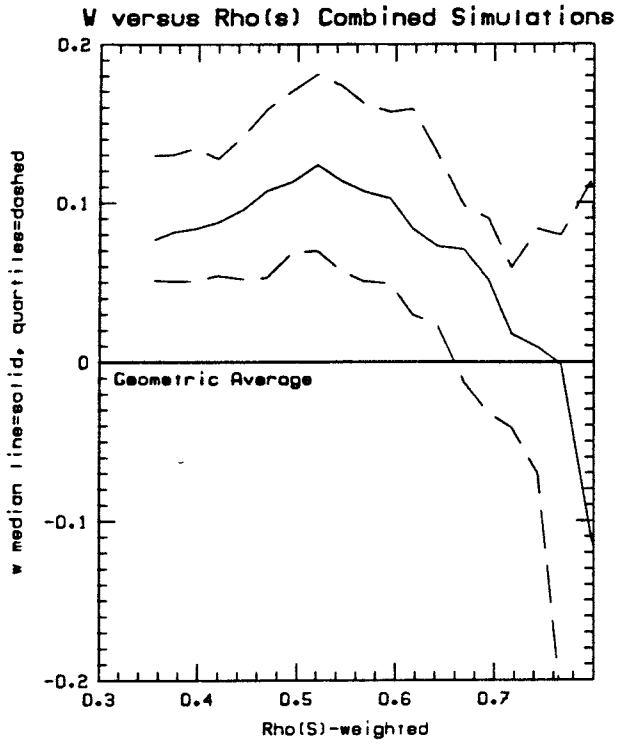

Figure 5.7: Power of Averaging (ω) versus $\overline{\rho}(S)$.
All the test data has been combined to determine the median and quartiles of ω based on small classes of $\overline{\rho}(S)$. For a large range of $\overline{\rho}(S)$, the averaging power appears quasi constant, a result comparable to that shown in figure 5.4.

Five Test Cases Considered

(all distances L are relative to the range of the variogram model)

(the discretization d gives the number of points within the variogram range)

Test Run	L_x	d_x	L_y	d_y	L_z	d_z	size
Base Case I	0.8	7.5	0.8	7.5	1.5	6.7	6x6x10
1. Discretization II	0.8	6.3	0.8	6.3	1.5	6.7	5x5x10
2. Small Block	0.4	12.5	0.4	12.5	2.0	5.0	5x5x10
3. Large Block	2.0	2.5	2.0	2.5	2.0	5.0	5x5x10
4. Large Block II	3.0	1.7	3.0	1.7	3.0	3.3	5x5x10

Table 5.1: Characteristics of the test cases considered.

For each case 500 simulations have been performed. The effective permeability (Ke), power of averaging (ω), proportion of shale (p), equal weighted $\overline{\rho}_{ew}(L)$, unequal weighted $\overline{\rho}(L)$, equal weighted $\overline{\rho}_{ew}(S)$, and the unequal weighted $\overline{\rho}(S)$ have been retrieved from each simulation.

Figure 5.8 shows the median lines for predicting omega on the basis of $\overline{\rho}(L)$ for all five test cases. On figure 5.9 the median lines for prediction of ω by $\overline{\rho}(S)$ are shown. The near horizontal nature of the median lines and the scatter observed leaves little hope to use $\overline{\rho}(S)$ in confidently predicting ω. A multiple linear regression has been used to estimate ω from both $\overline{\rho}(L)$ and $\overline{\rho}(S)$. The inclusion of $\overline{\rho}(S)$ increases only marginally the correlation from 0.694 to 0.704.

In summary, the following observations can be made:

1. The power of averaging (ω) appears independent of p (refer to figure 5.2).
2. The weighted $\overline{\rho}$ terms (ref. equations B.5 and B.7) are better correlated to ω than the equal weighted $\overline{\rho}_{ew}$ terms.

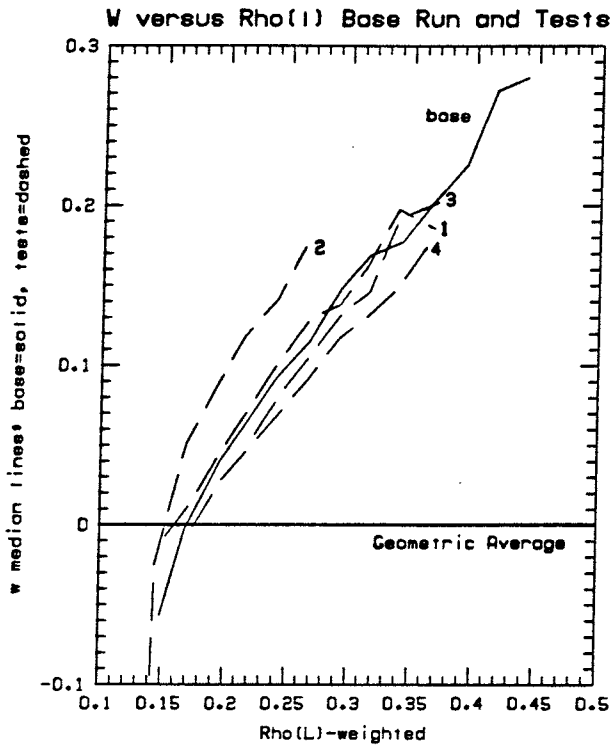

Figure 5.8: Power of averaging (ω) versus $\overline{\rho}(L)$.
Median lines for the four test runs and the base case are shown. The median relates to the distribution of the effective power average ω within classes of $\overline{\rho}(L)$. Note the definite positive correlation between ω and $\overline{\rho}(L)$.

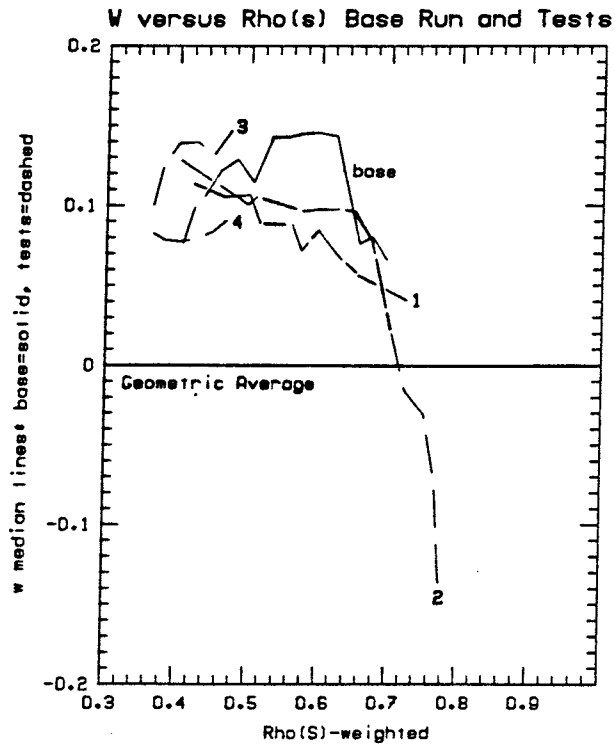

Figure 5.9: Power of averaging (ω) versus $\overline{\rho}(S)$.
Median lines for the four test runs and the base case are shown.
The averaging power ω appears poorly related to $\overline{\rho}(S)$.

3. For the test cases considered the relationship between ω and $\overline{\rho}(L)$ depends little on the block size or level of discretization, see figure 5.8.

4. A good approximation of ω may be made from regression using only the weighted $\overline{\rho}(L)$. The statistic $\overline{\rho}(S)$ does not assist in predicting ω except in extreme situations with very high $\overline{\rho}(S)$.

Referring to figure 5.6 a piecewise linear model for the median line can be adopted:

$$\omega = 6.0\,\overline{\rho}(L) - 1.00, \qquad \overline{\rho}(L) \leq 0.17 \tag{5.4}$$

$$\omega = 0.9\,\overline{\rho}(L) - 0.13, \qquad \overline{\rho}(L) > 0.17$$

This relationship is for vertical flow and should not be used for horizontal flow. Horizontal flow conditions (strong continuity of the shales in the flow direction) would yield a higher $\overline{\rho}(L)$ than is shown on the graph of figure 5.6. To test this regression model the following cross validation was performed. For each run the network effective permeability has been estimated first by the regressions proposed above and second by the traditional geometric average. The mean and variance of the relative error of estimation will give a measure of the bias and accuracy of each method, see table 5.2. The relative error is defined as the true network permeability minus the estimate divided by the true permeability. The closer the mean relative error to zero the less biased the estimator. The lower the variance of the relative errors the more accurate the estimator.

Statistics of the Relative Error				
Estimate	mean	variance	minimum	maximum
1. Geometric Average	-0.0093	62.29	-209.3	0.87
2. Power Average knowing $\overline{\rho}(L)$	-0.0062	0.28	-12.7	0.92

Table 5.2: Relative error statistics using a geometric average and the model proposed in equation 5.4.

The power averaging technique clearly outperforms the traditional geometric averaging. The geometric average is unbiased but not accurate. The constant power of averaging that would give exactly zero bias is $\omega = -0.0125$, a value indeed very close to the geometric average.

Figure 5.10 shows a cross plot of the true and estimated block effective permeability using successively a geometric average and a power average knowing $\overline{\rho}(L)$. All the 2500 runs are pooled in these figures. The bias and accuracy performance appears better for the power averaging technique. In practice the statistics $\overline{\rho}(L)$ need to be estimated. Estimation of a mean indicator correlation is not a particularly difficult exercise, however the estimation would entail some deviation (error) from the exact value $\overline{\rho}(L)$ used in figure 5.10 entailing a poorer performance than shown.

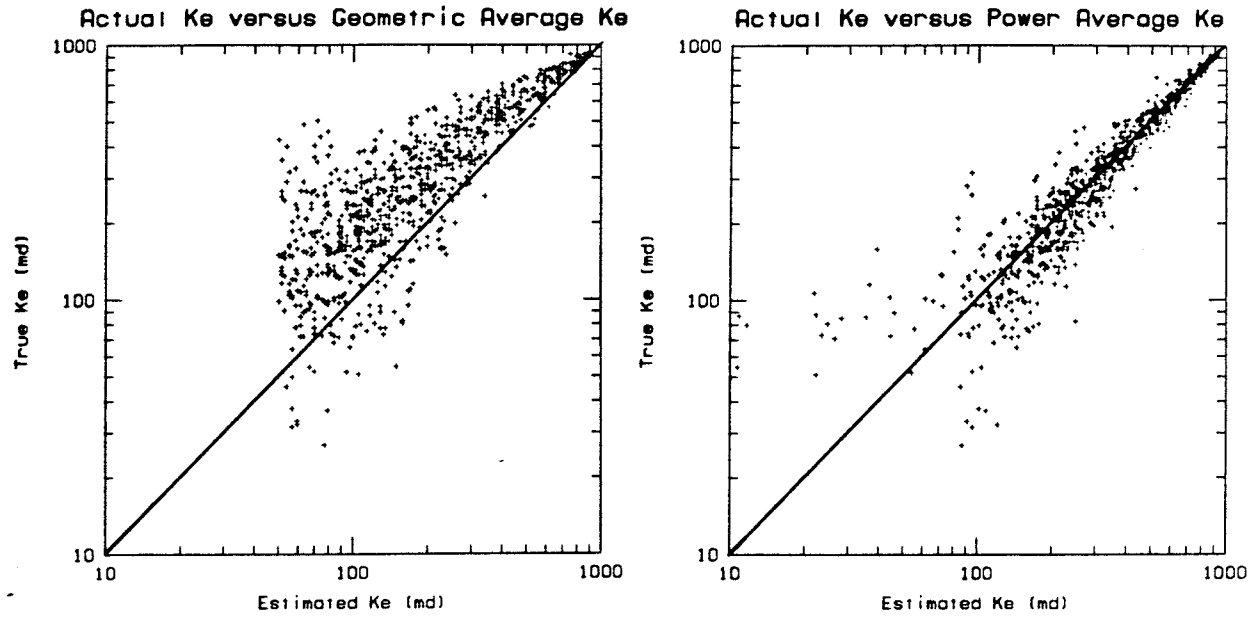

Figure 5.10: Actual Ke versus averaged Ke (Geometric average and Power average)
Note that the geometric average underestimates Ke for all ranges of estimated Ke. The power average is unbiased for all ranges of estimated Ke.

Estimation of K_e Based on $\overline{\rho}(L)$ and SFP

The approach used in this section is different from that taken in the previous section for the following reasons:

- Another geometrical simulation technique (the bombing model) is used to create possible sandstone/shale indicator networks. This change allows greater control over the geometry of the shale heterogeneities. With more controlled geometry it is hoped that the influences of heterogeneity may be observed more clearly. By filtering all the influences except a selected number of controlled parameters, more definitive statements about heterogeneity can be made. The bombing model also allows generation of large networks with a minimum of computer time.

- A commercial flow simulator (Eclipse) has been used. The solution of the finite difference flow equations is fully implicit in this simulator. The previous in-house program treated pressure implicitly and saturation explicitly. Another consideration for choosing Eclipse is that it allows two or three phase flow studies.

- In addition to the weighted indicator correlation $\overline{\rho}(L)$ measures of shortest flow path (see appendix F) will be considered. If these new measures can be inferred in practical circumstances they can be used to improve prediction of block effective permeability.

For a 3-d network there are measures of flow path distance that can assist in predicting the effective permeability. If one considers the sandstone as permeable and the shale as impermeable, flow paths are defined as a continuous sequence of sandstone indicators. From each starting point on the input face of a block there is a shortest flow path to reach the opposing face in the direction of flow. The corresponding array of shortest flow path measures relate to the effective

permeability of the block. An algorithm for calculating this shortest flow path (SFP) array is given in appendix F.

Before proceeding further it is important to recall the ultimate objective of this research. The goal is to develop *measureable* statistical parameters that can be used to infer the correct averaging power. The information required to calculate the measures of shortest flow path would rarely be available in practice except from outcrop studies and/or geological inference.

Bombing Model:

The technique for simulating the random geometry of uncorrelatable shales used in this section is the bombing model. This technique amounts to locate randomly the centers of shale units in space by a Poisson process. A Poisson process implies that the location of one particular center is independent from the location of any other center. This assumption is not fully realistic but it will be considered as a first approximation.

In this study ellipsoids of fixed geometry (axes: a_x, a_y, a_z) are considered. The anisotropy may be set such that the "shales" are extremely flat (a_z/a_x, a_z/a_y very small). Some important comments about the simulation procedure adopted:

1. All ellipsoids are all the same size, however overlapping of the shale units and truncation by the boundaries of the block cause the shapes to differ.
2. All ellipsoid major axes are in the 3 primary x, y, z directions.
3. The model is not as sophisticated, hence as realistic as the 2-d model developed by Srivastava(1986). However, a 3-d model was required that allows for a three dimensional continuity of the shales. A model that "stacks" 2-d realizations was not considered appropriate.
4. This method was employed for the major part of this thesis rather than the unconditional indicator simulation used by Desbarats(1986) because it

imposes no grid size limitation and the geometry of the resulting shales is better controlled.

Description of the Flow System:

A large 3-d rectangular block is discretized into elementary sub-blocks. The permeability within each sub-block is assumed to be constant. Specifically:

- The porosity is uniform and constant over the entire large block.
- The absolute permeability of each sub-block is the same in the vertical and horizontal directions. The software developed would allow for different horizontal and vertical permeabilities, however this additional factor of variability has not been investigated at this time.
- The sub-block permeability has a binary distribution with spatial correlation induced by the bombing model.

Figure 5.11 shows such a block discretized into 2000 sub-blocks (i.e., 10x10x20). This level of discretization has been used in all simulation runs. Each of the 2000 sub-blocks is filled with either shale or sandstone. Given a particular realization of the sandstone/shale mixture the block effective absolute permeability is then determined by running the flow simulation.

A waterflooding simulation has been used. For the block shown in figure 5.10 the following simulation parameters are used:

- *Rock Properties:* Porosity and absolute permeability ($\phi = 14.5\%$, $K_{ss} = 1000md$, $K_{sh} = 0.1md$).
- *Initial Condition:* The reservoir block is 100% water saturated. The relative size of the block versus the size of heterogeneities is the important feature while the absolute block size is not. However, the Eclipse simulator does require a physical size. The size used is:

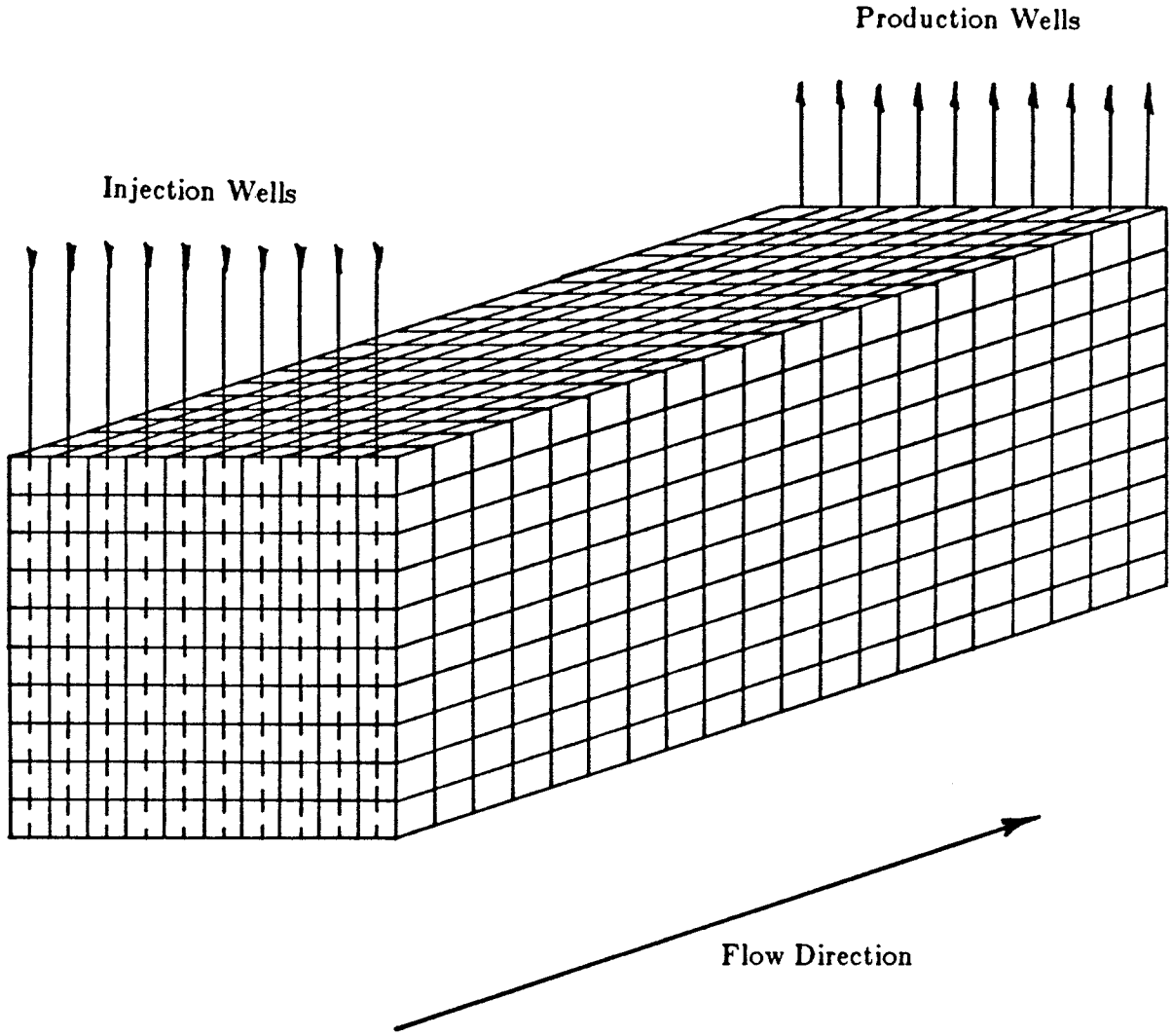

Figure 5.11: A block discretized into 2000 sub-blocks.

$$d_x = 100\ ft \qquad n_x = 20 \qquad L_x = 2000\ ft \text{ (flow direction))}$$
$$d_y = 100\ ft \qquad n_y = 10 \qquad L_y = 1000\ ft$$
$$d_z = 20\ ft \qquad n_z = 10 \qquad L_z = 200\ ft$$

- *Production Scheme:* Water will be injected at a constant pressure at one end of the reservoir. Fluid will be produced at constant pressure from the other end of the block. The flow rate will be determined by the block effective permeability.

- *Injection:* Water is injected into every sub-block on one end of the large block. This is achieved by 10 vertical wells completed throughout each of the 10 layers. Water is injected at constant bottom hole pressure (6500 psi which is below the fracture pressure). The injection pressure decreases linearly from the top of the well (due to gravity) so the average injection pressure is:

  P_{inj} = 6500 – effect of gravity

- *Production:* The reservoir is produced in every sub-block on the opposite end of the large block. Again, 10 vertical wells produce at constant bottom hole pressure (5000 psi which is above the bubble point). The average production pressure must be corrected for gravity and is given by:

  P_{pro} = 5000 – effect of gravity

  When the pressure difference between the injection face and the production face of the horizontal block is considered the gravity effect cancels out.

The flow system described above has been implemented on an Apollo DN660 computer system. The sandstone/shale network simulation was implemented and interfaced with the flow simulation. Relevant Fortran77 subroutines are included in Appendix G.

The software allows the user to generate a 3-d sandstone/shale model with the ellipsoidal shales located by the bombing model. The size of the ellipsoidal shales and their volume proportion are set by the user. Every sandstone/shale model is written to a file for direct input into the Eclipse flow simulator. Another program takes the output from Eclipse and files the effective permeability, averaging power, and the input statistics. Complete flexibility is allowed for input size and anisotropy of the shales, proportion of shales, directional permeability of the sandstone and shale within each sub-block (not used here). and so on.

This set of programs allows the investigation of flow in heterogeneous media to be approached in a very systematic way. Some results are now presented.

Some Results:

Shales of various sizes have been added to the grid network (see figure 5.11) to simulate both horizontal and vertical flow. Horizontal flow corresponds to shales elongated in the x direction while vertical flow is simulated by adding shales elongated in the z direction. Two cases for horizontal flow, one case for spherical shales, and two cases for vertical flow are considered. Each test cases has been tested with 12% and 25% shale. Twenty realizations of each case (10 for each shale fraction) were run. A total of 20x5=100 network realizations were thus considered. A summary of the results are shown in table 5.3.

Summary of Test Cases

No.	Description	Size of Shales			Proportion of	Averaging Power	
		x	y	z	shale	mean	s.d.
1a	Horz. flow	5	3	1	12.5	0.738	0.024
1b	Horz. flow	5	3	1	22.5	0.713	0.020
2a	Horz. flow	9	5	3	12.5	0.696	0.043
2b	Horz. flow	9	5	3	22.5	0.665	0.053
3a	Spherical	3	3	3	12.5	0.422	0.017
3b	Spherical	3	3	3	22.5	0.417	0.021
4a	Vert. flow	1	3	5	12.5	0.341	0.028
4b	Vert. flow	1	3	5	22.5	0.328	0.027
5a	Vert. flow	3	5	9	12.5	0.246	0.050
5b	Vert. flow	3	5	9	22.5	0.179	0.042

Table 5.3: Description of test cases.

Some Remarks:

- The important parameter that determines the averaging power seems to be the geometry of the shales. This can be observed in figure 5.12 where the averaging power for each run is plotted, and increasing from run 5b to run 1a.

- The results are consistent with those observed in the first phase of research i.e., the averaging power for vertical flow is around 0.2 and for horizontal flow around 0.7.

The two different measures for the spatial arrangement of the shale indicator grid (i.e., the indicator correlation $\overline{\rho}(L)$ and the shortest flow path measures) will now be considered for the test cases of table 5.3.

1. Shale Indicator Correlation:

In the sandstone/shale networks considered here the indicator correlation is induced solely by the size of the shales since the shale centers are Poisson located. The variogram for an indicator field of this type is developed analytically in appendix E. The indicator correlogram essentially does not depend on the proportion of shale. Figure 5.13 shows the correlogram (in the x direction) for runs 1a and 1b. The average correlogram corresponding to all 10 realizations is shown. The range of correlation is clearly found to be the size of the shales (i.e, the dimension of the ellipsoids). Appendix E contains an analytical development for the variogram (and correlogram) of Poisson located ellipsoids. The correlograms for the other runs have been computed and show similar matching results.

It is interesting to study how the experimental average indicator correlation $\overline{\rho}(L)$ is related to the averaging power. In the first phase of research it was noted that the averaging power was highly correlated to the correlogram values for short lags. This is shown to be the case on figure 5.14. All 200 runs have been

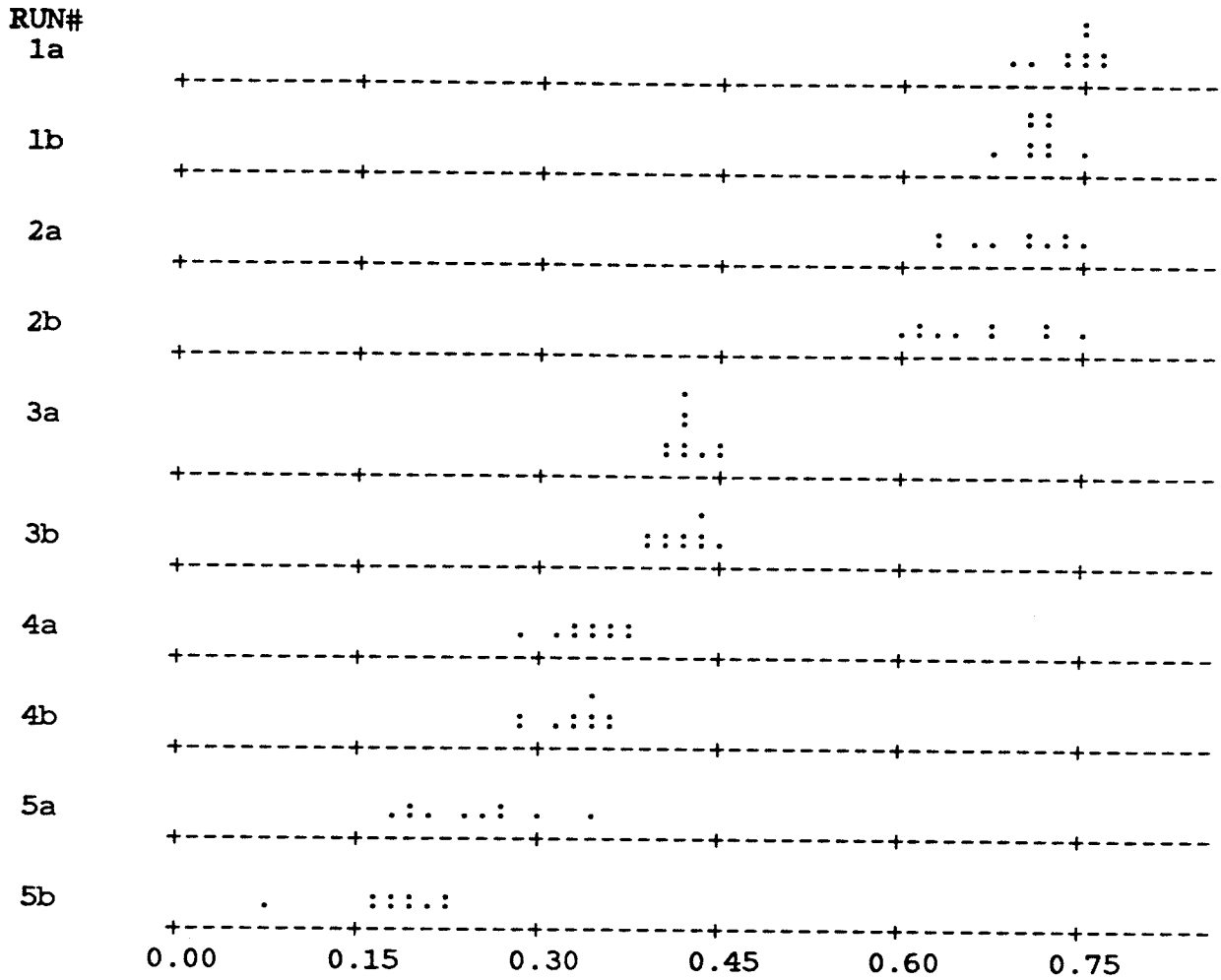

Figure 5.12: The averaging powers ω for all the test runs documented in table 5.3. Note the decrease in the averaging power as the shales become less continuous in the direction of flow (horizontal vs. vertical flow).

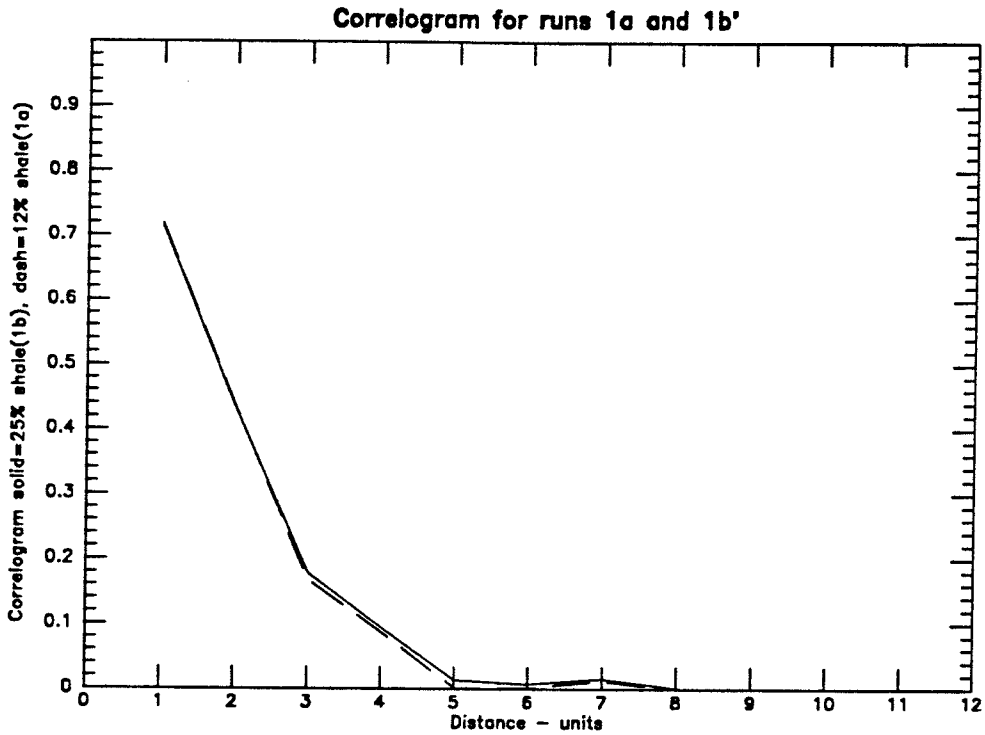

Figure 5.13: Mean indicator correlogram for runs 1a and 1b (see table 5.3). The correlograms for the x direction are shown. The range of correlation is the same as the length of the shales in the x direction (i.e. 5).

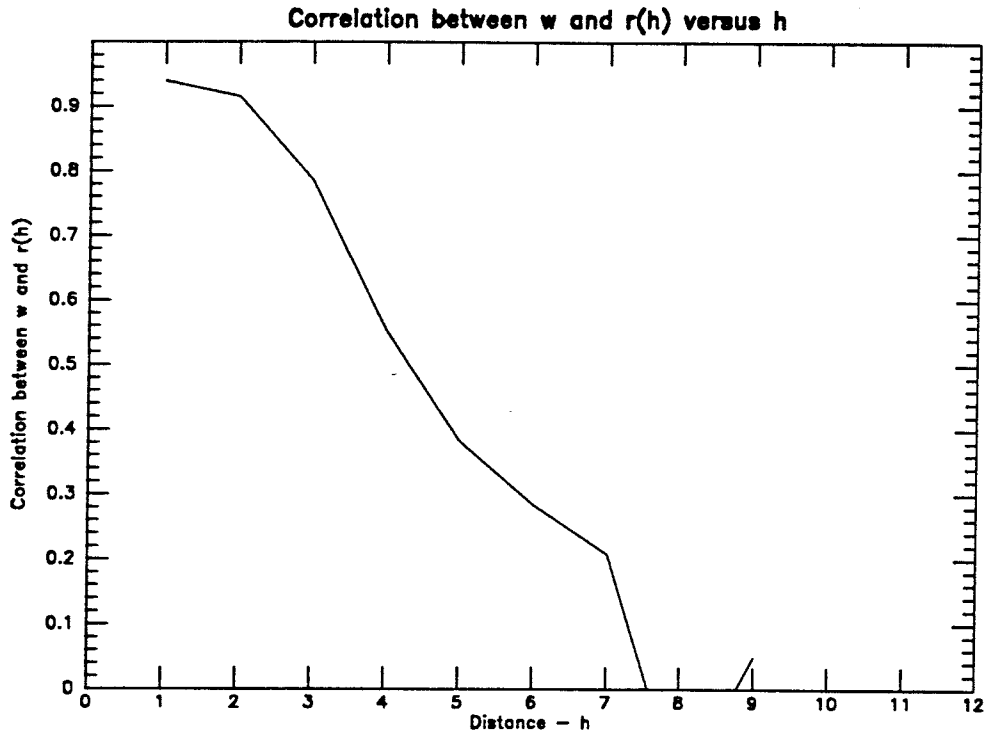

Figure 5.14: Plot of the correlation between ω and the $\rho(h)$ values for various lag distances (h). The correlation is the best for small h and decreases linearly to zero around 8. This led to the weighting system for $\overline{\rho}(L)$.

pooled for this figure.

If the indicator correlation structure could be inferred then the averaging power can be predicted reasonably well. The indicator variogram range and anisotropy are more important than the details of the correlation structure. The practical emphasis should then be directed toward determining the range and anisotropy of the shales. With this information the averaging power could be determined very closely.

1. Shortest Flow Path Statistics:

Although less accessible the shortest flow path (SFP) statistic should provide a much richer information about the flow properties of heterogeneous media and should be highly correlated to the averaging power ω. However, establishing the relationship between the SFP statistics and ω is not an easy task for the following reasons:

1. The SFP parameters are no longer independent of the proportion of shale. The volume fraction of shale will have a strong non-linear influence on the statistics of shortest flow path.
2. For a particular realization the averaging power should be highly dependent on the proportion of flow paths that are unobstructed. However, this proportion is not independent of the block size. As the block size increases for a constant shale size and volume proportion of shale there is a greater chance of hitting a shale obstacle. Thus, the proportion of shortest flow paths will decrease.
3. Not only the proportion of unobstructed flow paths must be accounted for but also their spatial arrangement. If the very short paths are clustered then there is essentially a channel for flow. If the paths are dispersed then the flow is, in general, more tortuous resulting in a lower K_e.

For these reasons the SFP statistics have not been considered in this thesis. The essential point of this research is to develop parameters that can be measured in real practice.

To conclude this phase of research: the averaging power is found to depend on the size and anisotropy of the shales (see figure 5.12). The averaging is also slightly dependent on the proportion of shale. A method to estimate the block effective permeability in a *real* situation can now be presented.

Chapter 6

Conclusions and Recommendations

A Procedure to Estimate Effective Absolute Permeability

A procedure can now be suggested to calculate the block permeability values that are required for reservoir simulators. The procedure outlined below is based on the experiments documented in this thesis.

The important question that should be kept in mind while reviewing this section is: *On the basis of sparse core data, imprecise well logs, and possibly a geological interpretation - how much can be inferred about the spatial distribution of heterogeneities away from the well bore area?*

If only the proportion of shale, the depositional environment, and the principal direction of sedimentation can be inferred - a power average approach to estimate effective absolute permeability is relevant. Other techniques which require more information (such as assumptions about how the shales are distributed...) should be reserved for situations where this information is available.

The following step by step procedure could be used in practice.

1. Infer the proportion of shale correctly everywhere. This will involve a *good* well log analysis that does not ignore small scale shales that may not be picked up by the gamma log. Beyond the well locations the proportion of shale can be estimated using either a conditional simulation (which will provide the "least smooth" estimate) or kriging.

2. Assign absolute permeabilities to the shale and sandstone. If more than one type of sandstone (or shale) is present the proportion of each component must be inferred in each block as well as the permeability of each component. It is important to note that assuming a binary or n-ary distribution for the permeability even when there is some mixing (spread about the modes) is not unrealistic and provides virtually identical results.

3. On the basis of the information available a power average can be applied. If enough information is available to perform flow simulations as was done in chapter 5 then this should be done. Otherwise, *expert judgement* or some previous data (from a nearby reservoir or same depositional environment) can be used. Averaging powers would have to be calculated on a case-by-case basis but the following approximations could only improve the estimate:

Power Averaging			
Continuity Horz	Continuity Vert	ω_h (Horizontal)	ω_v (Vertical)
Good	Poor	0.80	0.10
Average	Poor	0.70	0.15
Poor	Average	0.60	0.20
Poor	Good	0.50	0.25

Table 6.1: Some First Estimates of Averaging Powers.

This information has all the character of the qualitative information usually presented by geologists to engineers. However, in estimating the non-linear nature of averaging there is currently no experience that will quantify the property any better.

Conclusions

The following preliminary conclusions can be made regarding the scale averaging of absolute permeability.

A simulated reservoir model (ϕ, K_{horz}, K_{vert}) was used to assess the impact that scale averaging of absolute permeability has on waterflooding performance. The oil production rate and cumulative oil production were found not to be sensitive to the averaging process used. This is due to the initial unimodal distribution of permeability and the reservoir production practice considered. The injection and production rates were fixed while alternate averaging processes were used to generate the absolute permeability data for the reservoir simulator. The fixed total flow rate and the unchanging relative permeability curves caused the measured forecasting variables to be insensitive to the absolute permeability. The sensitive variable was the well pressures and not the flowrates.

It has been shown that if the distribution of permeability is unimodal (ex. lognormal) the block averaged permeability will not be sensitive to the averaging process. The distribution of permeability within homogeneous rock types (ex sandstone) will be unimodal but the distribution of permeability for two component mixtures of sandstone and shale will be bimodal at the scale of measurement. A binary approximation to this bimodal distribution is relevant given the two component aspect of the problem.

Permeability from this binary distribution is averaged into block effective permeabilities. The non-linear averaging process has been modeled as a power average. A power average amounts to transform the data by a power transformation, arithmetically average the transformed data, and then back transform this arithmetic average. This process allows a mapping of the problem of determining the effective absolute permeability to that of determining an averaging power that will identify the effective permeability. The averaging power is then estimated from characteristics of the shales spatial distribution.

The two limiting physical situations are when the shales are aligned perfectly in the direction of flow which leads to an arithmetic average ($\omega = 1$), and when the shales are perfectly aligned opposing flow which leads to a harmonic average ($\omega = -1$). The spatial arrangement of the shales can be inferred from well logs, outcrop data, and possibly from well tests. This information can be used to establish an averaging power that will give an estimate of the block permeability.

The statistical parameter that has been found to predict the averaging power accurately is the indicator correlogram describing the sandstone/shale transitions in the flow direction. More specifically a single parameter, a weighted average of the indicator correlogram values for different distances, can be used. The correlation at short distances is found to influence the averaging power more than the correlation at large distances.

Recommendations for Future Work

No research topic is ever closed and there are many avenues of research that relate to the topic of this thesis. Some of the more interesting and practical aspects of future work include:

1. The technique proposed to estimate the effective absolute permeability (K_e) needs practical validation.
2. The multimodal assumption for the permeability distribution in a heterogeneous media is certainly valid but a collection of permeability distributions from actual data would help support this assumption.
3. A systematic study relating the size of shales, the anisotropy, and the block size could be performed. Only a limited number of tests have been presented here. The statistical parameters of interest could be refined if such a study were to be carried out.
4. The structure of common depositional environments could be studied closely and the features that characterize such environments could be used to

predict appropriate averaging schemes. This would be in line with the approach of Weber(1982).

5. The fluid flow in an oil reservoir is multiphase and this work would have to extend to multiphase flow to be fully applicable in the petroleum industry. There are immediate applications in the field of hydrology and whenever single phase flow is considered. The problems of relative permeability and capillary pressure have yet to be tackled for a truly heterogeneous system.

Certain key aspects of fluid flow in heterogeneous media, must always be kept in mind. The three dimensional aspect of flow studies should be maintained because flow in the ground is inevitably three dimensional and translating results from two dimensions to three dimensions is not a straightforward task. The true aspect of heterogeneity is the presence of two or more rock populations (sandstone/shale or matrix/fractures) and the distribution of flow properties in such a medium is not continuous, hence is not likely to be well described by unimodal, small variance, statistical distribution models.

References

1. Abramowitz, M., and I. Stegun: "*Handbook of Mathematical Functions,*" Dover Pub., New York (1965)

2. Aziz, K., and Settari, A.: "*Petroleum Reservoir Simulation,*" Applied Science Publishers, New York, (1983)

3. Beck, A.E.: "*An Improved Method of computing the thermal conductivity of fluid filled sedimentary rocks,*" Geophysics, 41: 133-144 (1976)

4. Bennion, D.W., Moore, R.G.: "*Effect of Relative Permeability on the Numerical Simulation of the Steam Simulation Process,*" J. Can. Pet. Tech. (March-April 1985) 40-44

5. Chirlin, G.R.: "*Flow Through a Porous Medium with Periodic Barriers or Fractures,*" SPE Journal (June 1985) 358-362

6. Collins, R.E.: "*Flow of Fluids Through Porous Materials,*" Van Nostrand Reinhold, New York (1961)

7. Craft, B.C. and Hawkins, M.F.: "*Applied Petroleum Reservoir Engineering,*" Prentice-Hall Inc, Englewood Cliffs, N.J. (1959)

8. Dagan G.: "*Models of Groundwater Flow in Statistically Homogeneous Porous Formations,*" Water Resour. Res. Vol 15 no 1 pp 47-63 (1979)

9. Dake, L.P.: *Fundamentals of Reservoir Engineering,*" Elsevier, New York, (1978)

10. DeNevers, N,: "*Fluid Mechanics,*" Addison-Wesley Publishing Company, Menlo Park, California, (1977)

11. Desbarats, A.J.: "*Numerical Estimation of Effective Permeability in Sand - Shale Formations,*" Water Resources, In Press (1985)

12. Deutsch, C.V.: "*Estimating Block Effective Permeability with Geostatistics and Power Averaging,*" Submitted to SPE J #015991 (1986)

13. Fogg, G.E.: "*Groundwater flow and sand body interconnectedness in a thick multiple aquifer system,*" Water Resour. Res. Vol 22 no. 5 pp 679-694, Oct. (1986)

14. Freeze R.A.: "*A Stochastic Conceptual Analysis of One Dimensional Groundwater Flow in Nonuniform Homogeneous Media,*" Water Resour. Res. Vol 11 no. 5 pp 725-741, Oct. (1975)

15. Gelhar L.W.: "*Effects of hydraulic conductivity variations on groundwater flows,*" In proceedings 2nd Intl. IAHR symposium on stochastic hydraulics, Lund, Sweden, Intl. Ass. of Hydraulic Research (1976)

16. Gelhar L.W. and Axness C.L.: "*Three Dimensional Stochastic Analysis of Macrodispersion in Aquifers,*" Water Resour. Res. Vol 19 no. 1 pp 161-180, Feb. (1983)

17. Gutjahr A.L., Gelhar L.W., Bakr A.A. and McMillan J.R.: "*Stochastic Analysis of Spatial Variability in Subsurface Flows 2, Evaluation and Application,*" Water Resour. Res. Vol 14 no. 5 pp 953-959, (1983)

18. Grant, F.S. and West, G.F.: "*Interpretation Theory in Applied Geophysics.*" McGraw-Hill, New York,N.Y. (1965)

19. Haldorsen, H.H.: "*Reservoir Characterization Procedures for Numerical Simulation,*" Ph.D. dissertation, Univ. of Texas at Austin, Austin, (1983)

20. Haldorsen, H.H., Chang, D.M.: "*Stochastic Shales: From Outcrop to Simulation Model*" *in Proceedings of the NIPER "Reservoir Characterization Technical Conference", Dallas (May 1985)*

21. Haldorsen, H.H., Lake, L.W.: "*A New Approach to Shale Management in Field-Scale Models,*" SPE Journal (August 1984) 447-457

22. Hammersley J.M. and Welsh D.J.A.: "*Percolation Theory and its Ramifications,*" Contemp. Phys. Vol 21 no 6 pp 593-605 (1980)

23. Hewett, T.A.: "*Fractal Distributions of Reservoir Heterogeneity and their Influence on Fluid Transport,*" SPE Paper 15386, prepared for presentation at the 61st Annual Technical Conference of SPE in New Orleans, LA, October 5-8, 1986

24. Hubbert, M.K.: "*Darcy's Law and other Field Equations of the Flow of Underground Fluids,*" Trans. SPE of AIME, 207, pp 222-239 (1956)

25. Islam, M.R., Bentson, R.G.: "*A Dynamic Method for Measuring Relative Permeability,*" J. Can. Pet. Tech. (Jan - Feb 1986)

26. Johnson, N.L., and S. Kotz: "*Continuous univariate distributions - 1,*" John Wiley & Sons, New York (1970)

27. Journel, A.G.: "*Geostatistics: Models and Tools for the Earth Sciences,*" Math. Geol. (18(1), 1986) 119-140

28. Journel, A.G., Deutsch, C.V., Desbarats, A.J.: "*Power Averaging for Block Effective Permeability,*" SPE Paper 15128, prepared for presentation at the 56th California Regional Meeting of the SPE held in Oakland, CA, April 2-4 1986

29. Journel, A.G., Huijbrects, Ch.J.: "*Mining Geostatistics,*" Academic Press, San Francisco (1978)

30. Journel, A.G., Isaaks, E.H.: "*Conditional Indicator Simulation: Application to a Saskatchewan Uranium Deposit,*" Math. Geol. (16(7), 1984) 685-718

31. Korvin, G.: "*Axiomatic Characterization of the General Mixture Rule,*" Geoexploration, 19:267-276 (1981)

32. Mateker, E.J.Jr.: "*Lithologic predictions from seismic predictions,*" Oil Gas J. Nov 8, 1971 pp 96-100 (1971)

33. Meese, A.D. and Walther, H.C.: "*An investigation of sonic velocities in vugular carbonates,*" 8th SPWLA Symp., Denver

34. Mungan, N.: "*Relative Permeability Measurements using Reservoir Fluids,*" SPE Journal (October 1972) 398-402

35. Pryor, W.A., and K. Fulton: "*Geometry of reservoir type sand bodies in the Holocene Rio Grande delta and comparison with ancient reservoir analogs,*" SPE Preprint 7045, 81-92 (1976)

36. Rzhevsky, V. and Novik, G.: "*The Physics of Rocks,*" Mir Publishers, Moscow (1971)

37. Scheidegger, A.E.: "*Physics of Flow Through Porous Materials,*" 3rd edn., University of Toronto Press, Toronto (1974)

38. Schon, J.: "*Ein Beitrag zur Klassifizierung und Systematik petrophysikalischer Parameter,*" Neue Bergbautechnik, 1: 2-10 (1971)

39. Smith L. and Freeze R.A.: "*Stochastic Analysis of Steady State Groundwater Flow in a Bounded Domain 1: One Dimensional Simulations,*" Water Resour. Res. Vol 15 no. 3 pp 521-528, June (1979)

40. Smith L. and Freeze R.A.: "*Stochastic Analysis of Steady State Groundwater Flow in a Bounded Domain 2: Two Dimensional Simulations,*" Water Resour. Res. Vol 15 no. 6 pp 1543-1559, (1979)

41. Srivastava, R.M.: "*Probabilistic Approaches to the Problem of Calculating Effective Permeability: An Application of Percolation Theory,*" internal report, Dept. of Applied Earth Sciences, Stanford University (February 1985)

42. Srivastava, R.M.: "*Some Notes on the Second - Order Moments of the 3-d Bombing Model,*" internal report, Dept. of Applied Earth Sciences, Stanford University (November 1985)

43. Tegland, E.R.: "*Sand-shale ratio determination from seismic interval velocity,*" 23rd Ann. Midwestern Mtg., SEG, AAPG, Dallas (1970)

44. Warren, J.E., Price, H.S.: "*Flow in Heterogeneous Porous Media,*" SPE Journal (September 1961) 153-169

45. Weber, K.J.: "*Influence of Common Sedimentary Structures on Fluid Flow in Reservoir Models,*" J. Pet. Tech. (March 1982) 665-672

46. Whitaker,S.: "*The Equations of Motion in Porous Media,*" Chem. Eng. Sci., 21, pp 261-300 (1966)

47. Whitaker,S.: "*Advances in Theory of Fluid Motion in Porous Media,*" Indust. and Engineering Chemistry, 61, No 12, pp 14-28 (1969)

48. Woodside, W. and Messmer, J.H.,: "*Thermal conductivity of porous media,*" II. Consolidated Rocks. J. Appl. Phys., 32: 1696-1706 (1961)

Appendix A: Normal Approximation to the Binomial Distribution - Application to Power Averaging

In chapter 4 it was shown that under certain conditions the cumulative distribution function (cdf) for block averaged permeabilities could be approximated by a binomial distribution with the permeability scale depending on the averaging power. Each binomial probability corresponds to a specific volume fraction of shale. If the averaging is to be performed over blocks composed of n units there are $n+1$ possible fractions of shale. There could be $j=0,1,2,3,....,n$ units of shale in a block containing n units. The proportion of shale p_j is binomially distributed with an average volume fraction of shale p. If n becomes large this binomial distribution can be approximated by a normal distribution. The transform from the specific proportion of shale p_j to the permeability is made through a power average. i.e.

$$K_{e_j} = \left[p_j \cdot K_{sh}^{\omega} + (1-p_j) \cdot K_{ss}^{\omega} \right]^{\frac{1}{\omega}} \tag{A.1}$$

where:

$K_{sh} > 0$

$j = 0,1,2,...,n$ = the number of shale units in the block.

K_{e_j} = effective permeability of the block given j shale units.

$p_j = \frac{j}{n}$ = the fractional volume of shale.

ω = the averaging power.

Knowing that p_j is binomially distributed we would like to know the distribution of K_e given an averaging power ω. With n, K_{sh}, K_{ss}, and ω known the distribution of K_e may be determined.

$$F(k) = Prob(K_e \leq k) = F_1(k), \text{ for } \omega \geq 0$$

$$= F_2(k), \text{ for } \omega<0$$

Case 1:

$\omega \geq 0$, where k^ω is an increasing function of k:

$$\begin{aligned} F_1(k) &= Prob\,\{K_e^\omega \leq k^\omega\} \\ &= Prob\,\{p_j\,[K_{sh}^\omega - K_{ss}^\omega] + K_{ss}^\omega \leq k^\omega\} \\ &= Prob\,\{p_j > \frac{k^\omega - K_{ss}^\omega}{K_{sh}^\omega - K_{ss}^\omega} = \frac{K_{ss}^\omega - k^\omega}{K_{ss}^\omega - K_{sh}^\omega} = r\ \} \\ &= Prob\,\{j > n \cdot r\,\} \end{aligned} \tag{A.2}$$

with r being the relative argument.

It is known that j follows a binomial distribution given n and p and that the mean of this random variable is $n \cdot p$, and its variance is: $n \cdot p\,(1-p)$. Considering the normal approximation to the binomial the distribution $F_1(k)$ may now be written in terms of the standard normal cdf:

$$\begin{aligned} F_1(k) &= 1 - G\left(\frac{n \cdot r - n \cdot p}{\sqrt{n \cdot p \cdot (1-p)}}\right) \\ &= 1 - G\left(\frac{r - p}{\sqrt{\frac{p \cdot (1-p)}{n}}}\right) \end{aligned} \tag{A.3}$$

Where G is the standard normal cdf.

Case 2: $\omega<0$, where k^ω is a decreasing function of k:

$$\begin{aligned} F_2(k) &= Prob\,\{K_e^\omega > k^\omega\} \\ &= Prob\,\{p_j\,[K_{sh}^\omega - K_{ss}^\omega] + K_{ss}^\omega > k^\omega\} \\ &= Prob\,\{p_j < \frac{K_{ss}^\omega - k^\omega}{K_{ss}^\omega - K_{sh}^\omega} = r \end{aligned} \tag{A.4}$$

$$= Prob\{j < n \cdot r\} = G\left(\frac{r - p}{\sqrt{\frac{p \cdot (1-p)}{n}}}\right) \qquad \text{(A.5)}$$

The cdf takes a different form for negative averaging powers because K_{sh}^{ω} is greater than K_{ss}^{ω} for $\omega<0$. Regardless of the averaging power, p_j is binomially distributed and the distribution may be approximated by a normal distribution for large n. As shown above the actual expression for the cdf does change for $\omega<0$.

With equations A.3 and A.5 it is possible to compute the cdf of a block average permeability given the required information noted above and assuming that the various hypotheses discussed in chapter four are valid.

Appendix B: Calculation of Continuity Parameters ($\bar{\rho}(L)$):

To assist in predicting the averaging process for permeability some parameters must be devised to capture the spatial arrangement of the shale heterogeneities. Large scale shales will be handled deterministically in the finite difference grid model but the small scale shales can not. The spatial continuity and connectivity of the low permeability zones(shales) and high permeability zones (clean well-sorted sandstone) along with an estimate of the proportion of each component may be used to predict the effective permeability of large scale grid blocks. The continuity parameters derived hereafter are based on a binary model for the permeability field.

The proposed parameter $\bar{\rho}(L)$ may be calculated experimentally, given an indicator grid and an estimate of the range of the variogram defined over the larger stationary volume. Directional variograms are required to provide a range of correlation in each of the coordinate directions.

The spatial variance of $I(x)$ along a length L representing the dimension of the block in one of the coordinate directions may be written. Consider L in the coordinate direction x (ref. Journel and Huijbregts (1978) pp 67):

$$\bar{\gamma}_I(L,L) = \frac{1}{n_x^2} \sum_{i=1}^{i=n_x} \sum_{j=1}^{j=n_x} \gamma_I(x_i - x_j) \qquad \text{(B.1)}$$

The ergodic limit of this spatial variance is the variance of $I(x)$ ie. $p(1-p)$. To obtain a measure of spatial continuity the influence of the proportion of shale should be filtered. By standardizing $\bar{\gamma}_I(L,L)$ to its ergodic limit, the following continuity factor can be defined:

$$\bar{\rho}_{ew}(L) = 1 - \frac{\bar{\gamma}_I(L,L)}{p(1-p)}, \qquad \epsilon\,[0,1] \qquad \text{(B.2)}$$

This is the average shale indicator correlogram along the flow length L (hence the $\bar{\rho}$ notation). The subscript ew implies that the average correlogram is equal

weighted for all lag distances. As the continuity of the shales in a particular direction increases the $\overline{\rho}_{ew}(L)$ will get closer to its upper limit (1.0), as the continuity of the shales in a direction becomes very low, or the block becomes very large, $\overline{\rho}_{ew}(L)$ will approach its lower limit (0.0).

It is desirable to have a measure of continuity that may be used for any size block. In the work that is done here all the block dimensions are relative to the variogram range. As the dimension of the block becomes large (i.e., greater than the variogram range) $\overline{\rho}_{ew}(L)$ will asymptotically approach zero. The lack of correlation at large distances will dominate the calculation of $\overline{\rho}_{ew}(L)$ regardless of the short scale variogram structure.

What seems intuitively reasonable and is indeed the case, is that the correlation at small distances will be more important than the correlation at long distances. So in a situation where an experimental or actual measure of the spatial continuity is to be calculated a better estimate of $\overline{\rho}(L)$ would be weighted such that the short scale structure has more influence. For each lag distance h_l, in a particular coordinate direction, the average correlogram is defined as $\overline{\rho}(h_l)$. The average correlogram is calculated for each coordinate direction independently. The following elaboration will assume the coordinate direction z. The derivation for other coordinate directions is easily made.

The vector h_l is a vector in one of the three coordinate directions (i.e., z) with a magnitude equal to an integer multiple of d_l (ref. figure 5.1), that is: $h_l = n \cdot d_l$, n = integer$< n_z$.

The average correlogram for each lag distance is determined by centering the non-centered covariance and normalizing to its ergodic limit. Each $\rho(h_l)$, $l=0, \ldots . n_z-1$, is given by:

$$\rho(h_l) = \frac{A(h_l) - p^2}{p \cdot (1-p)} \tag{B.3}$$

where $A(h_l)$ is the non-centered covariance given by:

$$A(h_l) = \frac{1}{n_x \cdot n_y \cdot n_z} \sum_{i=1}^{i=n_x} \sum_{j=1}^{j=n_y} \sum_{k=1}^{k=n_z-l} I(x_i, y_j, z_k) \cdot I(x_i, y_j, z_{k+l}) \qquad \text{(B.4)}$$

A weighted sum of each $\rho(h_l)$ with appropriately chosen weights would have the properties that are desired. A weighted sum is written:

$$\overline{\rho}(L) = \sum_{l=0}^{l=n_z-1} \lambda_l \, \rho(h_l) \;, \quad \sum_{l=0}^{l=n_z-1} \lambda_l = 1 \qquad \text{(B.5)}$$

An equal weighted average equal to that given in equation B.2 would result if each λ_l is set to $\frac{1}{n_x}$.

It is considered that after double the variogram range the block effective permeability will not depend on the underlying variogram. This was shown in experiments performed by A.J. Desbarats (1986). This was also verified through experimentation documented in chapter 5. If we impose the condition that beyond two times the variogram range all the weights are set to zero, and that the weighting function will decrease linearly to zero at this point, the following weights may be assigned:

$$\begin{aligned} &\lambda_l = b_1 - b_2 h_l, \quad \text{all } h_l < 2a \\ &\quad a = \text{variogram range} \\ &\quad b_1, b_2 = \text{constants chosen such that } \sum_{l=0}^{l=n_z-1} \lambda_l = 1 \\ &\lambda_l = 0, \quad h_l > 2a \end{aligned} \qquad \text{(B.6)}$$

This system of weights is more justified than the unweighted average that is implicitly assumed in equation B.2. In actual network simulations it has been observed that the correlations $\rho(h_l)$ at small lags h_l are more influential that those at larger lags. Also the weighted $\overline{\rho}(L)$ may be used to predict the power of

averaging more precisely than the unweighted $\overline{\rho}_{ew}(L)$.

A measure of the spatial continuity of $I(x)$ in the plane perpendicular to flow may be similarly calculated. The plane perpendicular to flow will be denoted S. If the flow is vertical (z-direction) the x-y plane will be S. If horizontal flow (in the x-direction) is being considered S will be the y-z plane.

In the numerical modelling of the fluid flow there is no flow in any diagonal directions (except stepwise). For this reason the calculation of $\overline{\rho}(S)$ is essentially a sum of the $\overline{\rho}$ in the two directions defining S. If one was considering vertical flow (S is the $x-y$ plane):

$$\overline{\rho}(S) = \alpha \cdot \sum_{l=0}^{l=n_x-1} \lambda'_l \overline{\rho}(h_l) + (1-\alpha) \cdot \sum_{l=0}^{l=n_y-1} \hat{\lambda}_l \overline{\rho}(h_l) \quad \text{,with:} \tag{B.7}$$

$$\sum_{l=0}^{l=n_x-1} \lambda'_l = \sum_{l=0}^{l=n_y-1} \hat{\lambda}_l = 1.0 \quad \text{,and:}$$

$$\alpha = \frac{L_x}{L_x + L_y}$$

The weights λ'_l and $\hat{\lambda}_l$ are determined in an identical fashion to λ_i given in equation B.6. The expected variogram range in the x and y directions need not be the same. The weight α is introduced to correct for unequal L_x and L_y. It is important to note that if either L_x or L_y is greater than two times the variogram range they should be reset to $2 \cdot a$ for the calculation of α. This is equivalent to calculating $\overline{\rho}(S)$ by summing the contributing $\overline{\rho}(h_l)$ for all lags h_l in the x and y directions.

The $\overline{\rho}$ terms defined above may be calculated for any realization of an indicator grid where the underlying variogram is known or can be estimated. These terms do not capture all the information possible if detailed "real" small scale information is available. However, in practice it will not be possible to have information that can characterize a sand/shale sequence more accurately than

these summary bivariate statistics.

If a variogram model and a block size is provided or alternately if a shale geometry is provided the $\overline{\rho}$ terms may be analytically derived. It should be emphasized here that the $\overline{\rho}$ terms are intended to estimate the averaging power for a particular realization of an indicator grid and not for the general case of a known shale indicator variogram or the specific case of a known shale geometry. However, it is illuminating to briefly consider the development of $\overline{\rho}$ for these two cases. It may be possible to describe a particular reality by one of these ideal situations. Or, if no other knowledge is available the estimated indicator variogram may be the only information available.

The $\overline{\rho}$ terms are developed for an exponential variogram and for ellipsoidal shales (bombing model) in appendices C and D. The connection between experimentally calculated $\overline{\rho}$ terms and the averaging power is covered fully in chapter 5.

Inference of Continuity Parameters

Up until this point the inference of actual $\overline{\rho}$ values has not been discussed. The basic requirement to infer the $\overline{\rho}$ terms is an indicator variogram model. If experimental or actual $\overline{\rho}$ terms are to be determined more information is required.

The most accurate and reliable way to infer an indicator variogram model is to have data at a reasonable scale. The scale and spacing of the data would have to be less than the range of correlation. A variogram inferred from an outcrop in the central Sahara (ref. Desbarats, 1986 quoted by Haldorsen et.al. 1985) was fitted by an exponential model with a 15 m range of correlation in the horizontal direction of the outcrop and a 1 m range of correlation in the vertical direction.

Outcrop data would provide the most direct means to determine appropriate variogram models. Close to some oil fields there may be outcroppings of the same sedimentary units. In northern Alberta (Canada) there is mining of oil sands which provides direct access to the sedimentary structure of oil bearing strata

similar to those of nearby oil fields. It is known that some of these structures contain shale. In any case, a catalog of variograms for specific depositional environments may be constructed. The appropriate variogram can then be selected on this basis if other information is not available.

Well logs would provide the vertical variograms. On the basis of the gamma ray, S.P., or more recently lithology logging (P_e), the down hole shale indicator variogram could be inferred. More precisely the $\overline{\rho}(L)$ in the vertical direction could be calculated. This would provide a method to estimate the averaging process for vertical permeability from well logging. Depending on the direction of the drill hole the averaging process in other directions may also be estimated.

Appendix C: Development of $\overline{\rho}$ for an Exponential Variogram:

Given a variogram model and a block of fixed dimensions it is possible to calculate $\overline{\rho}(L)$ and $\overline{\rho}(S)$ analytically. This has been done for the exponential variogram model with no nugget effect: $\gamma(h) = 1 - e^{(\frac{-3h}{a})}$, with practical range a.

Having determined the mathematical expression for the weighting function $\lambda(h)$ (see equation B.6) and knowing the correlogram function for the exponential variogram we may write $\overline{\rho}(L)$ as a function of the practical range and the block size:

$$\overline{\rho}(L) = \int_0^L \left[\frac{1.0}{2 \cdot a \cdot L - \frac{L^2}{2}} \right] \cdot (2 \cdot a - h) \cdot e^{\frac{-3 \cdot h}{a}} \, dh, \quad L \leq a \tag{C.1}$$

The solution obtained:

$$\overline{\rho}(L) = \left(\frac{2}{36(\frac{L}{a}) - 9(\frac{L}{a})^2} \right) \left[5 + (3\frac{L}{a} - 5)e^{-3\frac{L}{a}} \right] \tag{C.2}$$

This function is plotted on figure C.1.

The testing and implementation was carried out on realizations of indicator networks. The regression developed to predict ω by $\overline{\rho}(L)$ (see chapter 6) is statistical in nature and will not accomodate each particular realization. Thus, if a particular realization is envisaged the $\overline{\rho}(L)$ that corresponds to the particular case should be used and the exponential model defined above should not be used.

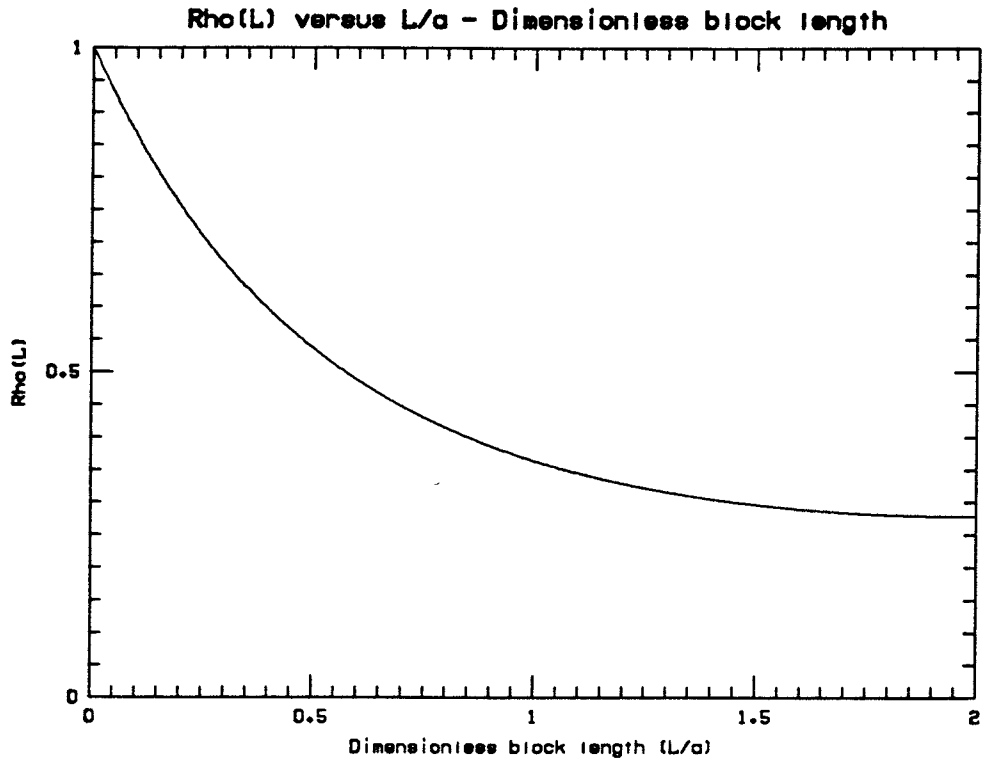

Figure C.1: $\overline{\rho}(L)$ versus Dimensionless Block Length (L/a) for an exponential variogram model of range a.

Appendix D: Development of $\overline{\rho}(L)$ for Poisson Located Ellipsoids

If ellipsoids of fixed geometry (axes: a_x, a_y, a_z; semiaxes: r_x, r_y, r_z) are located in space by a Poisson process it is possible to analytically derive the form of the shale indicator variogram and the weighted indicator correlation in any direction.

This will provide insight as to how the indicator correlation and thus the power of averaging relate to the ellipsoidal geometry of the shales. It is important to note that the initial study on power averaging was carried out using stochastic shales that do not neccesarily have an ellipsoidal shape. Although, the geometric anisotropy used would tend to create shale bodies in with this shape.

Appendix E shows the derivation of the indicator variogram for spheres placed by a Poisson process in a random media. It has been shown (Srivastava, 1985) that the indicator variogram for an indicator field generated by this process is given by:

$$\gamma_I(h') = p_1(1-p_1^{Sph(h')}) \tag{D.1}$$

where:

$\gamma_I(h')$ = indicator variogram of $I(x)$.

$p_1 = 1-p$ = volume fraction of sandstone.

h' = lag distance in a given direction (vector distance).

a' = diameter of the imbedded spheres.

$Sph(h')$ = spherical variogram function

$$= \frac{3}{2}\frac{h'}{a'} - \frac{1}{2}\left(\frac{h'}{a'}\right)^3, \quad h' < a'$$

$$= 1, \quad h' \geq a'$$

To account for the presence of ellipsoids (not spheres) it is necessary to correct for the geometric anisotropy. A standardized range and lag measurement

may be used:

$$a = a_x \tag{D.2}$$

$$h = \sqrt{h_x^2 + \left(h_y \frac{a_x}{a_y}\right)^2 + \left(h_z \frac{a_x}{a_z}\right)^2} \tag{D.3}$$

This is equivalent to transforming the ellipsoids into spheres.

The variogram and correlogram may be written as functions of the a and h given above:

$$\gamma_I(h) = p_1(1 - p_1^{Sph(h)}) \tag{D.4}$$

$$\rho(h) = \frac{p_1^{Sph(h)} - p_1}{(1 - p_1)} \tag{D.5}$$

The complete bivariate statistics of an indicator field generated by ellipsoidal shales in a sandstone matrix are now known. The proposed continuity factor $\overline{\rho}(L)$ may be calculated. The calculation of $\overline{\rho}(L)$ may be written as an integral (i.e., assume infinite discretization):

$$\overline{\rho}(L) = \int_0^L \lambda(h)\rho(h)dh \quad , \qquad L \leq 2 \cdot a \tag{D.6}$$

The weighting function $\lambda(h)$ is a linear weighting of $\rho(h)$ that decreases with increasing h to become nought at $2 \cdot a$ and beyond:

$$\lambda(h) = b - c \cdot h \quad \text{,where:} \tag{D.7}$$

b and c = constants

h = lag distance

The conditions on $\lambda(h)$ may be written:

$$\int_0^L \lambda(h)dh = 1 \quad , \qquad L \leq 2 \cdot a \quad \text{,and} \tag{D.8}$$

$$\lambda(h) = 0 \text{ at } h = 2 \cdot a$$

For these conditions the constants b and c are found to be:

$$b = \frac{2 \cdot a}{2 \cdot a \cdot L - \frac{L^2}{2}}, \text{ and} \qquad (D.9)$$

$$c = \frac{1}{2 \cdot a \cdot L - \frac{L^2}{2}}$$

Substituting into equation D.4 the following analytical expression for $\overline{\rho}(L)$ is found:

$$\overline{\rho}(L) = \int_0^L \left[\frac{1}{2 \cdot a \cdot L - \frac{L^2}{2}} \right] (2 \cdot a - h) \left[\frac{p_1^{Sph(h)} - p_1}{1 - p_1} \right] dh \qquad (D.10)$$

The author being reluctant to perform the integration required to obtain a closed form solution has solved the integral for various L and a values on a computer. A plot of $\overline{\rho}(L)$ versus the dimensionless block length $\frac{L}{a}$ is shown on figure D.1.

Remarks:

1. The $\overline{\rho}(L)$ continuity term used is now a function of the volume fraction of shale in the mixture. This was not suspected from the previous work. However, the dependence of $\overline{\rho}(L)$ on p is very small, the form of the solution is identical for all p. Figure D.1 corresponds to $p = 0.2$ with $\overline{\rho}(L)$ reaching a minimum of 0.312. Other runs were made with different proportions of shale, at $p = 0.1$ the minimum would be 0.319, or if $p = 0.3$ the minimum would have been 0.305. This does not have an effect on the results presented in this study, although this result may be interesting for other more detailed studies.

2. In theory, the correlation does not change beyond the variogram range. In practice the observed correlation up to double the underlying variogram range is found to be important. This is why the weighting scheme is set up

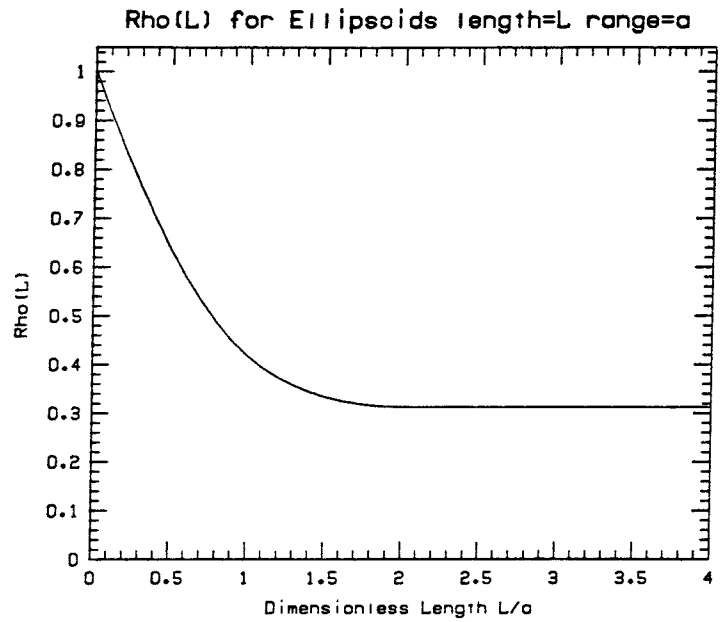

Figure D.1: $\overline{\rho}(L)$ versus dimensionless block length $\frac{L}{a}$ for ellipsoidal shales. Length of Block $=L$. Axis of ellipsoid in direction $(L) = a$.

to decrease to nought at double the variogram range. With the weighting system used the theoretical $\overline{\rho}(L)$ will change between the range and double the range.

Appendix E: Variogram Model for Poisson Located Ellipsoids

This presentation is extracted from an internal note by R. Mohan Srivastava (November, 1985). The 3-d bombing model is a process where spheres of equal radius r and diameter a have their centers located in space randomly according to a Poisson process. In this development an indicator $I(x)$ will be defined as 0 if the point falls inside a sphere and 1 if it falls outside. The variogram may be written:

$$\gamma(h) = C(0) - C(h)$$

$$= p_1(1-p_1) - C(h)$$

where p_1 is the probability that the indicator at a point is 1 (i.e. the volume fraction outside the spheres). The covariance function is defined as follows:

$$C(h) = E[I(x) \cdot I(x+h)] - p_1^2$$

$$\gamma(h) = p_1(1-p_1) - (E[I(x) \cdot I(x+h)] - p_1^2)$$

$$= p_1 - E[I(x) \cdot I(x+h)]$$

There are only four outcomes of $I(x)$ and $I(x+h)$:

$$I(x) = 0, \; I(x+h) = 0$$

$$I(x) = 0, \; I(x+h) = 1$$

$$I(x) = 1, \; I(x+h) = 0$$

$$I(x) = 1, \; I(x+h) = 1$$

Only the last of these will produce a non-zero product, and its product is always 1, therefore:

$$E[I(x) \cdot I(x+h)] = p_{11}(h)$$

where p_{11} is the probability that both $I(x)$ and $I(x+h)$ equal 1.

$$\gamma(h) = p_1 - p_{11}(h)$$

If spheres with radius r have their centers laid down according to a Poisson process in a volume V, then the number of spheres can be calculated from the volume fraction that the spheres span. The number of centers falling in a volume v follows a Poisson distribution with parameter av, where

$$p_1 = e^{-a\frac{4}{3}\pi r^3}$$

$$a = \frac{-ln\,(p_1)}{\frac{4}{3}\pi r^3}$$

The probability that both indicators are 1 is then

$$p_{11}(h) = Prob\,[I(x)=1 \cap I(x+h)=1]$$

$$= Prob\,[I(x)=1 \mid I(x+h)=1]\cdot Prob\,[I(x+h)=1]$$

$$= p_1 \cdot Prob\,[I(x)=1 \mid I(x+h)=1]$$

For $h > a$, $I(x)$ and $I(x+h)$ are independent and $p_{11}(h) = p_1^2$.

For $h < a$,

$$Prob\,[I(x)=1 \mid I(x+h)=1] = Prob\,[no\ centers\ exist\ in\ V(x) \cap (V(x+h))^c]$$

$$= e^{-av(h)}$$

Where $v(h)$ is the shaded region on figure E.1.

$$v(h) = \pi r^2 h - \frac{\pi h^3}{12}$$

$$p_{11} = p_1 \cdot e^{-av(h)}$$

$$= p_1 \cdot e^{\left[\frac{\ln p_1}{\frac{4}{3}\pi r^3}(\pi r^2 h - \frac{\pi h^3}{12})\right]}$$

$$= p_1 \cdot p_1^{\frac{3}{4}\frac{h}{r} - \frac{1}{16}\frac{h^3}{r^3}}$$

$$= p_1 \cdot p_1^{\frac{3}{2}\frac{h}{a} - \frac{1}{2}(\frac{h}{a})^3}$$

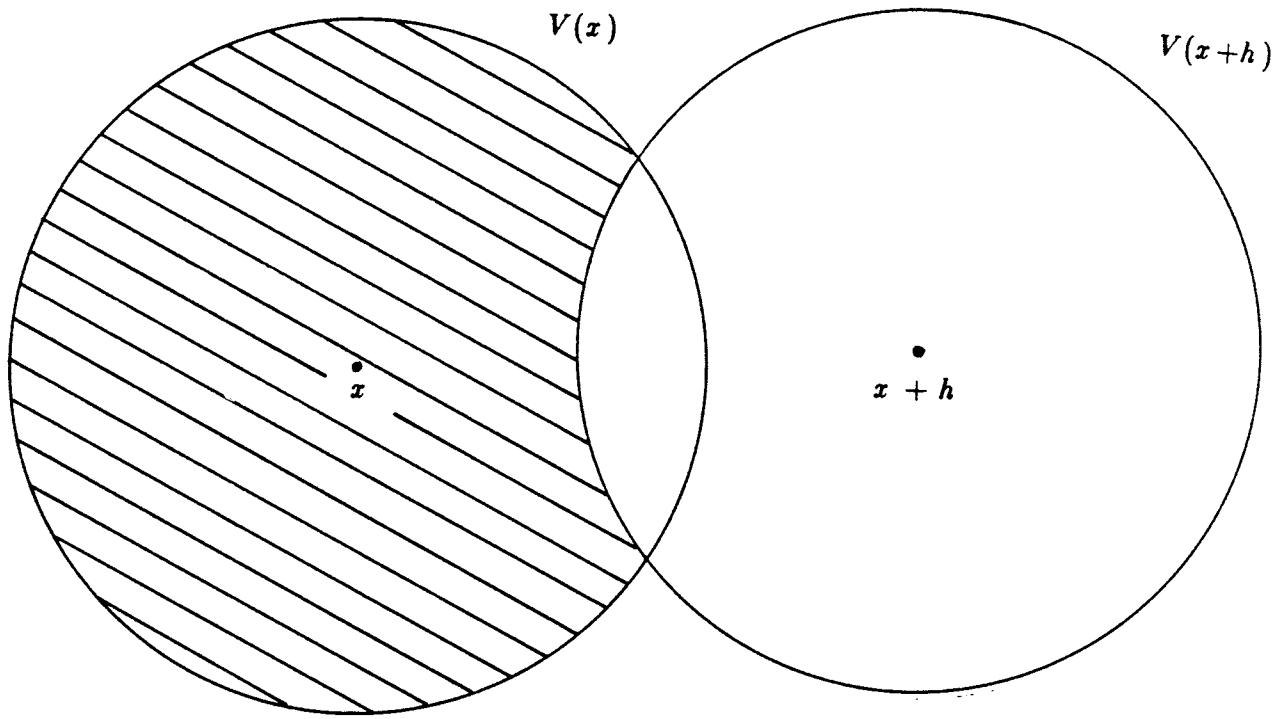

Figure E.1: The area $v(h)$ noted in Appendix E is shown.

$$= p_1 \cdot p_1^{Sph(h)}$$

where Sph(h) is the spherical variogram function.
The variogram model can now be written as:

$$\gamma(h) = p_1 - p_1^2 = p_1(1-p_1) \qquad \text{for } h > a$$

$$= p_1 - p_{11}(h) \qquad \text{for } h \leq a$$

$$= p_1 - p_1 \cdot p_1^{Sph(h)}$$

$$= p_1(1 - p_1^{Sph(h)})$$

The variogram model expressed above is in a form similar to the familiar $p(1-p)$ with the exponent simply the spherical variogram model. This form suggests what the corresponding variograms should be for analagous processes in different dimensions. In 1D the exponent becomes a linear variogram up to the range a; in 2D the exponent becomes the circular variogram. In any dimension the exponent should be the corresponding hyperspherical variogram function. This model is used in chapter 4 of this thesis where different continuity parameters are calculated for ellipsoids.

It should be noted that the variogram is asymmetric (i.e. The variogram of the pores is not the same as the variogram of the spheres.

Appendix F: Shortest Flow Path (SFP) Statistics

Within a three dimensional sandstone/shale sequence the effective permeability is determined by the available paths in sandstone for the fluid to move through the sequence. Some statistics that attempt to capture this information should be very helpful in predicting the block effective permeability. In practice these statistics will be more difficult to infer than the indicator correlation discussed previously but may be calculated on the basis of a digitized geologic drawing or geometric simulation results. Starting from any fixed point on the face of the 3-d block, which the fluid element is to pass through, there is a shortest distance to reach the opposing face. This distance may be calculated for any specific point on the input face of the reservoir block.

So, a 2-d array of "shortest flow path" measures is available. There are certain summaries of this array that may be useful in predicting flow properties. Some evident summaries include:

1. An unobstructed flow path is a path where the fluid element can move from one end of the block to the other without being diverted around a shale obstacle. The proportion of the 2-d array of shortest flow path measures that are unobstructed is a useful summary.
2. Some of the flow paths will be infinite because they have no way to reach the other side of the block within the sandstone. The proportion of infinite flow paths is another useful summary.
3. The clustering of shortest flow paths - creating channels for flow. It should be possible to determine a critical flow length beyond which the fluid path is too tortuous. The clustering of shortest flow paths that are less than this critical length may be described by a correlogram of an indicator which is created on the basis of this critical flow path length.

Calculation Procedure:

Given a 3-d rectangular network that is filled with either sandstone or shale the goal is to compute the shortest flow path that a fluid element must take to get from a fixed point on one face to any point on the other face. Certain assumptions are required:

1. The fluid element must begin in sandstone. If a starting point is in shale the starting point must be moved.
2. The shortest *unobstructed* flow path will be a path directly from the starting point to an opposite point on the other end, hence of length equal to the length of the block in the flow direction. If a shale obstacle is reached the fluid must move (in sandstone) around the object.
3. If the fluid element can no longer go forward or in any perpendicular direction the flow path is assigned an infinite value.

It is easy to see that the process described above may not always return the shortest flow path. The decision of which direction to take when a shale is reached may affect what happens in the next step. If the network is large the effect of such previous decisions is very important. At the limit there are almost an infinite number of paths that may be taken but there is only one shortest distance. This shortest distance can be approximated by considering (sampling) several flow paths. On the basis of some experimentation the following algorithm was retained to obtain the "shortest" flow path with a reasonable probability of success in all cases (begin with SFP=0):

Note: a flow chart is shown on figure F.1.

1. Begin in sandstone or move vertically away from the starting point if it is in shale (SFP=SFP+1). The restriction to a vertical movement is a physical constraint of the particular flow simulation used. The fluid is injected through vertical wells and the fluid is assumed to enter the system through a vertical column.

One Flow Distance Calculation

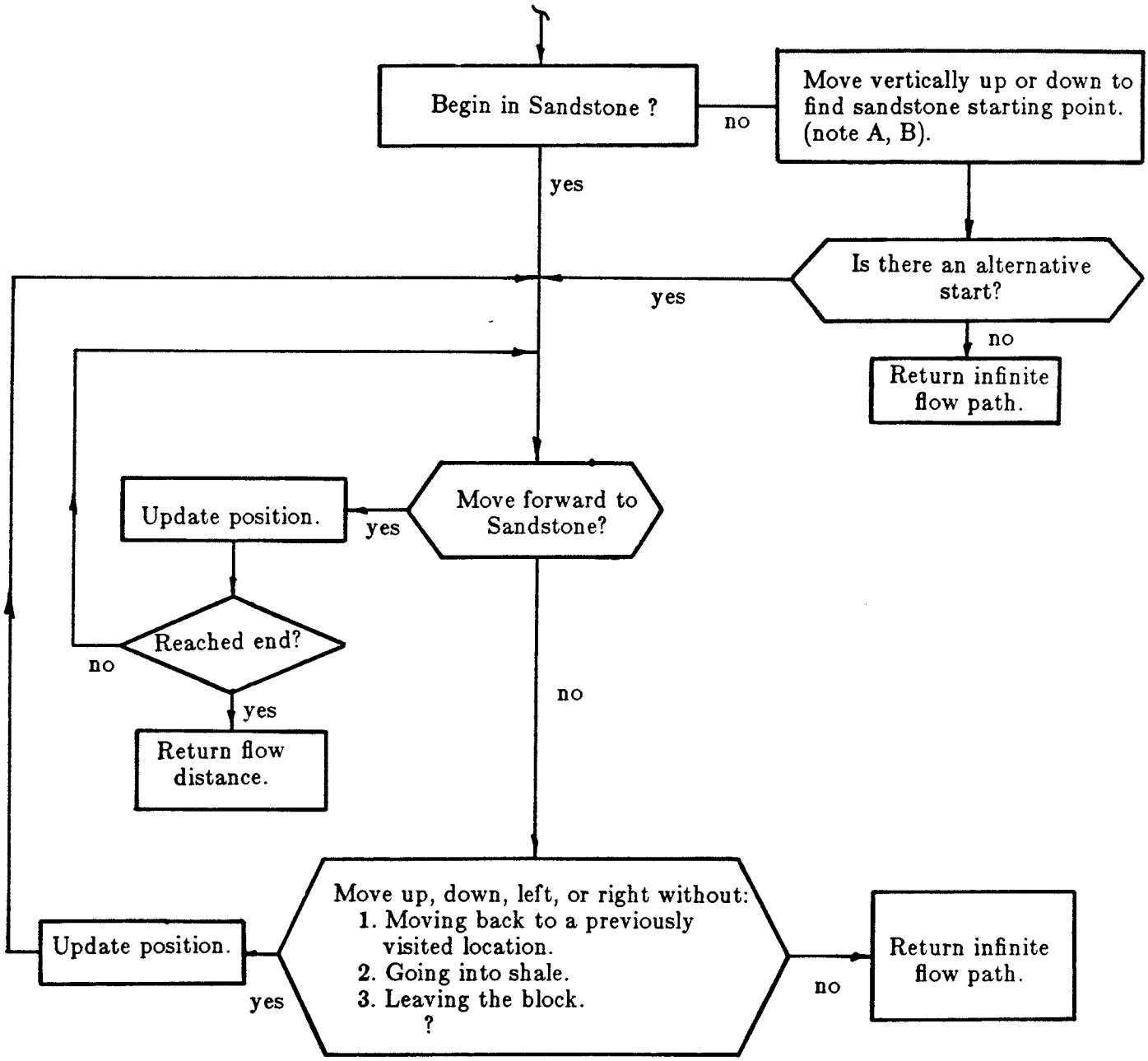

NOTE:

A. If there are multiple possibilities for movement the ties are broken randomly.

B. Consider a vertical well bore connecting the blocks.

Figure F.1: Flowchart showing the procedure to calculate the shortest flow path starting from any point on the end of a 3-d indicator grid.

2. Try to move forward in sandstone. If the path is blocked, try to move in a perpendicular direction, as long as the move will not place the current position in a sub-block that has been previously passed through. If more than one alternative site is available, break the tie by drawing a random number. If there are no possible moves - return an infinite flow path. Otherwise, move(SFP=SFP+1) and go back to the start of step two.
3. This procedure will return either a flow path distance (possibly not minimal) or an infinite flow distance.
4. This procedure can be repeated with different random number seeds as many times as required. Repeating the procedure with a different random number seed causes the breaking of ties to be done differently. If this is repeated enough times the minimum distance found will likely be the true shortest distance.

There are certain geometries of shale obstructions for which this algorithm will not return a finite flow path even though one may exist. The fluid element is not capable of looking more than one step ahead and fore-seeing a trap. One can imagine a situation where a shale is reached and no perpendicular direction is available but if the fluid element had moved prior to reaching the shale it would have succeeded to reach the opposite face. This is a rare case for the situations that will be considered here. This is due to the low proportion of shale typically present and the simulation of ellipsoidal shales rather than a convoluted geometry that may create traps more readily.

The remaining question is: How many calculations are sufficient to obtain reasonable estimates of the shortest flow path? To test the method a difficult test case has been selected. The test case is difficult due to the alignment of the shales perpendicular to the direction of flow and the high volume fraction of shale. The test grid network has the following properties:

1. 20 nodes in the flow direction, 10 nodes in each perpendicular direction for a total of 2000 nodes.
2. 35% of the blocks are shale.
3. A very large number of alternative paths are thus possible.

Given such a difficult test network documented above, the SFP calculation has been made. The 35% shale have been placed to simulate vertical flow (i.e., the maximum continuity is in the two directions perpendicular to flow).

There are 100 possible starting points for the flow calculation. At each of these starting points the flow calculation must be performed a number of times so that the *shortest* flow path can be found or reasonably approximated. The shortest flow path for a node is the minimum flow path for all the attempts from that node.

With the network used as a test there are a number of starting nodes that do not have a finite flow path. If not enough attempts are made this proportion will be overestimated. Figure F.2 shows the proportion of non-infinite flow paths versus the number of attempts made from each node. The solution appears stable after 100 iterations. The calculations for a certain number of attempts has been made independently of the others, i.e., the result for 51 iterations is not the result for 50 iterations plus one additional iteration.

It is not only important to estimate the proportion of non-infinite flow paths. The calculated flow distance for the finite flow paths should also be the *true* shortest. Figure F.3 shows the average flow distance (non-infinite paths only) versus the number of attempts from each starting node. This average should reach a minimum as each of the shortest flow paths is found correctly. This result also appears stable after 100 iterations.

This test case is more difficult than the cases considered in practice (see chapter 5), so it is evident a reliable calculation of the SFP statistics can be made

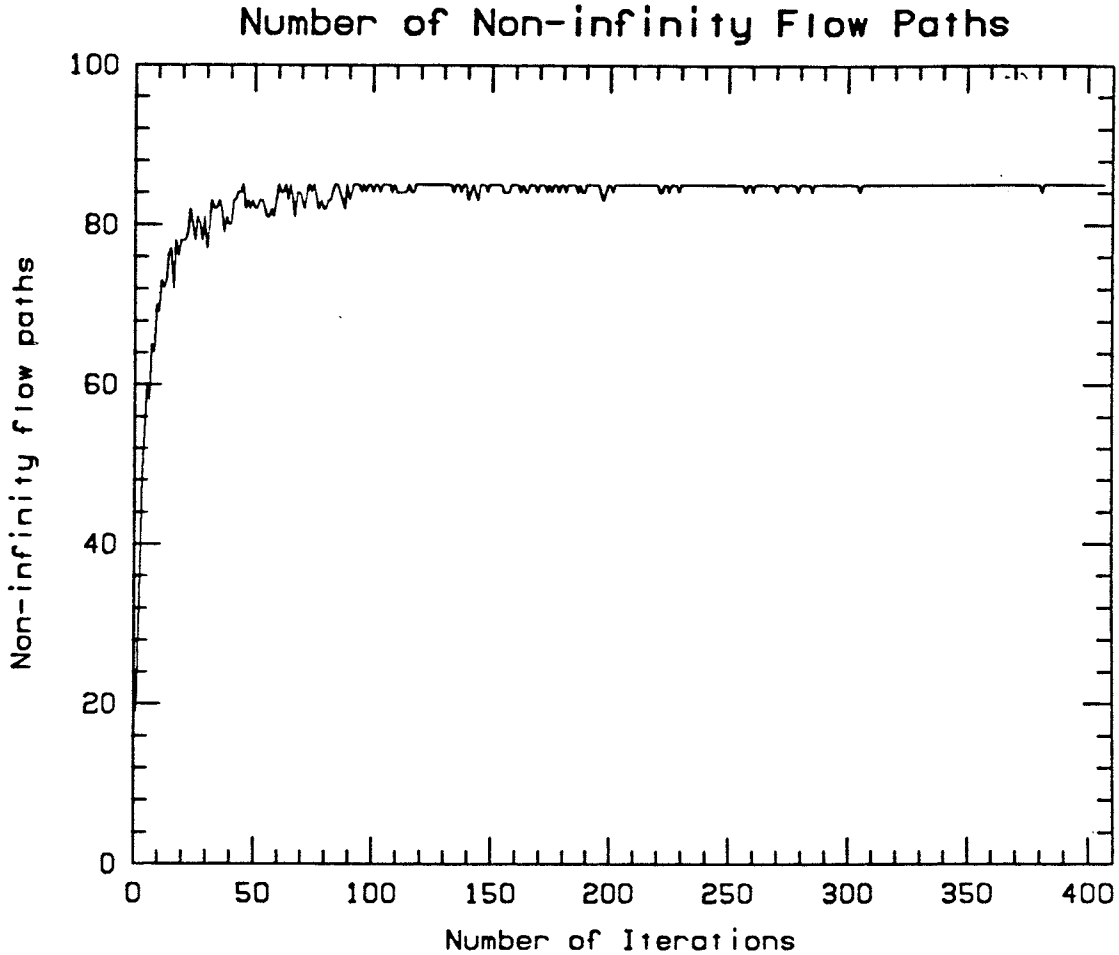

Figure F.2: The proportion of starting points for a particular network realization yielding non-infinite flow paths. The sfp calculation is performed for an increasing number of iterations (1 through 400). Each trial (i.e., given number of iterations) was carried out on the same network independently of the other trials. The calculation is stable after 100 iterations.

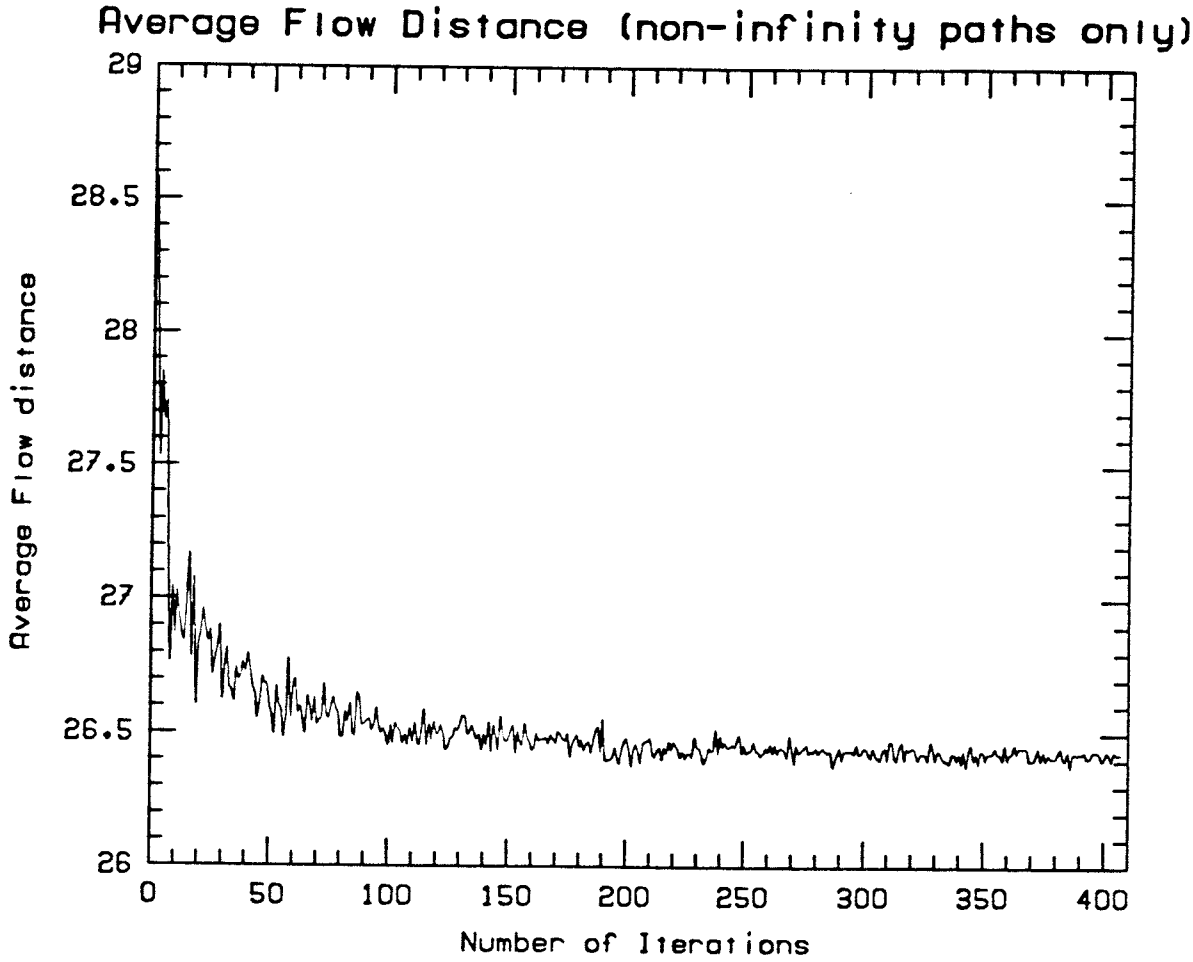

Figure F.3: The average of the shortest flow paths (for the non-infinity cases) versus the number of attempts made from each point on the face perpendicular to flow. The shortest flow path for each of the 100 (10x10) nodes are averaged and plotted versus the number of iterations used to find the shortest flow path (1 to 400). Only the non-infinite flow paths are averaged.

is a suitably large number of iterations is used (i.e., 100).

The problem with the measurement of the shortest flow path statistics as discussed here is that a model for the sandstone/shale network is necessary. How could such a model be obtained? If a simulation program (ex. bombing model) is used the output is only as good as the data that is input into the simulation program. The only direct way to inform such a model is through outcrop data or through extrapolation from other sedimentary formations. In many respects these SFP statistics are too rich for the task at hand. These statistics are discussed more in chapter 5.

Appendix G: Fortran77 Subroutines

Various computerized schemes have been used in this thesis. Often in practice more time is spent on developing good working programs than in conceptualizing the problem. This is why the following subroutines have been provided. The subroutines have been tested and used through the course of the thesis. No extra effort has been made to optimize the computer coding, rather, the simplest possible programming is used. The following fortran77 subroutines are appended:

1. RHOL - Subroutine to calculate the indicator correlation in the three primary directions of a 3-d indicator grid.
2. SFP - Subroutine to compute the 2-d array of shortest flow paths given a 3-d array of indicators. Some summaries of the shortest flow paths are also returned.
3. RAND - Subroutine to compute random numbers uniformly distributed between 0 and 1.
4. OMEGA - Subroutine to determine the averaging power from the effective permeability, the sandstone permeability, the shale permeability, and the proportion of shale.
5. GAUSCDF - This function computes the value of the cdf for a gaussian probability distribution.

```
      subroutine rhol(in,name,pmssh,pmssv,pmshh,pmshv,lsumm)
c-----------------------------------------------------------------
c
c      CALCULATE THE SUMMARY STATISTICS OF AN INDICATOR GRID
c      ****************************************************
c
c The summary characteristics of a 3-d indicator grid are calculated.
c  In particular the indicator correlation for all lags in the
c  three principal directions are computed.
c
c NOTES:
c  1. The correlation for the first 10 lags are output in this
c     version of the subroutine. This can be changed easily in the
c     code if more or less are desired.
c
c INPUT:
c  1. The folowing arguments are passed in blank common:
c        psh      = The proportion of shale (1's).
c        nx,ny,nz = The size of the grid in thex,y, and z directions.
c        n        = nx*ny*nz = total number of units.
c        ptar     = The target proportion of shale (not used).
c        nxed,y,z = The semiaxis of the ellipsoids generated.
c        sed      = The random number seed that was used to generate
c                   the grid.
c  2. in(nx,ny,nz) = The indicator grid (1's or 0's).
c  3. name = the name associated with the run.
c  4. pmssv = The vertical sandstone permeability.
c  5. pmssh = The horizontal sandstone permeability.
c  6. pmshv = The vertical shale permeability.
c  7. pmshh = The horizontal shale permeability.
c  8. lsumm = 1 if final summary requested, =0 if not.
c
c OUTPUT:
c  1. Summary information is written into a file called "name.summ1"
c     This information if for the single network considered.
c  2, The same information is written to an intermediate summary
c     file where summaries for various runs can be saved.
c     This file should be opened (unit 15) prior to calling the
c     subroutine. The format can be found at the end of this program.
c
c AUTHOR: Clayton  Deutsch                    DATE: January 1987
c
c-----------------------------------------------------------------
      dimension in(100,25,25),rhox(50),rhoy(50),rhoz(50),num(40)
      character name*4,blank*4,appl*6,filel*10
      common psh,nx,ny,nz,n,ptar,nxed,nyed,nzed,sed
      data blank/'    '/,appl/'.summ1'/
c
c The file where the readable summary is written:
c
```

```
        file1=name//app1
        open(10,file=file1)
c
c Compute the indicator correlation in the X - DIRECTION
c
        nlagx=nx-1
        do 10 lag=1,nlagx
        acov=0.0
        npairs=0
        do 11 j=1,ny
        do 12 k=1,nz
        do 13 i=1,nx
        index=i+lag
        if(index.gt.nx) go to 13
        acov=acov+in(i,j,k)*in(index,j,k)
        npairs=npairs+1
13         continue
12         continue
11         continue
        acov=acov/npairs
        rhox(lag)=(acov-(psh*psh))/(psh*(1.0-psh))
10     continue
        range=float(2*nxed+1)
        call wtrho(rhox,range,nlagx,wtrx,ewrx)
c
c Compute the indicator correlation in the Y - DIRECTION
c
        nlagy=ny-1
        do 30 lag=1,nlagy
        acov=0.0
        npairs=0
        do 31 i=1,nx
        do 32 k=1,nz
        do 33 j=1,ny
        index=j+lag
        if(index.gt.ny) go to 33
        acov=acov+in(i,j,k)*in(i,index,k)
        npairs=npairs+1
33         continue
32         continue
31         continue
        acov=acov/npairs
        rhoy(lag)=(acov-(psh*psh))/(psh*(1.0-psh))
30     continue
        range=float(2*nyed+1)
        call wtrho(rhoy,range,nlagy,wtry,ewry)
c
c Compute the indicator correlation in the Z - DIRECTION
c
        nlagz=nz-1
```

```
      do 50 lag=1,nlagz
      acov=0.0
      npairs=0
      do 51 j=1,ny
      do 52 i=1,nx
      do 53 k=1,nz
      index=k+lag
      if(index.gt.nz) go to 53
      acov=acov+in(i,j,k)*in(i,j,index)
      npairs=npairs+1
53       continue
52       continue
51       continue
      acov=acov/npairs
      rhoz(lag)=(acov-(psh*psh))/(psh*(1.0-psh))
50    continue
      range=float(2*nzed+1)
      call wtrho(rhoz,range,nlagz,wtrz,ewrz)
c
c
      write(10,100)name
100   format(25x,'RUN # ',a10)
      write(10,*)blank
      write(10,99)nx,ny,nz
99    format('Grid size: nx= ',i2,' ny= ',i2,' nz= ',i2)
      write(10,101)pmssh,pmssv
101   format('Permeability of sandstone horz=',f6.1,' vert=',f6.1)
      write(10,102)pmshh,pmshv
102   format('Permeability of shale     horz=',f6.2,' vert=',f6.2)
      write(10,98)sed
98    format('Random Number Seed =',f12.1)
      write(10,*)blank
      write(10,103)psh,ptar
103   format('Proportion of shale = ',f6.4,' Target = ',f6.4)
      write(10,*)blank
      write(10,104)
104   format('Ellipsoidal Shales:')
      write(10,105)nxed
      write(10,106)nyed
      write(10,107)nzed
105   format(2x,'range in x direction = ',i2)
106   format(2x,'range in y direction = ',i2)
107   format(2x,'range in z direction = ',i2)
      write(10,*)blank
      write(10,108)
108   format('Indicator Correlation:')
      write(10,*)blank
      rho1=1.0
      do 5 i=1,30
      num(i)=i-1
```

```
5       continue
c
c  X - DIRECTION
c
        write(10,*)blank
        write(10,109)
109     format(2x,'X - Direction:')
        write(10,110)ewrx
        write(10,111)wtrx
        write(10,112)rhox(1)
        write(10,*)blank
110     format(4x,'Equal Weighted = ',f6.4)
111     format(4x,'      Weighted = ',f6.4)
112     format(4x,'     First lag = ',f6.4)
c
c  Y - DIRECTION
c
        write(10,118)
118     format(2x,'Y - Direction:')
        write(10,110)ewry
        write(10,111)wtry
        write(10,112)rhoy(1)
        write(10,*)blank
c
c  Z - DIRECTION
c
        write(10,121)
121     format(2x,'Z - Direction:')
        write(10,110)ewrz
        write(10,111)wtrz
        write(10,112)rhoz(1)
        write(10,*)blank
c-------------------------------------------------------------
c           WRITE OUT TO INTERMEDIATE FILE - SUMMARY
c-------------------------------------------------------------
        write(15,999)name,sed,nxed,nyed,nzed,psh
999     format(a4,2x,f9.0,2x,i3,2x,i3,2x,i3,2x,f5.3)
        write(15,998) (rhox(i),i=1,5)
998     format(1x,5(1x,f6.4))
        write(15,998) (rhox(i),i=6,10)
        write(15,998) (rhoy(i),i=1,5)
        write(15,998) (rhoy(i),i=6,10)
        write(15,998) (rhoz(i),i=1,5)
        write(15,998) (rhoz(i),i=6,10)
c
c
c
        return
        end
c
```

```
c                              WTRHO
c                              *****
c
      subroutine wtrho(rh,range,nd,wtr,ewr)
c-----------------------------------------------------------------------
c SUBROUTINE TO CALCULATE THE WEIGHTED INDICATOR CORRELATION
c  GIVEN THE INDICATOR CORRELATION FOR EACH LAG AND THE RANGE.
c
c INPUT:
c  1. rh(i) = The indicator correlation function.
c  2. range = The range to be used in the weighting.
c  3. nd    = The size of the grid to use for calculation.
c
c OUTPUT:
c  1. wtr  = The weighted indicator correlation.
c  2. ewr  = The equal weighted correlation.
c
c-----------------------------------------------------------------------
      dimension rh(50)
      nrang=ifix(range+0.5)
      swtrx=0.0
      if(nrang.le.1) then
      wtr=rh(1)
      do 10 k=1,nd
10     swtrx=swtrx+rh(k)
      ewr=swtrx/float(nd)
      return
      endif
      alamt=0.0
      blamt=0.0
      blam=1.0
      do 20 i=1,nd
      if(i.gt.nrang) then
      alam=0.0
      else
      alam=float((-1/nrang)*i+1)
      endif
      swtrx=swtrx+alam*rh(i)
      alamt=alamt+alam
      blamt=blamt+blam*rh(i)
20    continue
      ewr=blamt/float(nd)
      if(alamt.le.0.0) alamt=0.01
      wtr=swtrx/alamt
c
c
c
      return
      end
```

```
      subroutine sfp(nx,ny,nz,in,niter,nsfp,nsfpmn,nninf,sfpavg,sed)
c-----------------------------------------------------------------------
c
c            CALCULATE THE SHORTEST PATH FOR A 3-D NETWORK
c            *********************************************
c
c NOTES:
c  1. x is the flow direction
c  2. z is the vertical direction
c
c INPUT:
c  1. nx,ny,nz      = size of the grid in the x,y, and z directions
c  2. in(nx,ny,nz)  = indicator network (1=impermeable, 0=permeable)
c  3. niter         = number of iterations for each node
c
c OUTPUT:
c  1. nsfp(ny,nz)   = array of shortest flow paths
c  2. nsfpmn        = number of minimum "shortest flow paths"
c  3. nninf         = number of non-infinity flow paths
c  4. sfpavg        = average shortest flow path (non-infinity)
c
c AUTHOR: Clayton Deutsch                          DATE: January 1987
c-----------------------------------------------------------------------
      dimension in(100,25,25),nsfp(25,25),vector(1),nsel(4)
      common /unusual/itab(55),n1,n2,nseed
      integer stfg
c
c
c
      nrand=1
      call rand(sed,nrand,vector)
      seed=0.0
c
c
c
      nsfpmn=0
      inf=9999
      do 1 jblk=1,ny
      do 2 kblk=1,nz
      nsfp(jblk,kblk)=inf
      do 3 iter=1,niter
      stfp=1
            icur=1
      jcur=jblk
      kcur=kblk
c
c                 GET A SANDSTONE STARTING PLACE
c
      if(in(icur,jcur,kcur).eq.1) then
            ihope=0
```

```
99              ihope=ihope+1
                if(ihope.ge.5) then
                stfp=inf
                go to 4
                endif
                        kt1=kcur+ihope
                kt2=kcur-ihope
                ikt1=1
                ikt2=1
                if(kt1.gt.nz) then
                        ikt1=0
                go to 95
                endif
                if(in(icur,jcur,kt1).eq.1) ikt1=0
95              if(kt2.le.0) then
                ikt2=0
                go to 96
                endif
                if(in(icur,jcur,kt2).eq.1) ikt2=0
96              continue
                kup=-1
                if(ikt1.eq.1.and.ikt2.eq.1) then
                call rand(seed,nrand,vector)
                ipick=ifix(2.0*vector(1))
                if(ipick.eq.0) kup=kt1
                if(ipick.eq.1) kup=kt2
                else
                if(ikt1.eq.1) kup=kt1
                if(ikt2.eq.1) kup=kt2
                endif
                if(kup.eq.-1) go to 99
                stfp=stfp+ihope
                kcur=kup
        else
                continue
        endif
c
c                       MOVE FORWARD TO THE END
c
        jpast=jcur
        kpast=kcur
98      it=icur+1
        if(in(it,jcur,kcur).eq.0) then
        icur=it
        stfp=stfp+1
        if(it.eq.nx) go to 4
        go to 98
        endif
c
c                       MUST MOVE AROUND SHALE
```

```
c
      jt1=jcur-1
      jt2=jcur+1
      kt1=kcur-1
      kt2=kcur+1
      ijt1=1
      ijt2=1
      ikt1=1
      ikt2=1
      if(jt1.le.0.or.jt1.eq.jpast) then
      ijt1=0
            go to 93
      endif
      if(in(icur,jt1,kcur).eq.1) ijt1=0
93    if(jt2.gt.ny.or.jt2.eq.jpast) then
      ijt2=0
      go to 92
      endif
      if(in(icur,jt2,kcur).eq.1) ijt2=0
92    if(kt1.le.0.or.kt1.eq.kpast) then
      ikt1=0
      go to 91
      endif
      if(in(icur,jcur,kt1).eq.1) ikt1=0
91    if(kt2.gt.nz.or.kt2.eq.kpast) then
      ikt2=0
      go to 94
      endif
      if(in(icur,jcur,kt2).eq.1) ikt2=0
94    continue
c
      iii=0
      if(ikt2.eq.1) then
      iii=iii+1
      nsel(iii)=1
      endif
      if(ijt2.eq.1) then
      iii=iii+1
      nsel(iii)=2
      endif
      if(ikt1.eq.1) then
      iii=iii+1
      nsel(iii)=3
      endif
      if(ijt1.eq.1) then
      iii=iii+1
      nsel(iii)=4
      endif
      if(iii.eq.0) then
      stfp=inf
```

```
          go to 4
          endif
          call rand(seed,nrand,vector)
          index1=ifix(vector(1)*float(iii))+1
          index=nsel(index1)
          if(index.eq.1) then
          kpast=kcur
          kcur=kt2
          stfp=stfp+1
          endif
          if(index.eq.2) then
          jpast=jcur
          jcur=jt2
          stfp=stfp+1
          endif
          if(index.eq.3) then
          kpast=kcur
          kcur=kt1
          stfp=stfp+1
          endif
          if(index.eq.4) then
          jpast=jcur
          jcur=jt1
          stfp=stfp+1
          endif
          go to 98
4        continue
          if(stfp.lt.nsfp(jblk,kblk)) nsfp(jblk,kblk)=stfp
3        continue
2        continue
1        continue
c
c                    COMPUTE FINAL STATISTICS
c
          nninf=0
          sfpavg=0.0
          nsfpmn=0
          do 100 i=1,ny
          do 101 j=1,nz
          itest=nsfp(i,j)
          if(itest.eq.nx) nsfpmn=nsfpmn+1
          if(itest.lt.9999) then
                  nninf=nninf+1
                  sfpavg=sfpavg+float(itest)
          endif
101      continue
100      continue
          sfpavg=sfpavg/float(nninf)
c
c                    FINISHED THE SUBROUTINE
c
          return
          end
```

```
      subroutine rand(seed,n,vector)
c-----------------------------------------------------------------------
c          Marsaglias handy dandy random number generator.
c This random number generator generates random numbers in ]0,1[
c Note that if the seed value is zero on the first call, a default
c value of 1369 will be used  in a linear congruential generator to
c generate 55 odd integers for the array 'itab()'. These values are
c preserved by a common statement, so that they may be used in sub-
c sequent calls by setting the seed to zero.If the value of 'seed'
c is greater than zero in a call to the subroutine, then the array
c 'itab' will be initialized and a new seed value will be returned
c by the subroutine. Best results are obtained by making the initial
c call with a seed of your choice and then setting the seed to '0'
c for all subsequent calls.
c
c-----------------------------------------------------------------------
      dimension vector(n)
      common /unusual/itab(55),n1,n2,nseed
      integer rn1,seed
c
c test to see if 55 odd integers must be generated.
c
      if((seed.le.0).and.(nseed.ge.1)) go to 11
      nseed = seed
      if(seed.le.0) nseed  = 7931
c
c generate 55 odd integers in array itab().
c
      do 10 i=1,55
      rn1=mod(nseed*9069,32768)
      if(mod(rn1,2).eq.0) rn1 = rn1-1
      itab(i) = rn1
      nseed = rn1
10    continue
c
c generate "n" random components for the vector "VECTOR"
c
      n1 = 0
      n2 = 24
11   do 30 i=1,n
      itab(55-n1) = mod(itab(55-n2)*itab(55-n1),32768)
      nseed = itab(55-n1)/2
      vector(i) = float(nseed)/float(16384)
      n1 = mod(n1+1,55)
      n2 = mod(n2+1,55)
30    continue
      if(seed.gt.0) seed=nseed
      return
      end
```

```
      subroutine omega(pke,pksh,pkss,psh,w)
c-----------------------------------------------------------------
c              CALCULATE THE POWER OF AVERAGING
c              ********************************
c
c INPUT:
c  1. pke   = effective permeability.
c  2. pksh  = shale permeability.
c  3. pkss  = sandstone permeability.
c  4. psh   = proportion of shale.
c
c OUTPUT:
c  1. w     = the averaging power.
c
c AUTHOR: Clayton Deutsch                    DATE: January 1987
c
c-----------------------------------------------------------------
      wn=-0.001
      wp=0.001
      dop=del(pke,pksh,pkss,psh,wp)
      dnp=del(pke,pksh,pkss,psh,wn)
      w=0.0
      if(dop.gt.0.0) w=-1.0
c
c
c
      w=w+0.005
      dow=del(pke,pksh,pkss,psh,w)
      do 10 i=1,100
      w=w+0.01
      doa=del(pke,pksh,pkss,psh,w)
      test=doa*dow
      if(test.le.0.0) go to 20
      dow=doa
10    continue
c
c
c
20    w=w-0.01
      do 30 i=1,100
      w=w+0.001
      doa=del(pke,pksh,pkss,psh,w)
      test=doa*dow
            if(test.le.0.0) go to 40
      dow=doa
30    continue
c
c
c
40    w=w-0.0005
```

```
      return
      end
c
c     function delta
c
      real function del(pke,pksh,pkss,psh,w)
c
      if(w.gt.-0.0009.and.w.lt.0.0009) go to 291
      del=psh*(pksh**w)+(1.0-psh)*(pkss**w)-pke**w
      go to 292
291   del=0.0
292   continue
      return
      end
```

```
      real function gauscdf(m,s,x)
c-----------------------------------------------------------------
c
c  This function computes the value of the cdf for a gaussian
c    probability distribution of mean m , standard deviation s
c
c  Reference : Abramovitz and Stegun , p.932
c
c-----------------------------------------------------------------
      data c1,c2,c3,c4/0.196854,0.115194,0.000344,0.019527 /
      real m
c
      if(s.eq.0.0) stop 'Error in gauscdf '
      y1=(x-m)/s
      y=abs(y1)
      gaus=1.0+y*(c1+y*(c2+y*(c3+y*c4)))
      g1=1.0/gaus
      g4=g1*g1*g1*g1
      gauscdf=1.0-0.5*g4
      if(y1.lt.0.0) gauscdf=1.0-gauscdf
c
      return
      end
```